Open access • Journal Article • DOI:10.1098/RSPA.1985.0043

The kinetics of solvent-mediated phase transformations — Source link

P.T. Cardew, Roger J. Davey

Published on: 09 Apr 1985 - Proceedings of The Royal Society A: Mathematical, Physical and Engineering Sciences (The Royal Society)

Topics: Dissolution and Supersaturation

The kinetics of solvent-mediated phase transformations.

INFORMATION TO USERS

The most advanced technology has been used to photograph and reproduce this manuscript from the microfilm master. UMI films the text directly from the original or copy submitted. Thus, some thesis and dissertation copies are in typewriter face, while others may be from any type of computer printer.

The quality of this reproduction is dependent upon the quality of the copy submitted. Broken or indistinct print, colored or poor quality illustrations and photographs, print bleedthrough, substandard margins, and improper alignment can adversely affect reproduction.

In the unlikely event that the author did not send UMI a complete manuscript and there are missing pages, these will be noted. Also, if unauthorized copyright material had to be removed, a note will indicate the deletion.

Oversize materials (e.g., maps, drawings, charts) are reproduced by sectioning the original, beginning at the upper left-hand corner and continuing from left to right in equal sections with small overlaps. Each original is also photographed in one exposure and is included in reduced form at the back of the book.

Photographs included in the original manuscript have been reproduced xerographically in this copy. Higher quality 6" x 9" black and white photographic prints are available for any photographs or illustrations appearing in this copy for an additional charge. Contact UMI directly to order.

U·M·I

University Microfilms International
A Bell & Howell Information Company
300 North Zeeb Road, Ann Arbor, MI 48106-1346 USA
313/761-4700 800/521-0600

Order Number 9022118

The kinetics of solvent-mediated phase transformations

Wu, Hsiu-Jean, Ph.D.

The University of Arizona, 1990

U·M·I
300 N. Zeeb Rd.
Ann Arbor, MI 48106

THE KINETICS OF SOLVENT-MEDIATED PHASE TRANSFORMATIONS

by

Hsiu-Jean Wu

A Dissertation Submitted to the Faculty of the

DEPARTMENT OF PHARMACEUTICAL SCIENCES

In Partial Fulfillment of the Requirements
For the Degree of

DOCTOR OF PHILOSOPHY

In the Graduate College

THE UNIVERSITY OF ARIZONA

1 9 9 0

THE UNIVERSITY OF ARIZONA
GRADUATE COLLEGE

As members of the Final Examination Committee, we certify that we have read the dissertation prepared by Hsiu-Jean Wu

entitled The Kinetics of Solvent-Mediated Phase Transformations

and recommend that it be accepted as fulfilling the dissertation requirement for the Degree of Doctor of Philosophy.

Marc Rodriguez-Hornedo	11/30/89 Date
Michael Mayersohn	11/30/89 Date
[signature]	11-30-89 Date
G.K. Venkatapathi	11/30/89 Date
M.F. Burke	11/30/89 Date

Final approval and acceptance of this dissertation is contingent upon the candidate's submission of the final copy of the dissertation to the Graduate College.

I hereby certify that I have read this dissertation prepared under my direction and recommend that it be accepted as fulfilling the dissertation requirement.

Marc Rodriguez-Hornedo	12/20/89
Dissertation Director	Date

STATEMENT BY AUTHOR

This dissertation has been submitted in partial fulfillment of requirements for an advanced degree at The University of Arizona and is deposited in the University Library to be made available to borrowers under rules of the Library.

Brief quotations from this dissertation are allowable without special permission, provided that accurate acknowledgement of source is made. Requests for permission for extended quotation from or reproduction of this manuscript in whole or in part may be granted by the head of the major department or the Dean of the Graduate College when in his or her judgement the proposed use of the material is in the interests of scholarship. In all other instances, however, permission must be obtained from the author.

SIGNED: John Jean Wu

ACKNOWLEDGEMENTS

I would like to give my special gratitude to my advisor, Dr. Nair Rodriguez, for her guidence and encourgement throughout my graduate education.

I would like to thank Dr. Michael Mayersohn, Dr. Samuel Yalkowsky and Dr. Arnold Martin for their support and academic input.

I would also like to thank Dr. Michael Burke and Dr. Krishna Vemulapalli for their time and support in my graduate committe.

TABLE OF CONTENTS

TABLE OF CONTENTS (Continued)

TABLE OF CONTENTS (Continued)

TABLE OF CONTENTS (Continued)

TABLE OF CONTENTS (Continued)

LIST OF ILLUSTRATIONS

LIST OF ILLUSTRATIONS (Continued)

LIST OF ILLUSTRATIONS (Continued)

LIST OF ILLUSTRATIONS (Continued)

LIST OF ILLUSTRATIONS (Continued)

LIST OF TABLES

LIST OF TABLES (Continued)

LIST OF TABLES (Continued)

ABSTRACT

The objectives of this work are to characterize and model the solvent-mediated phase transformation process of theophylline anhydrous crystals to the monohydrate crystals in an aqueous system. In order to model the transformation, the following processes are taken into account : (1) the dissolution kinetics of theophylline anhydrous crystals, (2) the kinetics of the formation of theophylline monohydrate nuclei, and (3) the growth kinetics of the monohydrate crystals. The driving forces for the above processes are determined from the concentration of theophylline in the solution and the solubilities of theophylline anhydrous and monohydrate. The solubilities of theophylline anhydrous and the monohydrate, and these three distinct processes along with the overall transformation phenomena were investigated in the present study.

By using theophylline as a model compound we have gained some understanding of the kinetics of the solvent-mediated phase transformation between the metastable anhydrous form and the stable hydrated form of an organic compound and we were able to model the transformation

process. By identifying the mechanisms for nucleation, growth of the hydrate form and the dissolution of the anhydrous form one can predict and control the transformation process.

The growth kinetics of thymine monohydrate crystals at various temperatures are also investigated in the present study.

CHAPTER 1

INTRODUCTION

1.1 : GENERAL OVERVIEW

Many solids can exist in a number of different polymorphs, hydrates or other solvates as well as amorphous solids. Under a given set of conditions such as temperature, pressure and composition, only one solid phase will be consistent with a minimum free energy of the system and hence will be the thermodynamically stable phase, any other phase that appears will be metastable with respect to the stable phase. However, the metastable phase can often exist for a relatively long time when left undisturbed. Enantiotropic polymorphs can interconvert below the melting points of the polymorphs, while monotropic polymorphs can not.

During crystallization from solution, the resulting crystals may consist of a pure component or may be a molecular compound. Molecular compounds may contain two or more constituents crystallized together as a new single crystalline entity. Solvates are molecular

complexes that have incorporated the crystallizing solvent molecules in their lattice. When the solvent incorporated is water, it is called a hydrate. To distinguish solvates from polymorphs, the term pseudo-polymorph has been used. Just as different chemical compounds can have different polymorphs, solvates can also exhibit polymorphism. The stoichiometric ratio of the compound molecule to the solvent molecule may also vary. For example, the crystal forms of sulfameter have been identified for three polymorphs, two solvates and an amorphous phase (Moustafa, 1971; Khalil,1972). Urapidil, a new antihypertensive drug, can exist as three unsolvated polymorphs, a methanol solvate and three hydrates as monohydrate, trihydrate and pentahydrate (Botha, 1986, 1988, 1989).

Pseudopolymorphs, or solvates, sometimes behave similarly to polymorphs. The crystalline lattice, reactivity, chemical and physical properties of the anhydrous form are different from those of the hydrate form. The anhydrous form usually has a higher solubility than the hydrate form in an aqueous system (Haleblian, 1969). The solvent-mediated transformation between the anhydrous and the hydrate form can usually be

explained by the same principle as the transformation between polymorphs.

The existence of polymorphs and solvates has some advantages in pharmaceutical applications. For example, the bioavailability of chloramphenicol palmitate suspensions and aspirin tablets can be significantly improved by utilizing the high solubility (or high energy) of the metastable form (Haleblian, 1969; Tawashi, 1969). However, most of the problems encountered with metastable forms are related to their physical and chemical instabilities. For example, tolbutamide exists as forms A and B; during tableting, the plate-like form B causes powder bridging in the hopper and capping problems, whereas, form A does not have such problems (Simmons, 1972). Lactose, a commonly used tablet diluent, exists as monohydrate and anhydrous crystals with different mechanical behavior (Wong, 1988). Polymorphic transformations can cause physical, chemical and therapeutic problems with tablets, suspensions, suppositories, creams and other pharmaceutical dosage forms. Pharmaceutically important solvates, which have been studied, include steroids, barbiturates, hydrocortisone acetate, prednisolone, antibiotics, sulfa

drugs, caffeine, ouabain, theophylline, etc. (Haleblian, 1975).

Most of the studies of polymorphs and solvates have been involved with their characterization, stability, solid state transition, solid state dehydration and their dissolution. Only a few investigations have focused on the kinetics of solvent-mediated phase transformations. The transformation kinetics of calcium oxalate trihydrate and dihydrate to the thermodynamically stable monohydrate have been studied in batch precipitation experiments by Brecevic and Sketic (1986). The solvent-mediated phase transformation of copper phthalocyanine has been analyzed by Cardew and Davey (1985).

Solvent-mediated transformations involve the nucleation and the subsequent growth of the more stable (less soluble) form at the expense of the dissolution of the metastable phase. In order to construct the kinetic profile for the phase transformation process, the individual kinetics of the nucleation, growth and dissolution process must be fully understood. In the present study, we use a model compound, theophylline, which exists as anhydrous or monohydrate form, to investigate the following processes : (1) the growth

kinetics of the stable monohydrate crystals, (2) the dissolution kinetics of the metastable anhydrous form, and (3) the solvent-mediated phase transformation between the metastable and the stable form, and the nucleation process during the transformation. From these kinetic data, the growth, dissolution and the transformation processes can be modeled and predicted, and the rate controlling process for the transformation can also be elucidated. These are the advantages of measuring the kinetics of these processes over only the characterization of solid phase.

1.2 : THEOPHYLLINE SOLVATES

Theophylline exists in both the anhydrous and the monohydrate forms. The structure of theophylline anhydrous is shown in Figure 1.1. Theophylline is a weak organic acid with a pKa value of 8.6 (Maulding, 1971), and also a weak base with pKb of 13.5 (Linek, 1969). It has a molecular weight of 180.17 and a melting point of 272°C.

The monohydrate crystals can be obtained from water (Suter, 1958). They belong to the monoclinic space group $P2_1$, nearly $P2_1/a$, with unit cell dimensions a = 13.3, b = 15.3, c = 4.50 Å, and β = 99.5°. The anhydrous form can be crystallized from chloroform (Nagvi, 1981) or by drying finely powdered monohydrate at 150°C for three hours (Cohen,1975) or at 100°C overnight (Merk Index, 1952). The anhydrous crystals are orthorhombic, $Pna2_1$, with a = 24.63, b = 3.83 and c = 8.50 Å.

1.2.1 : Previous Work on the Phase Transformation of Theophylline

Several studies have been done to investigate the phase transformation between theophylline anhydrous and the monohydrate form. Lin and Byrn (1979) demonstrated that by cutting the end of a long plate monohydrate crystal, it gradually became opaque due to the loss of water. Shefter (1973) studied the kinetics of the dehydration of theophylline monohydrate crystals in the solid state, with nitrogen (dried over sulfuric acid) constantly flushed through the reaction chamber, from 38°C to 54°C by X-ray powder diffraction.

Bogan (1983) confirmed that the monohydrate form was always the stable phase in a water-dioxane system as long as the water content was higher than 5%. Shefter and Higuchi (1963) showed that theophylline anhydrous was the metastable form in water below the transition temperature (73°C). Pearson and Varndy (1969) studied the crystal growth from the anhydrous form by hydration in an aqueous suspension using photomicrography. Fokkens (1983) showed that the powdered anhydrous theophylline formed a cake in the interfacial area between water and paraffin. The

caking phenomenon was independent of the pH of the aqueous phase, and was due to the formation of the monohydrate crystalline needles.

In the present study we investigate the growth kinetics of theophylline monohydrate crystals, the dissolution kinetics of the anhydrous crystals and the transformation process between these two forms in an aqueous suspension.

Figure 1.1 : The Structure of Theophylline

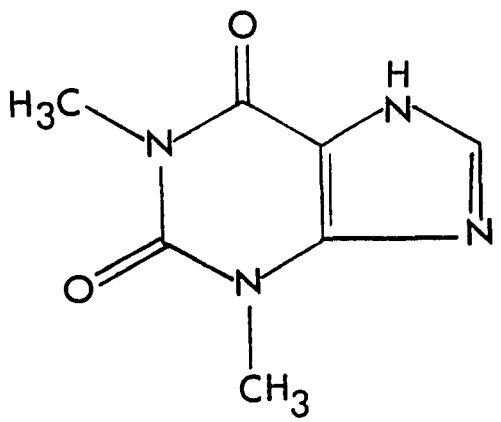

1.3 : SOLUBILITY

In order to define the driving force for the processes under consideration, the solubilities of theophylline anhydrous and the monohydrate need to be known.

Thermodynamically, the driving force for nucleation, crystal growth and dissolution is the difference between the chemical potential (or Gibb's free energy) of a molecule in the solution and the saturated solution (Boistelle *et al*, 1988). The driving force, ΔG , can be written as,

$$\Delta G = RT \ln \left(\frac{C}{C_S}\right) \qquad (1.1)$$

where R is the gas constant (1.987 cal deg^{-1} $mole^{-1}$), T is the absolute temperature, C is the concentration of the solute in the system, and C_S is the solubility of the solute. The magnitude of the driving force will affect the kinetics and the mechanisms of the nucleation, growth and dissolution processes.

1.3.1 : Measurement of Solubility

The solubility of the stable form, theophylline monohydrate, was measured by allowing the solid phase to come to equilibrium with theophylline in solution. The solid-solution equilibrium of theophylline monohydrate in an aqueous system can be expressed as,

$$A.H_2O_{(S)} \underset{}{\overset{K_S}{\rightleftharpoons}} A_{(aq)} + H_2O \qquad (1.2)$$

where A represents a theophylline molecule. The equilibrium constant K_S is essentially the solubility of the monohydrate form.

Theophylline anhydrous crystals undergo transformation to the monohydrate form in aqueous solution before its solubility is reached. Instead of using the equilibrium method, the solubility of the anhydrous form is estimated from the initial dissolution rate obtained from disk dissolution experiments with a constant surface area of the solid.

The release of a solid substance from a disk is generally treated as a diffusion controlled process (Wagner, 1970). The dissolution rate for a diffusion

controlled process can be described by the Noyes-Whitney equation as shown in equation 1.3 (Noyes and Whitney, 1897),

$$\frac{dC}{dt} = \frac{A\ D\ (C_S - C)}{h\ V} \qquad (1.3)$$

where A is the surface area of the compound in contact with the dissolution medium, V is the volume of the dissolution medium, h is the diffusion layer thickness, D is the diffusion coefficient of the solute in the dissolution medium, and C_S and C are the solubility and the concentration of the solute in the dissolution medium, respectively. The surface area of exposed solid (Seitz, 1958), intensity of agitation (Nicklasson et al, 1982), and temperature (Gapson, 1926) will affect the dissolution behavior.

Equation 1.3 can be written as equation 1.4,

$$\frac{dC}{dt} = K_A\ D\ (C_S - C) \qquad (1.4)$$

where K_A is equal to A/hV. Under sink conditions (i.e., the concentration of the solute in the dissolution medium is less than 10% of its solubility), such as during the initial dissolution of a solid, the solubility term C_S in equation 1.4 is the determining factor for dissolution rate.

When the conditions for the dissolution of both the anhydrous and the monohydrate form are the same, the value of K_A will be the same. The diffusion coefficient, D, which is concerned with the diffusion of the molecule in solution, is the same for both forms. The ratio of the initial dissolution rate of the anhydrous form to the monohydrate form will be equal to the ratio of the corresponding solubility at a given temperature. This is the basic assumption in using the ratio of dissolution rate to obtain the solubility of the unstable anhydrous form in this study.

By knowing the solubility of the monohydrate form and the dissolution rates of both forms, the solubility of the anhydrous form can be estimated.

1.3.2 : Thermodynamic Parameters Involved in the Phase Transformation Process

The thermodynamic parameters involved in the phase transformation process are the free energy, enthalpy and entropy of transition and the transition temperature. These can be determined from the dissolution rates and the solubilities of the solid forms involved in the transformation process.

The dissolution rate of a solid under sink conditions can be expressed in terms of the diffusion coefficient and the solubility of the compound, as shown in equation 1.5,

$$\frac{dC}{dt} = K_A \, D \, C_S \qquad (1.5)$$

The temperature dependence of the dissolution rate can be obtained from the temperature dependence of the diffusion coefficient and solubility (DeSmidt, 1986).

Within the temperature range where Arrhenius law is followed, the dependence of the diffusion coefficient on temperature can be expressed by equation 1.6,

$$D = D_o\, e^{-Ea/RT} \qquad (1.6)$$

where D_o is a constant, depending on the molecular weight of the solute, and Ea is the activation energy of diffusion. Likewise, the dependence of solubility on temperature is described by equation 1.7,

$$C_S = C_{So}\, e^{-\Delta Hs/RT} \qquad (1.7)$$

where C_{So} is a constant, ΔHs is the heat of solution. Equation 1.5 may be written as equation 1.8 by incorporating equations 1.6 and 1.7,

$$\frac{dC}{dt} = K_B\, e^{-(Ea+\Delta Hs)/RT} \qquad (1.8)$$

where $K_B = K_A D_o C_{So}$. Equation 1.8 predicts a linear relationship between the logarithm of the dissolution rate and the reciprocal of the absolute temperature, with a slope equal to $-(Ea + \Delta H_S)/R$. The quantity $(Ea+\Delta H_S)$, referred to as the heat of dissolution, ΔH_{diss}, can be determined for any dissolving solid.

For a compound with different crystalline forms, the species in solution is independent of the solid phase, so the diffusional contribution to the heat of dissolution is identical for different forms. As a result, the difference in the heat of dissolution of different forms of a compound is determined by the difference in their heat of solutions.

The enthalpy of transition (ΔH_{trans}) is the difference in the heats of dissolution of any two crystalline forms of the same compound, and is also equal to the difference in their heats of solution.

Under the conditions of constant pressure and temperature, the difference in free energy of any two solid forms of a compound involved in the transition is given by equation 1.9,

$$\Delta G_T = RT \ln\left(\frac{C_{S1}}{C_{S2}}\right) = RT \ln\left(\frac{IDR_1}{IDR_2}\right) \qquad (1.9)$$

where the subscripts 1 and 2 represent the metastable and the stable forms, respectively. C_S is the solubility and IDR is the initial dissolution rate. At the transition

temperature, where ΔG_T is zero, the two solid forms will have the same solubility and dissolution rate.

The entropy of transition at a given temperature can be calculated from equation 1.10,

$$\Delta S_T = \left(\frac{\Delta H_{trans} - \Delta G_T}{T}\right) \qquad (1.10)$$

The thermodynamic parameters metioned here can indicate whether the transformation processes are likely to occur.

1.4 : NUCLEATION AND CRYSTAL GROWTH KINETICS

Reviews on crystallization phenomena from liquid solution in the literature include those of Randolph (1988, 1980), Mullin (1979), Rosenberger (1979), Ohara (1973), Garside (1984), Brice (1986), Wey (1985), Strickland (1968), Nyvlt (1971), Hartman (1973) and Pamplin (1980).

The deposition of a solid crystalline phase from liquid solutions can only occur if a certain degree of supersaturation has first been achieved in the system. The attainment of the supersaturation state is essential for any crystallization operation, and the degree of supersaturation, or the deviation from the equilibrium saturated condition, is the prime factor controlling the crystallization process. Any crystallization process can be considered to comprise three distinct steps : (1) achievement of supersaturation, (2) formation of crystal nuclei, or nucleation, and (3) the subsequent growth of the crystals.

The supersaturation of a system may be achieved by cooling, evaporation, the addition of a precipitant or diluent or as a result of a chemical reaction between two

homogeneous phases. The degree of supersaturation can affect the rates and mechanisms of nucleation and growth, and consequently the internal structure and the habit of crystals.

1.4.1 : Nucleation

Two major mechanisms for nucleation have been identified, primary and secondary nucleation, and are shown in the following diagram,

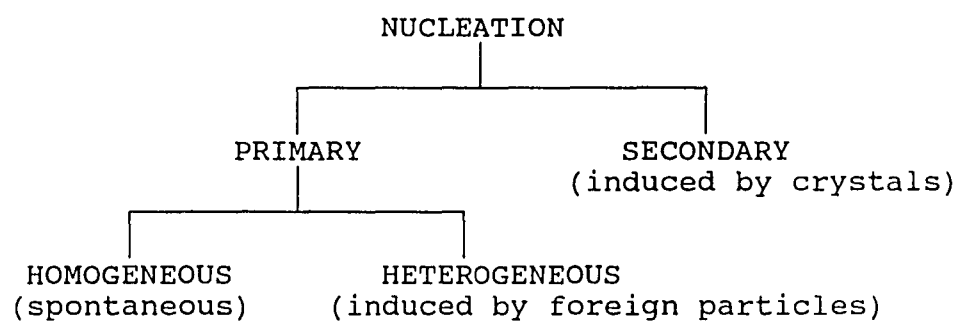

(a) Primary Nucleation :

Primary nucleation is the formation of the crystal nuclei in the absence of the solid phase of the crystallizing substance. It can be a spontaneous

(homogeneous) process or it may be induced by foreign particles (heterogeneous process). In order to form stable nuclei, the molecular aggregates or clusters must overcome an energy barrier, as shown in Figure 1.2. The Gibb's free energy associated with a spherical cluster for homogeneous nucleation can be expressed as in equation 1.11,

$$\Delta G = -\left(\frac{4}{3}\right) \pi r^3 V R T ln(S) + 4 \pi r^2 \tau \qquad (1.11)$$

and the maximum energy barrier needed to be overcome (i.e., the activation energy) can be expressed as follows,

$$\Delta G_{MAX} = \frac{16 \pi \tau V}{3 R T \ln(S)} \qquad (1.12)$$

where ΔG is the Gibb's free energy, R is the Boltzmann constant, T is the absolute temperature, r is the radius of the cluster, V is the molecular volume, τ is the surface free energy and S is the supersaturation. Only those clusters or nuclei surpassing this energy barrier,

ΔG_{MAX}, will be able to continue to grow, otherwise, they will redissolve (Adamson, 1982). The higher the supersaturation the lower the energy barrier. In order to overcome the energy barrier, homogeneous nucleation usually occurs when the supersaturation is high.

Heterogeneous nucleation occurs most frequently when the supersaturation is low and when the solute molecules have some affinity for solid substrates which may be the walls of the crystallization vessel, the surface of the stirrer or any other solid like dust or foreign crystals in the crystallization medium. With such a nucleation mechanism, the nucleus develops onto the substrate with which it makes a contact angle α. Figure 1.3 shows a special situation for a cap-shaped nucleus where involves three areas and surface free energies (substrate/nucleus, substrate/solution and nucleus/solution). The activation energy for heterogeneous nucleation (ΔG_{MAX}^{*}) is the product of the activation energy for homogeneous nucleation and a term depending on the value of α, and can be expressed in equation 1.13,

$$\Delta G_{MAX}^{*} = \Delta G_{MAX} \left(\frac{1}{2} - \frac{3}{4}\cos\alpha + \frac{1}{4}\cos^{3}\alpha\right) \quad (1.13)$$

The influence of α can be demonstrated by using three particular values. For $\alpha = 180°$, the nucleus has no affinity for the substrate, the term in parenthesis is one and $\Delta G_{MAX}^{*} = \Delta G_{MAX}$. For $\alpha = 90°$, $\Delta G_{MAX}^{*} = \Delta G_{MAX}/2$ and for $\alpha \approx 0$, $\Delta G_{MAX}^{*} \approx 0$. The smaller α, the smaller the energy required for forming nucleus. Therefore, the substrate catalyzes the nucleation and the nucleus may form at a very low supersaturation (Boistelle, 1988).

(b) Secondary Nucleation :

Secondary nucleation refers to the production of crystal nuclei by a seed crystal. The nuclei do not have to come directly from the seed, but the presence of the seed crystal is essential to the nucleation process. Strickland-Constable (1968), Clontz and McCabe (1971) and Botsaris *et al.*(1967) have outlined some of the ways in which secondary nucleation could occur as follows :
(1) Initial breeding : This occurs only when a crystal is first introduced to a solution. It is attributed to the existence of crystal dust already present on the surface of the seed crystal, these are washed off and grow as new crystals. (2) Needle or dentrite breeding : The needles

or dentrites grow out of the body of the crystal, and they may break off and cause breeding. (3) Poly-crystalline breeding : This occurs only at high supersaturation, the crystal grows as a polycrystalline mass which may break up rather easily and give rise to further crystals. (4) Collision breeding : This occurs very readily when a crystal collides with or slides along another solid body in a supersaturated solution, the number of crystals usually increase rapidly as the supersaturation increases. Collision breeding appears to be the principal cause of secondary nucleation in most agitated seeded crystallizers. The formation of the nuclei from all kinds of secondary nucleation will depend on the seed crystals added and it occurs at a lower supersaturation than primary nucleation (Botsaris, 1976, Boistelle, 1988).

1.4.2 : General Growth Models

It is generally thought that the growth of crystals from solution involves two steps occuring in series : the transport of solute from bulk supersaturated solution to the crystal surface; and the incorporation of solute into the crystal lattice, or surface integration (Liu *et al*, 1971). Several growth models have been developed and they fall into one of the following four classes, depending on the rate-limiting step : (a) boundary layer solute transport model, (b) rough surface model, (c) surface nucleation model, and (d) screw dislocation model.

(a) Solute Transport Model :

For the solute transport model, the growth of crystals is controlled by the transport of the molecules across a boundary diffusion layer (Ohara, 1973a). The growth rate G is given by equation 1.14,

$$G = \frac{D\, V_S\, (C - C_S)}{h} = K\,(C - C_S) \qquad (1.14)$$

where D is the solute diffusion coefficient, V_S is the molecular volume of the solute in the crystal, C is the concentration of solute in the solution and C_S is the solubility of the solute. h is the boundary layer thickness around the crystals which will be affected by the agitation intensity of the crystallization system. The overall growth rate will depend on the hydrodynamic condition (stirring rate) for the diffusion model.

(b) Rough Surface Model :

The assumption for the models in the second category is that, a rough surface, on a molecular scale, provides many randomly distributed favorable sites, at which an incoming molecule can form multiple bonds to the crystal (Weeks, 1979, Jetten, 1984 and Gilmer, 1977). Since growth results from many, essentially independent molecular attachment processes, G is expected to be a linear function of supersaturation $(C-C_S)$,

$$G = K_X (C-C_S) \qquad (1.15)$$

where K_X is a constant, which is independent of C, but may depend on the crystal face because of different binding energies of different faces.

(c) Surface Nucleation Model :

For the two dimensional surface nucleation model, the attachment sites for the growth unit are present at the edges of two-dimensional clusters (or nuclei) on the surface. In order to form the nuclei, surface nucleation usually occurs at a high supersaturation. The nuclei will grow, expand and merge to form new layers. Three different submodels : mononuclear model, polynuclear model and the birth and spread model are shown in Figure 1.3. The spreading rate of the clusters will influence the overall crystal growth rate. A general relation between the growth rate and supersaturation can be expressed in equation 1.16,

$$G = A\, S^{P}\, e^{(-B/S)} \qquad (1.16)$$

where S is the supersaturation, p is a constant with a value dependent on the spreading velocity, p is equal to 1/2, -3/2 and 5/6 for mononuclear, polynuclear and birth

and spread model, respectively (Hillig, 1966). The parameters A and B can be described by equations 1.17, 1,18 and 1.19.

$$A = \left(\frac{2\pi C_o}{3}\right)^{1/3} \left(\frac{2\lambda_s}{a_s}\right) C' \qquad (1.17)$$

$$B = \left(\frac{\pi}{3}\right) \left(\frac{\Gamma_e}{R\,T}\right)^2 \qquad (1.18)$$

$$C' = \frac{D_s\, n_{so}\, \Omega}{\lambda_s^{\,2}} \qquad (1.19)$$

where C_o is the fraction of the crystal surface occupied by growth units, λ_s is the mean diffusion distance of growth units on surface, a_s is the lattice spacing, Γ_e is the edge energy, D_s is the surface diffusion coefficient, n_{so} is the equilibrium value of surface solute density, Ω is the molecular volume in the crystal and R is Boltzmann constant (van der Eerden, 1978).

(d) Screw Dislocation Model :

In this model, the steps for the attachment of molecules are generated by a screw dislocation, shown in

Figure 1.4. Molecules diffuse through the essentially smooth surface and only attach to the crystal when they reach the steps at the edge of a growing layer, which are the most favorable attachment sites (Bennema, 1984, Nielsen, 1964). The surface advances in a spiral pattern. Since the steps are always present, adsorbed solute molecules are more easily trapped than in the surface nucleation model. Therefore, screw dislocation model usually occurs at a lower supersaturation than surface nucleation model, and the growth is much more regular. One of the screw dislocation models, the BCF model, developed by Burton, Cabrera and Frank (Burton *et al*, 1951) is the most successful one in this class. The equation for the BCF model is,

$$G = \frac{K_1}{K_2} S \, ln(1+S) \tanh\left(\frac{K_2}{ln(1+S)}\right) \qquad (1.20)$$

where S is the supersaturation, and K_1 and K_2 are constants and can be expressed by equations 1.21, 1.22 and 1.23.

$$K_1 = \beta C' \qquad (1.21)$$

$$\beta = [1 + (\frac{D_s \tau_k}{a_s \lambda_s}) \tanh(\frac{K_2}{S})]^{-1} \quad (1.22)$$

$$K_2 = \frac{9.5 \Gamma_e a_s}{n_s \lambda_s R T} \quad (1.23)$$

Where β is the retardation factor which is a measure of the resistance experienced by the growth units on entering the kinks in the steps. n_s is the number of co-operating spirals or strength of the step source. C', Ds, τ_k, a_s, k_s, and Γ_e have the same meaning as discussed in the surface nucleation model.

When $ln(1+S) \approx S$, equation 1.20 can be simplified as equation 1.24,

$$G = K_1 (\frac{S^2}{K_2}) \tanh(\frac{K_2}{S}) \quad (1.24)$$

It is important to note that at low supersaturation,

$$G = K_1 \frac{S^2}{K_2} \quad (1.25)$$

the growth rate is proportional to the second order of the supersaturation. At high supersaturation,

$$G = K_1 S \qquad (1.26)$$

the growth rate is directly proportional to the supersaturation.

(e) Exponential Model :

Many of the constants involved in the BCF and surface nucleation models are unknown, a simple semiempirical growth rate equation in the form of,

$$G = K_g S^a \qquad (1.27)$$

has been frequently used to describe the growth process. Such an equation can represent the two limiting cases of the BCF equation when **a** equals 2 or 1 at low and high supersaturation, respectively. It is also a good approximation in the intermediate region when $1 < a < 2$. For the surface nucleation model, the value of **a** is usually larger than 2 (Nielsen *et al*, 1984). For diffusion controlled process, equation 1.27 will be

first-order (**a** = 1), and the overall growth rate will depend on the hydrodynamics of the system. The growth rate constant K_g and the exponent **a** in equation 1.27 are determined experimentally.

The goal of the present study is to investigate the growth kinetics of the already existing seed crystals at various supersaturations, temperatures and stirring rates, and to establish a suitable model for the growth process.

Figure 1.2 : Gibb's Free Energy (ΔG) Versus Nucleus Size for Homogeneous Nucleation. ΔG_S and ΔG_V Are Contributed From the Surface and Volume Free Energies. ΔGmax Is the Activation Energy.

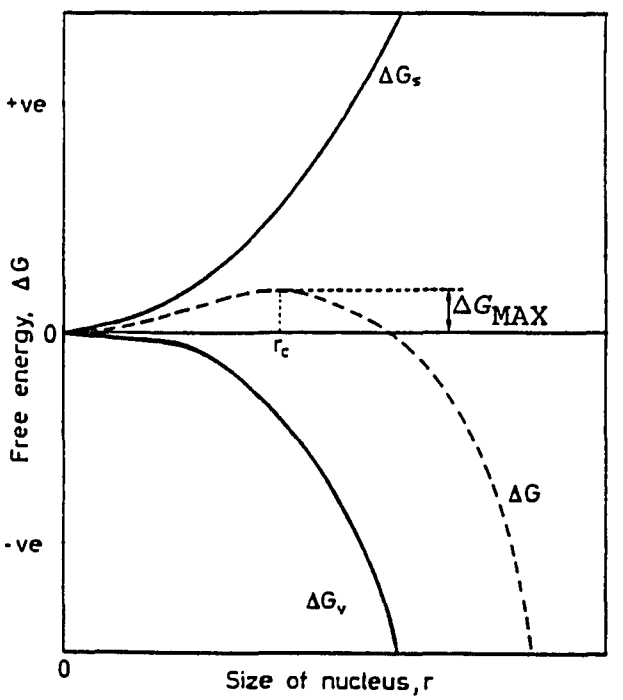

Figure 1.3 : Cap-Shaped Nucleus of Radius r Forming on a Solid Substrate, with Which It Forms the Contact Angle α, for Heterogeneous Nucleation (Boistelle, 1988).

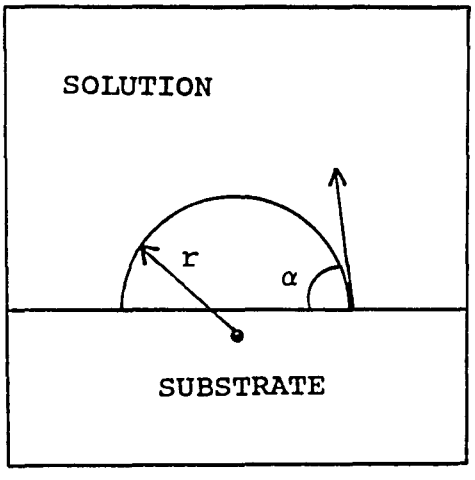

Figure 1.4 : Two Dimensional Surface Nucleation Growth Model. **(A)** Mononuclear Model, **(B)** Polynuclear Model and **(C)** Birth and Spread Model. (Ohara and Reid, 1973).

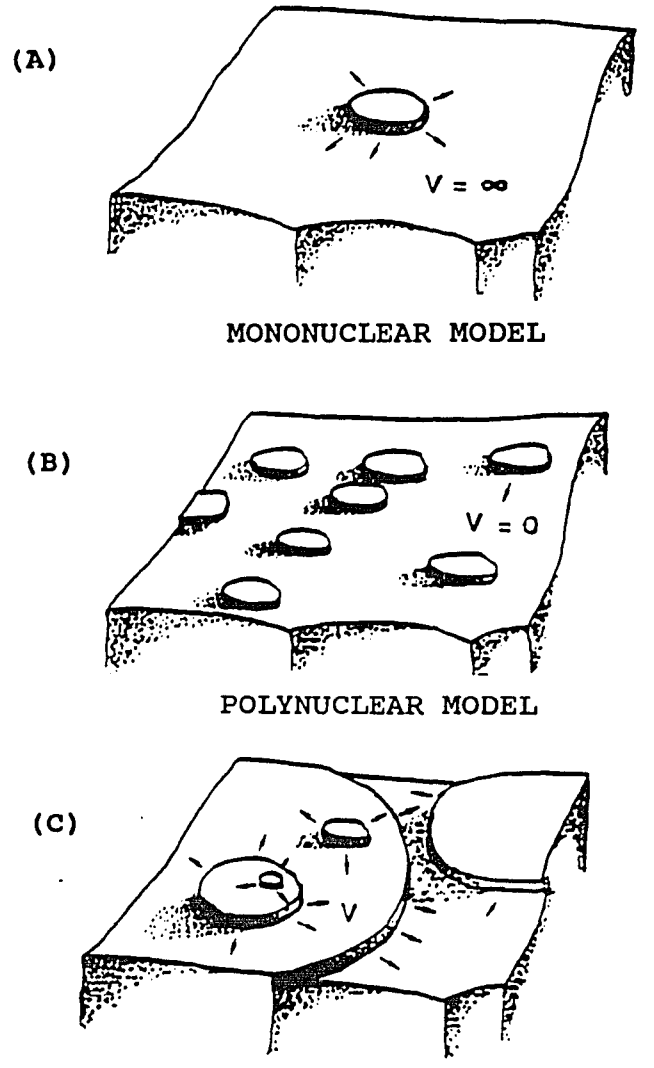

Figure 1.5 : Diagram of a Screw Dislocation
BCF Model (Garside, 1977)

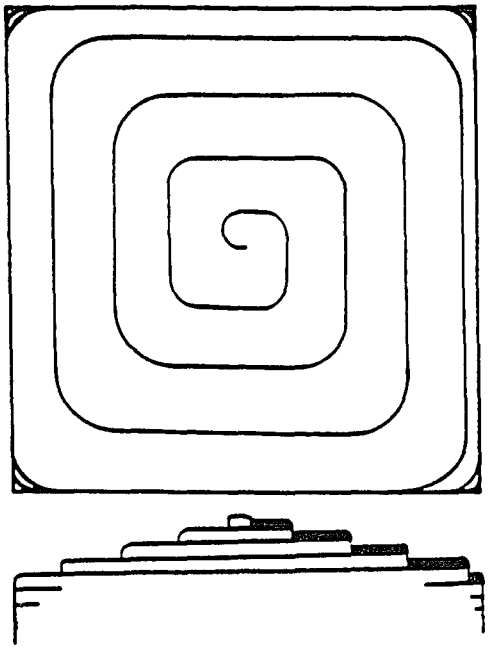

1.5 : DISSOLUTION

1.5.1 : General Dissolution Models

The dissolution process of a solid phase has been regarded as involving two principal stages : the solvation of the molecules at the solid-liquid interface (surface reaction) and the transport of the dissolved solute away from the surface into the bulk solution (Wurster et al, 1965). The solid-liquid interfacial reaction could be considered as three distinct steps : wetting of the solid by the solvent, fusion of the solid and, finally, solvation of the solute molecules (Hsia, 1977). These three steps are very difficult to elucidate by independent means. Depending on the relative rates of the two principal stages, the dissolution mechanism of a compound may be considered to be surface controlled or transport controlled or dependent on both mechanisms.

The interfacial step emphasizing the removal of the dissolution units (atoms, ions or molecules) from the surface of the crystal has seldom been investigated. The kinetics of this step are described only empirically,

usually by a second order law (Gohar, 1986). It has been shown that highly soluble ionic crystals dissolve according to a rate-determining diffusion law, whereas, poorly soluble crystals satisfy a rate-determining interfacial law (Konak, 1785, Jenin, 1968). The dissolution of magnesium fluoride was considered to be surface reaction controlled (Hamzat et al, 1985). The dissolution of aluminium floride trihydrate crystals in aqueous solution investigated by Nielsen and coworker was considered to be controlled by a surface spiral mechanism (Nielsen *et al*, 1984). Generally speaking, few studies focus on surface controlled dissolution, and the mechanism of the interfacial step has not yet been elucidated.

For most compounds, the rate of the solid-liquid transfer at the interface is more rapid than the rate of removal from the interface. A saturated solution exists at the solid-liquid interface, and the dissolution is controlled by the transport of the solute molecules across the stagnant layer around the solid surface. Noyes and Whitney developed the first dissolution model based on Fick's diffusion law, which has been discussed in section 1.3.1. In the Noyes-Whitney equation (as

shown in equation 1.3), the dissolution rate is directly proportional to the concentration driving force and the surface area exposed to the dissolution medium. Based on the Noyes-Whitney equation, Hixson and Crowell derived a cubic root rate law for the dissolution of monodispersed powders (Hixson and Crowell, 1931), which can be expressed as equation 1.28,

$$(W_o)^{1/3} - (W)^{1/3} = K_p\, t \qquad (1.28)$$

where W_o is the initial weight of the powder, W is the weight of undissolved powder at time t, and K_p is an apparent dissolution rate constant. The assumptions made in the derivation of equation 1.21 are : (a) all particles dissolve isotropically, (b) the particles are isometric, (c) the thickness of the diffusional layer is constant, (d) there is no particle-size solubility effect, and (e) sink conditions exist. Most of the dissolution studies or models in the literature are established from these two fundamental models.

In the present study we will investigate the effect of undersaturation and particle size on dissolution rate by using the following experimental equation,

$$DR = P\ (Su)^{Q}\ (Size)^{R} \qquad (1.29)$$

where DR is the dissolution rate in terms of dL/dt (dL is the decrease in particle size in a time interval dt), P, Q and R are constants, and Su is the undersaturation.

1.5.2 : Methods to Measure Dissolution Rate

The basic approaches to investigate dissolution behavior include the rotating disk method, flow through cell for single crystal, suspended multi-particulate method and column dissolution method. Many studies have been done with the rotating disk and flow through cell technique to incorporate hydrodynamic factors into the Noyes-Whitney model, or to investigate the intrinsic dissolution rates of compounds. For example, the studies by Nicklasson and Brodin (1982), Shah and Nelson (1975), Summers and Enever (1972), Higuchi and Young (1973), Amidon and McNamara (1986), and Burt and Mitchell (1980).

The modeling and simulation of the dissolution patterns of polydispersed powders have been investigated by Carstensen and Patel (1975), Mauger and Howard (1976), Higuchi and Rowe (1963), Brooke (1974), Niebergall and

Goyan (1963) and Veng Pedersen and Brown (1975). Column dissolution has been investigated by Langenbucher (1969), Chu and Wetteroth (1953), Carstensen and Dhupar (1976) and Tingstad and Riegelman (1970).

The use of a Coulter Counter to monitor particle size distributions during the dissolution process has been investigated by Marshall and Meakin (1972) with hydrocortisone acetate. They found that the equivalent sphere diameter decreased linearly with time, which agreed with the Hixson-Crowell cube root law. The study of the dissolution of griseofulvin with the coulter counter has been demonstrated by NystrÖm and coworkers (1985); they suggested that the dissolution process was not diffusion controlled. Garside and Jancic (1976) also studied the growth and dissolution of potash alum with an in situ Coulter Counter method. NystrÖm and Bisrat (1986) studied the solubility and the dissolution of griseofulvin and felodipine in micellar solution with a coulter counter.

The advantage of using a coulter counter to study the dissolution rate of polydispersed powders is that the number versus size distribution of the crystals during the dissolution process can be monitored. From the

change of the number-size distribution, the change in the surface area, volume, weight of the particles and the concentration change in the dissolution medium during the dissolution process can be calculated (Randolph and Larson, 1988). From the number versus size distribution, the size dependence of the dissolution rate can also be monitored.

1.5.3 : Determination of Dissolution Rate

A typical plot of the oversize cumulative number versus size distribution for the dissolution process is illustrated in Figure 1.6. The dissolution rate (DR) of a particle at size L is expressed as (Wey, 1985),

$$DR\ (L,t) = \frac{(L - dL) - L}{(t - dt) - t} = \frac{dL}{dt} \qquad (1.30)$$

where dL is the decrease of the particle size in a time period dt. The cumulative curve at time t will parallel the curve at time t-dt when the dissolution rate is size independent.

The number versus size distribution of theophylline anhydrous crystals during dissolution was monitored with an Elzone particle counter in the present study. The dependence of the dissolution on the undersaturation and crystal size were investigated in the present study.

Figure 1.6 : Determination of Dissolution Rate From Cumulative Size Distribution Plot

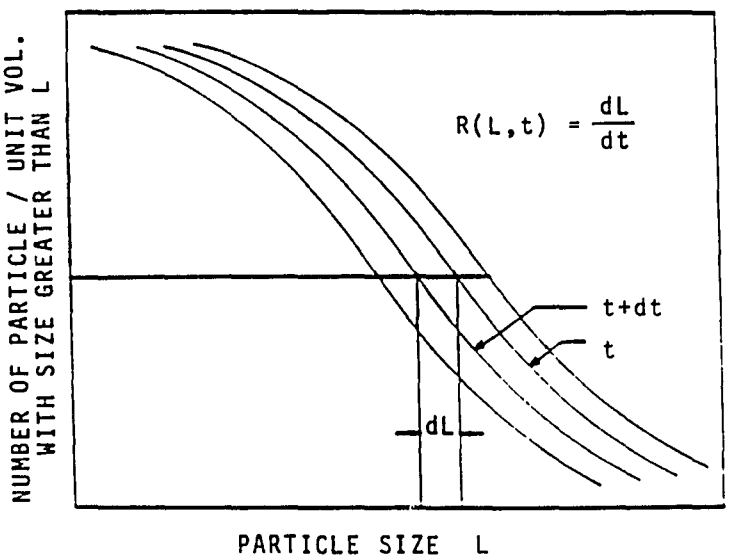

1.6 : PHASE TRANSFORMATIONS

1.6.1 : An Overview of Phase Transformations

Phase transformations of compounds with different polymorphs and solvates in pharmaceutical systems have long been recognized. The transformation may occur within a solid as it rearranges its structure to a more stable state, or it may occur through the formation and growth of the more stable form at the expense of the metastable one. Polymorphic transformations can occur in a solid state during storage, upon compression or exposure to heat and humidity; it may also occur when the compound is in contact with a solvent. Solvent-mediated phase transformations are especially important in a solvated or hydrated system.

A review of the pharmaceutical literature on polymorphism reveals work focusing on solid state transitions. These include the characterization of the solid phases, crystallographic studies, the factors influencing the phase transformations, the stability of the polymorphs and the kinetics of solid state transitions. Kuhnert-Brandstätter applied a thermo-

microscopic method to investigate the polymorphs of steroids, barbiturates and antihistamines (Kuhnert-Branstätter *et al.* 1961, 1963, 1967). Haleblian *et al.* (1971) used IR spectrophotometry to characterize different solid phases of fluprednisolone and X-ray diffraction to differentiate fluprednisolone polymorphs from fluprednisolone solvates. Behme and coworkers studied three polymorphs of gepirone hydrochloride by DSC, dissolution and solubility (Behme *et al.* 1985). The desolvation of solvated organic crystals, caffeine, theophylline and cycloserine has been studied by Lin and Byrn (1979). The dehydration of crystalline hydrates of ergosterol, dialuric acid and hydrocortisone have been related to their crystal packings (Callow, 1931; Brener, 1969; Clay, 1982). Ampicillin hydrate polymorphs have been investigated by Shefter (1973).

For a compound that undergoes solvent-mediated phase transformation, the stable form resulting from the transformation can be either the unsolvated polymorph or the solvate. Rawe and Anderson (1984) investigated the polymorphism of tolbutamide in an aqueous suspension system. Tolbutamide aqueous suspension was found to thicken to an unpourable state after several weeks of

occasional shaking (prior to daily dosing), due to the partial crystalline conversion of the original plate-like crystals to very fine needle-shaped crystals, which tend to form a highly flocculated structure. The stable tolbutamide crystals were identified as a polymorphic form rather than a solvate or habit change. Pearson and Varney (1969) studied the growth of crystals involving phase transformations in aqueous suspensions with oxyclozanide and theophylline. The growth of oxyclozanide crystals in quiescent suspensions was the result of an isothermal, solvent-mediated phase transition between two unsolvated polymorphs; while theophylline hydrated crystals grew at the expense of the dissolution of the anhydrous form. Water-mediated transformations in protein crystals have been shown by Salunke and coworkers (Salunke *et al.* 1985). The transformations appeared to involve changes in crystal packing as well as conformational transitions in lysozyme, pancreatic ribonuclease A and 2Zn insulin. Carless (1968) demonstrated that the unstable form of cortisone acetate dissolved and the stable hydrated crystals grew in an aqueous suspension by examining the

change in particle size distribution with a coulter counter.

Most of the studies on phase transitions of hydrated compounds in the pharmaceutical literature have focused on the description of the system, identification of the compounds and collection of thermodynamic data. Very few studies deal with the kinetics of the phase transitions. It is the purpose of this work to study the kinetics of solvent-mediated phase transitions using theophylline as a model compound, and to model the transformation process by combining the nucleation and growth kinetics of the stable form and the dissolution kinetics of the metastable form.

1.6.2 : The Kinetics of Solvent-Mediated Phase Transformations

The phase transformation of a hydrated compound in an aqueous system involve two processes : the dissolution of the metastable phase and the formation and growth of the nuclei of the stable phase. The kinetics of such transformations are controlled by the relative rates of dissolution and growth of these two phases, which are dependent on the relative solubility, or the energy, of these two forms. The best way of quantifying the kinetics is through the measurement of the concentration profile in solution during the transformation processes (McEwan and Sadler, 1986). The growth and dissolution rates are determined by the concentration, and correspondingly the concentration is influenced by the growth and dissolution rates.

Consider the phase diagram of a monotropic compound in Figure 1.7, where 2 is the stable phase and 1 is the metastable phase. A solution of composition X_1 at temperature Tx°C, with excess phase 1 crystals present, is saturated with respect to the metastable phase and supersaturated with respect to the stable phase. At this

point crystals of phase 2 could nucleate and grow. This sets the starting point for the transformation process, namely a slurry of phase 1 crystals in contact with the saturated solution containing the nuclei or seeds of the stable phase. As these seeds or nuclei grow, the solution composition falls towards the solubility of phase 2, and hence becomes undersaturated with respect to phase 1. Then phase 1 crystals start to dissolve and produce the supersaturation for the growth of phase 2. This dissolution-growth process continues until all of phase 1 has disappeared and the transformation is complete. The growth of the stable phase continues until the concentration drops to its solubility, with a solution composition at X_2.

The concentration profile during the transformation process is controlled by the following factors : the initial amount and size distribution of each phase (or the surface area of each phase), the solubility of each phase, and the relative dissolution and growth kinetics of each phase.

Further insight into the concentration profile, or the supersaturation profile, during the transformation process is gained by studying the system when the

dissolution and growth are balanced. The mass balance equation can be expressed as,

$$- \frac{dM_1}{dt} = \frac{dM_2}{dt} \tag{1.31}$$

where dM_1 is the decrease of the mass of phase 1, dM_2 is the increase of the mass of phase 2. The solution composition, X, will remain constant during this period and denoted as Xp. Two supersaturation values, S_{12} and Sp, can be defined as follows,

$$S_{12} = \frac{(X_1 - X_2)}{X_2} \tag{1.32}$$

$$S_P = \frac{(X_P - X_2)}{X_2} \tag{1.33}$$

where X_1 and X_2 are the solubility of phase 1 and phase 2, respectively. S_{12} is the initial supersaturation at the beginning of the transformation. When $X = X_P$, the supersaturation, S_P, is referred to as the plateau supersaturation.

By assuming linear dissolution kinetics for the metastable form, parabolic growth kinetics for the stable phase, and constant shape factors for both forms, equation 1.31 becomes,

$$K_d\ (S_{12} - S_p)\ A_1\ f_1\ \sigma_1 \;=\; K_g\ S_p^2\ A_2\ f_2\ \sigma_2 \qquad (1.34)$$

where the subscripts 1 and 2 refer to the metastable and stable phase, respectively. A is the total surface area, f is the shape factor and σ is the density of each phase. K_d and K_g are the rate constants for the dissolution and the growth, respectively. Rearranging equation 1.34 gives the plateau supersaturation as a fraction of S_{12},

$$S_P \;=\; S_{12}\ [(\ 1 + 4\ \theta\ S_{12}\ )^{1/2} - 1\ ]\ /\ 2\theta \qquad (1.35)$$

$$\text{with}\quad \theta \;=\; \frac{K_g\ A_2\ f_2\ \sigma_2}{K_d\ A_1\ f_1\ \sigma_1} \qquad (1.36)$$

This leads qualitatively to an expected trend of the experimental supersaturation-time relationship as shown in Figure 1.8. At the beginning of the transformation the supersaturation is S_{12}, and there is an initial drop

in the supersaturation until the plateau S_p is reached. S_p corresponds to the steady state balance between growth and dissolution. After all of phase 1 has dissolved, S_p can no longer be maintained and the supersaturation drops to zero due to the growth of phase 2 from solution.

The profile of relative supersaturation versus time can be simulated for different ratios of Kd versus Kg, as shown in Figure 1.9. For a growth controlled transformation, where Kg « Kd, the plateau supersaturation is relatively very high and occurs at a very early stage during the transformation; while for a dissolution controlled process, Kd « Kg, the plateau is lower and occurs later. For the transformation process where the growth and dissolution are comparable, the supersaturation profile is controlled by both processes and shows a trend between the above two extremes.

The goal of the present study is : (a) to obtain the supersaturation (concentration) profile for the transformation process from theophylline anhydrous crystals to the monohydrate crystals, and (b) to investigate the kinetics of the transition by incorporating the detailed kinetics of nucleation, growth and dissolution processes.

Figure 1.7 : Typical Phase Diagram for a Monotropic System. Phase 2 is the Stable Form and Phase 1 is the Metastable Form.

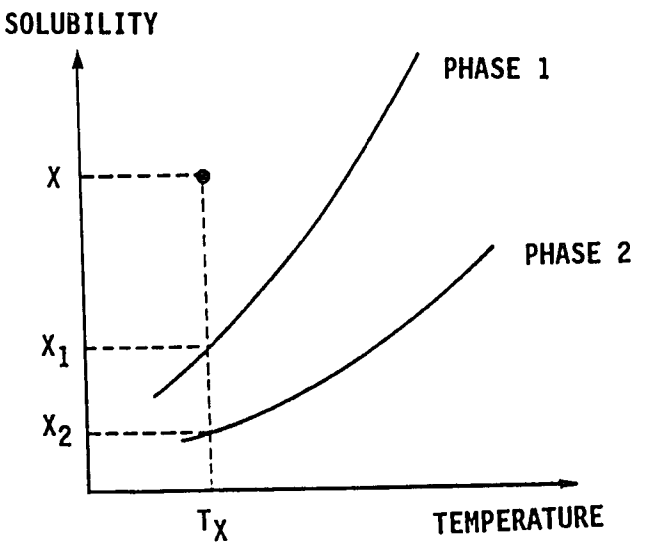

Figure 1.8 : Expected Form of Change in Relative Supersaturation With Time During the Solvent-Mediated Phase Transformation for a One-Dimensional Particle.

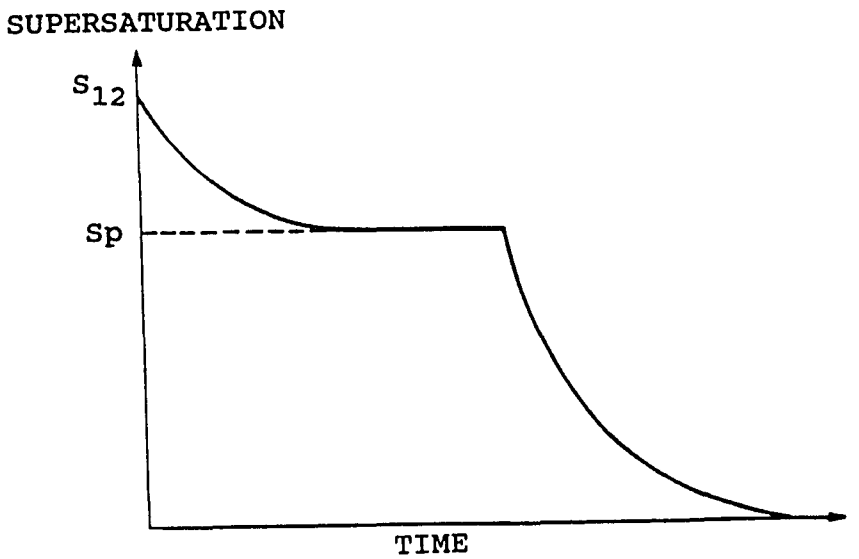

Figure 1.9 : Desupersaturation Profiles for Growth (●) and Dissolution (▲) Controlled Phase Transformations (Davey and Cardew, 1986).

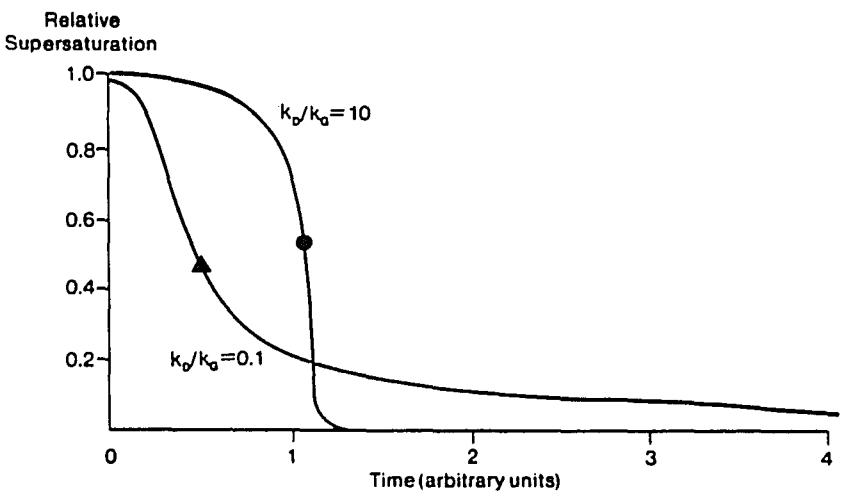

CHAPTER 2

EXPERIMENTAL

2.1 : MATERIALS AND INSTRUMENTS

The materials used in this study were :

(1) Theophylline anhydrous crystals :

Purchased from Sigma Chemical Company (St. Louis, MO). They were dried at 100°C for 24 hours and then cooled to room temperature in a desiccator with Drierite to absorb moisture.

(2) Theophylline monohydrate crystals :

Obtained from recrystallization of theophylline anhydrous crystals from pH 6 Sorensen's phosphate buffer and dried at room temperature overnight, then stored in a tightly closed container at a relative humidity of 60% (DeSmidt, 1986).

(3) Water used in this study was processed through a double deionized purification system (Milli Q Water System) from Millipore Product Company (South San Francisco, CA).

(4) Buffer system :

Sorensen's pH 6 phosphate buffer was prepared from 1/15 molar potassium phosphate monobasic solution and 1/15 molar sodium phosphate dibasic solution. These chemicals were purchased from Aldrich Chemical Company (Milwaukee, Wisconsin). The ionic strength of the buffer was adjusted to 0.15 mole by the addition of potassium chloride.

The instruments used in this study were :

(1) Beckman DU-8 spectrophotometer (Beckman Company, Fullerton, CA) for the assay of theophylline.
(2) pH meter, PHM84, from Radiometer American (Cleveland, Ohio).
(3) Endocal refrigerated circulating bath (RTE-400) from Neslab (Portsmouth, NH) for the control of temperature with an accuracy of ± 0.3°C.
(4) Beckman IR33 (Beckman, Fullerton, CA) for the identification of theophylline anhydrous and monohydrate crystals.
(5) Dupont 1090 Thermal Analyzer (Du Pont Company, Wilmington, DE) for the performing of differential scanning calorimetry (DSC).

(6) Standard testing sieves (CE Tylor Inc.), which meet the American Standard Testing Method (ASTM) requirements, with sieve numbers of 140, 170, 200, 230, and the corresponding sizes of 106 μm, 90 μm, 75 μm and 63 μm, respectively.

(7) Hydraulic press (Fred S. Carver Inc., N.Y.) with an applicable pressure range from 100 lb per square inch to 16000 lb per square inch.

(8) Tablet die with holder for a constant surface area (0.5 inch square) for the experiment to measure the intrinsic dissolution rate.

(9) Magnetic stirrer and one inch Teflon coated stirring bar were used in the disk dissolution experiment. The stirring rate was set at 1500 RPM.

(10) 3 ml syringes for the withdrawal of sample solutions, and Swinney filter units with 0.45 μm Durapore Hydrophilic membrane filter (Millipore Product Company, South San Franciso) for the filtration of the samples.

(11) Elzone 180XY particle counter (Particle Data Labs., Elmhurst, Illinois) with the following features :

a. Jacketed crystallization beaker (250ml).

b. Double bladed glass impeller and stirring motor.

c. 300 μm orifice tube for the measurement of particle size range from 12 μm to 120 μm.
d. This particle counter functions by the electrical conductivity blocking principle, which expresses the diameter of a particle as the diameter of a sphere with an equivalent volume. It can express the size distribution of particles in terms of differential and cumulative distributions on a length, area or volume basis.

2.2 : CALIBRATION OF THE ELZONE 180XY PARTICLE COUNTER

Calibrations of the Elzone 180XY particle counter fitted with a 300 μm orifice tube and a 1 ml manometer were done for pH 6 Sorensen's phosphate buffer with an ionic strength of 0.15, at various theophylline concentrations. The buffer solutions were filtered through 0.45 μm Durapore Hydrophilic membrane filter.

The standards were prepared by suspending particles of known mean size and narrow size distribution in the buffer solution. Two standard particles (polymer latex spheres) with the mean sizes of 19.16 μm and 87.25 μm were used.

The peak of the number versus size distribution of the spheres appeared in different size channels when the current and gain controls were adjusted to different levels. Two points on the scale were thus established at the known sizes and two size channels. These two points, particle mean sizes and the channels in which they appeared, established the calibration at a given current and gain setting. The particle counter interpolated (or extrapolated) between these two points for particles of other size.

There was no difference in the calibrations of the buffers at various theophylline concentrations. This indicated that the presence of theophylline in the buffer did not change the conductivity of the buffer solution. The current and gain were set at 5.5 and 2.0 for the calibration, and the latex spheres at 19.16 μm and 87.25 μm showed at channel 22 and 106.

2.3 : ASSAY AND IDENTIFICATION OF THEOPHYLLINE

2.3.1 : Assay of Theophylline

Theophylline concentration in solution was determined by UV spectrophotometry. The Ultraviolet spectrum of theophylline in 0.1N HCl is shown in Figure 2.1 with a maximum absorption at 270 nm. The wavelength of the maximum absorptivity will shift in solution at different pH values. In order to be consistent, all the necessary dilutions for the assay were performed with 0.1N HCl. The standard curve of theophylline for the assay at 270 nm is shown in Figure 2.2

2.3.2 : Identification of Theophylline

Infrared spectroscopy and thermal analysis were used to identify the anhydrous and the monohydrate forms of theophylline.

(a) Differential scanning calorimetry (DSC).

The DSC thermograms of theophylline monohydrate and anhydrous with a heating rate of 10°C per minute are shown in Figures 2.3a, 2.3b. The DSC of theophylline

monohydrate shows a large endothermic peak from 60°C to 80°C due to the loss of water. The second peak in the thermogram is due to the melting of theophylline anhydrous between 271°C to 274°C.

(b) Infrared spectroscopy.

Due to the O-H bond stretch in water molecules and the interaction between water and theophylline molecules, the IR spectrum of the monohydrate form shows a different pattern from the anhydrous form in the region between 2800 nm to 3800 nm. The IR spectrum for the monohydrate and the anhydrous forms were obtained with potassium bromide disk method in this study and are shown in Figures 2.4a and 2.4b.

Figure 2.1 : Ultraviolet Spectrum of Theophylline in 0.1N HCl.

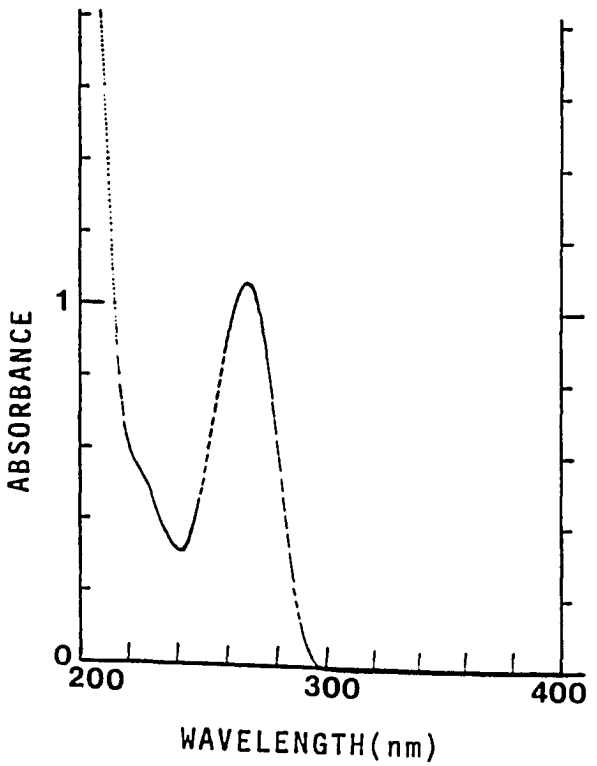

Figure 2.2 : Standard Curve for the Assay of Theophylline at 270nm.

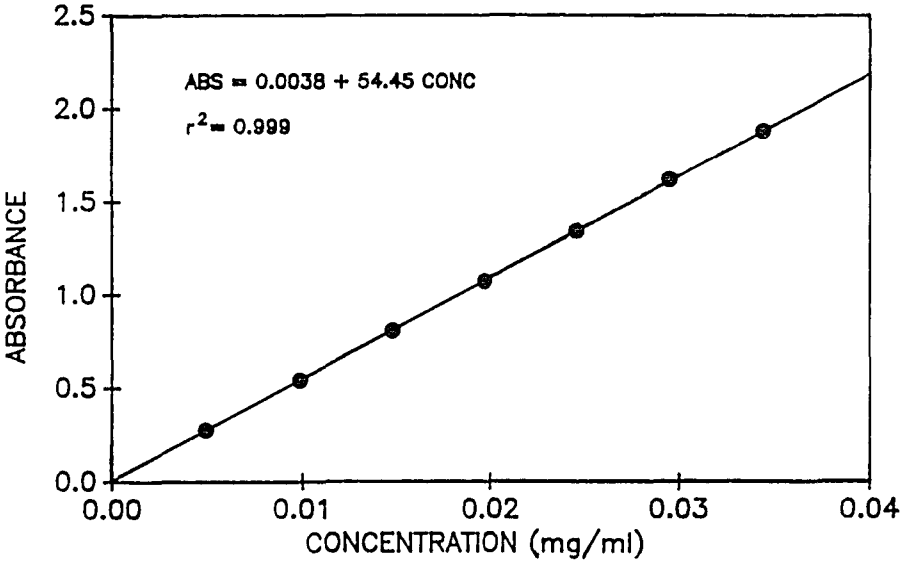

Figure 2.3 : Thermal Analysis of Theophylline. **(A)** DSC for Theophylline Monohydrate, **(B)** DSC for Theophylline Anhydrous.

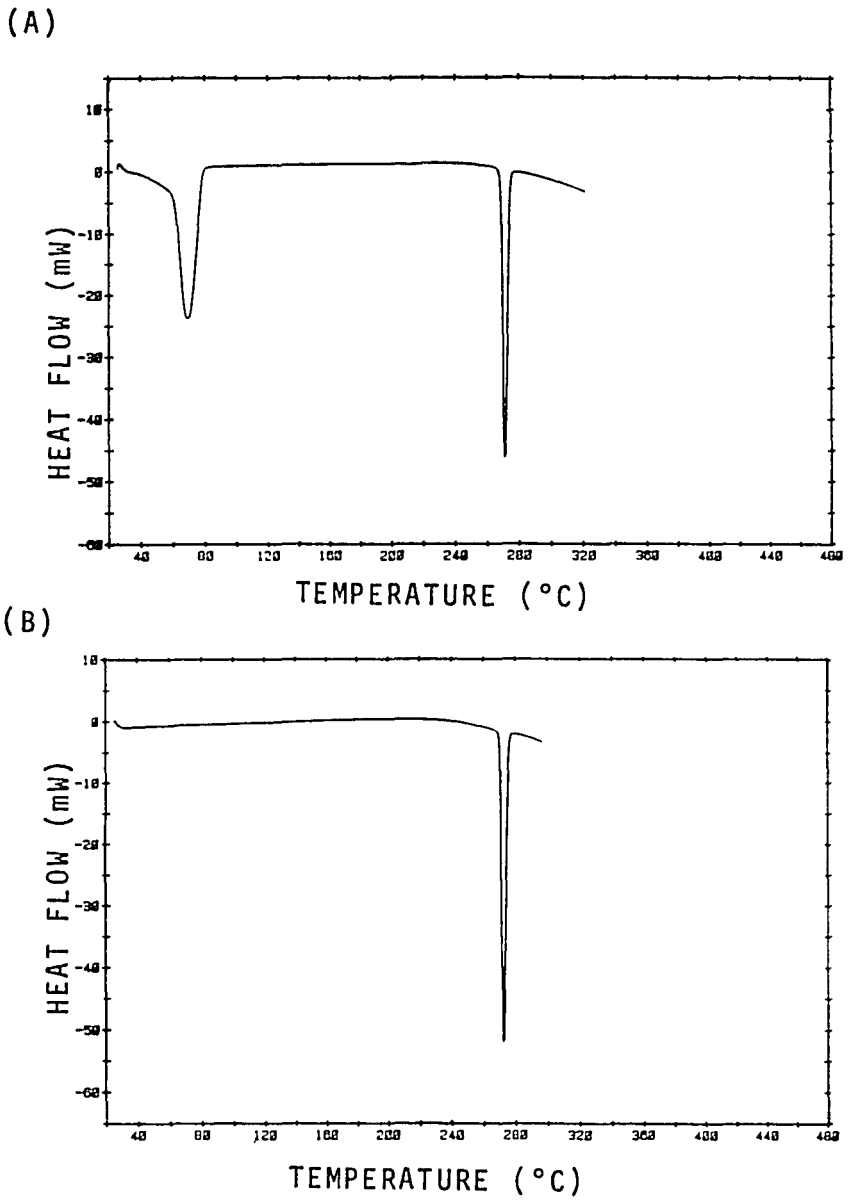

Figure 2.4 : IR Spectrum for **(A)** Theophylline Monohydrate and **(B)** Theophylline Anhydrous.

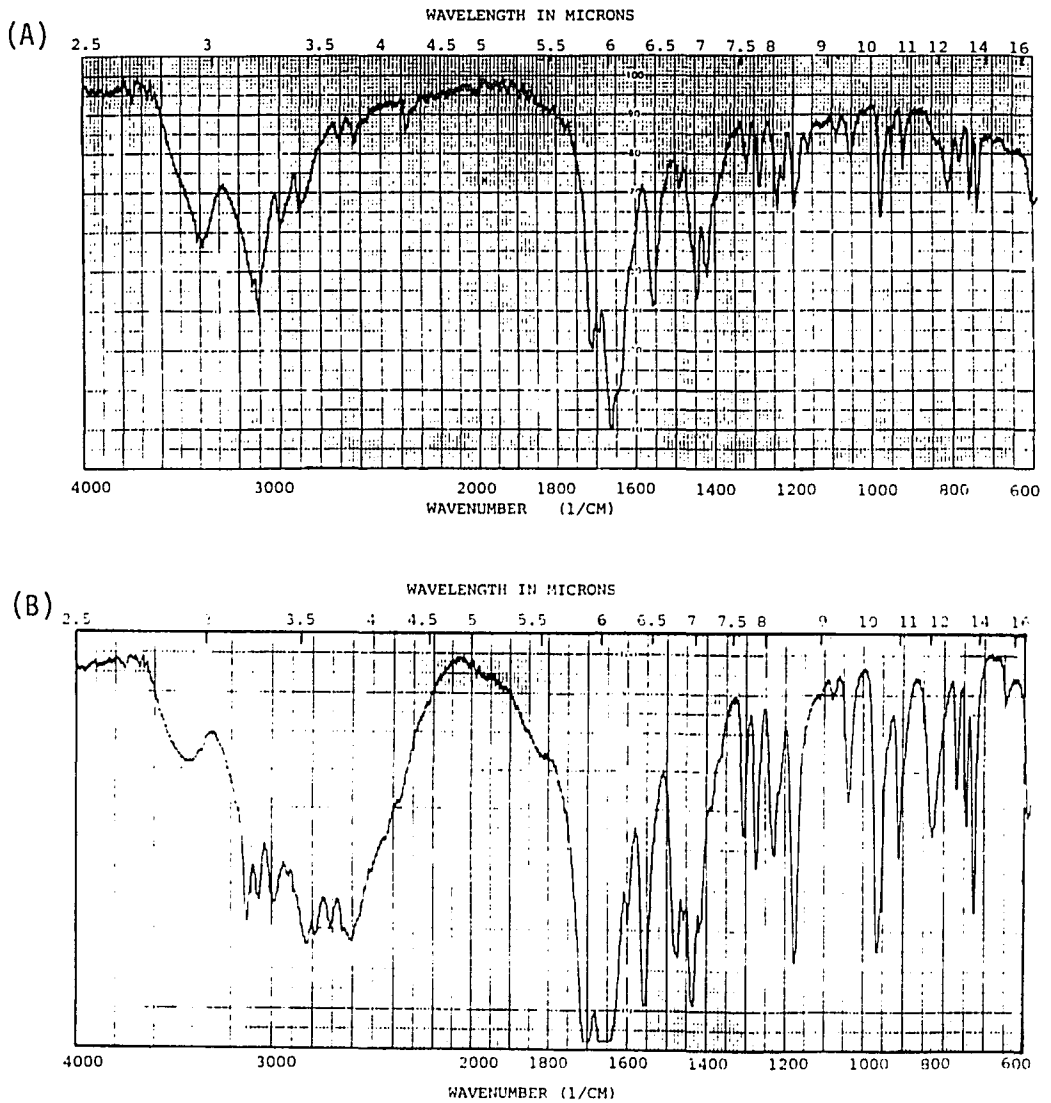

2.4 : SOLUBILITY MEASUREMENT

2.4.1 : Solubility of Theophylline Monohydrate

The solubility of theophylline monohydrate was obtained by approaching equilibrium from supersaturated and undersaturated solutions. For the supersaturation approach, an excess amount of theophylline anhydrous crystals, 2 gm, was stirred in a covered jacketed beaker with 100ml pH 6 Sorensen's phosphate buffer by a magnetic stirrer at 1000 RPM for 24 hours. Theophylline anhydrous crystals transformed into the monohydrate crystals during the process. Two ml samples were withdrawn at various times. The absorbance of each sample was measured by UV spectrophotometry following proper dilution. The experiments were conducted at various temperatures from 8°C to 50°C.

For the undersaturation approach, the monohydrate crystals were added to pH 6 Sorensen's phosphate buffer. The sampling and assay procedures were the same as those in the previous approach.

2.4.2 : Initial Dissolution Rate

The dissolution disk and apparatus are shown in Figure 2.5, which consist of a disk holder, immersed in the dissolution medium (pH 6 Sorensen's phosphate buffer) contained in an 800 ml glass beaker.

The amount of 0.5g anhydrous crystals or monohydrate crystals were compressed at a pressure of 3000 lb/in^2 for 5 minutes in a 0.5 inch diameter die. The die was then placed in a holder and lowered into the dissolution medium. The 400ml dissolution medium had already been equilibrated at the desired temperature and stirred by a magnetic stirrer at 1500 RPM. Two ml aliquots were taken at various times for assay.

The dissolution rates were determined for both theophylline anhydrous and monohydrate at 10.3°C, 17.0°C, 23.3°C and 30.5°C.

Figure 2.5 : Disk Dissolution Apparatus

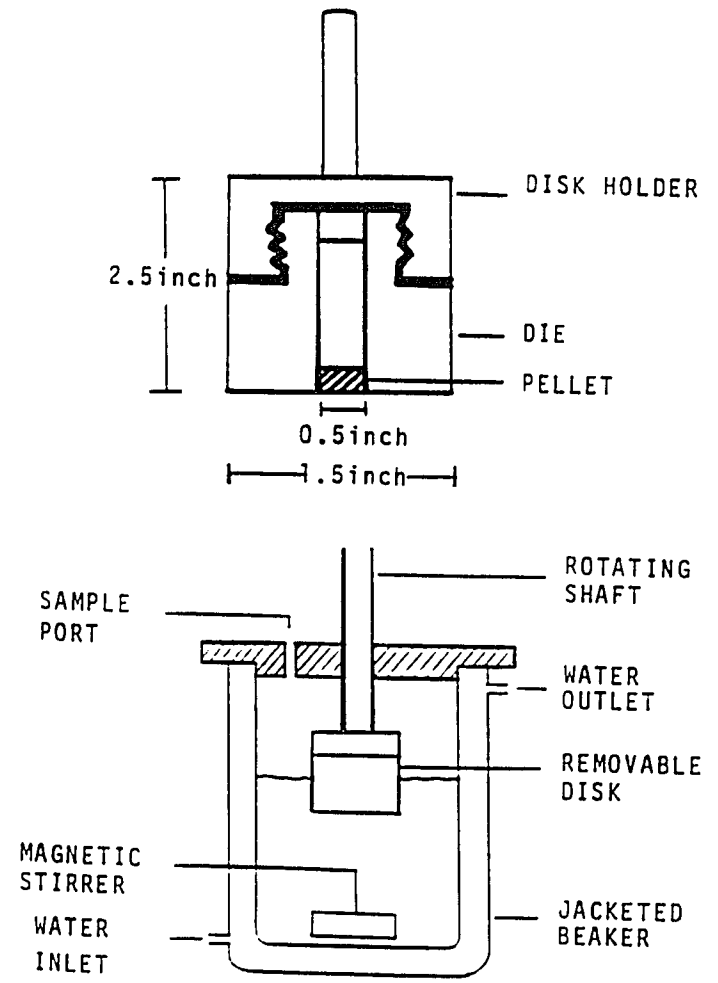

2.5 : PREPARATION OF MONOHYDRATE SEEDS AND ANHYDROUS CRYSTALS

2.5.1 : Preparation of Theophylline Monohydrate Seeds

A pH 6 Sorensen's phosphate buffer saturated with theophylline monohydrate was filtered through a 0.45 μm Durapore membrane filter at 25°C. One Hundred ml of this solution was chilled in an ice bath (10g NaCl in 250 ml ice) with constant stirring. The seed crystals appeared at 8 minutes. After stirring for another 10 minutes, the suspension was filtered through a 0.45 μm Durapore membrane filter. The seeds were resuspended and aged in pH 6 phosphate buffer for a period of two weeks at room temperature. The seeds were identified by IR spectroscopy to be theophylline monohydrate.

The number versus size distribution of the monohydrate seeds was obtained by the Elzone particle counter with a dispersing solution of 200 ml pH 6 Sorensen's phosphate buffer saturated with theophylline monohydrate.

2.5.2 : Theophylline Anhydrous Crystals

Theophylline anhydrous crystals were sieved in Taylor standard sieves. The fraction between 90 μm and 75 μm was used for the present study.

The size distribution of the anhydrous crystals was measured by an Elzone particle counter. The dispersing solution was 200 ml pH 6 phosphate buffer with a theophylline concentration equal to the solubility of the anhydrous form.

2.5.3 : Mass Balance of Theophylline Monohydrate Seeds Anhydrous Crystals

The mass of the solid per volume of suspension of the aged monohydrate seeds and the anhydrous crystals were obtained by the following two methods. (a) By weighing : 5ml of the suspension was filtered and dried to a constant weight at room temperature. (b) From the volume and density terms : the total volume of a known amount of the monohydrate seeds was obtained from the Elzone particle counter, and the mass of the monohydrate

seeds was calculated by multiplying the density of the monohydrate crystals by the volume of the seeds.

2.6 : THE SETUP FOR CRYSTAL GROWTH, DISSOLUTION AND TRANSFORMATION EXPERIMENTS

The setup for the batch crystallization, dissolution and transformation experiments is shown in Figure 2.6. All the experiments were carried out in a jacketed beaker connected to a temperature controlled water bath. A 300 μm orifice tube and a platinum electrode, which were connected to the Elzone particle counter, were immersed in the buffered system for the measurement of the crystal size distribution. The system was stirred with a double bladed glass impeller at various speeds.

Two hundred ml pH 6 Sorensen's phosphate buffer with an ionic strength of 0.15 at various theophylline concentrations was used for each experiment.

Low supersaturation, with respect to theophylline monohydrate, (or high undersaturation with respect to the anhydrous form) was created by a temperature change (cooling). High supersaturation, with respect to the monohydrate form, (or low undersaturation with respect to the anhydrous form), was obtained by both the temperature change and the addition of a small volume of a highly concentrated theophylline solution (60 mg/ml) in 0.1N

NaOH. This did not significantly change the ionic strength and the pH of the system.

The initial concentration of the solution for each experiment was assayed by UV spectrophotometry.

Figure 2.6 : The Setup for Batch Crystallization, Dissolution and Transformation Experiments

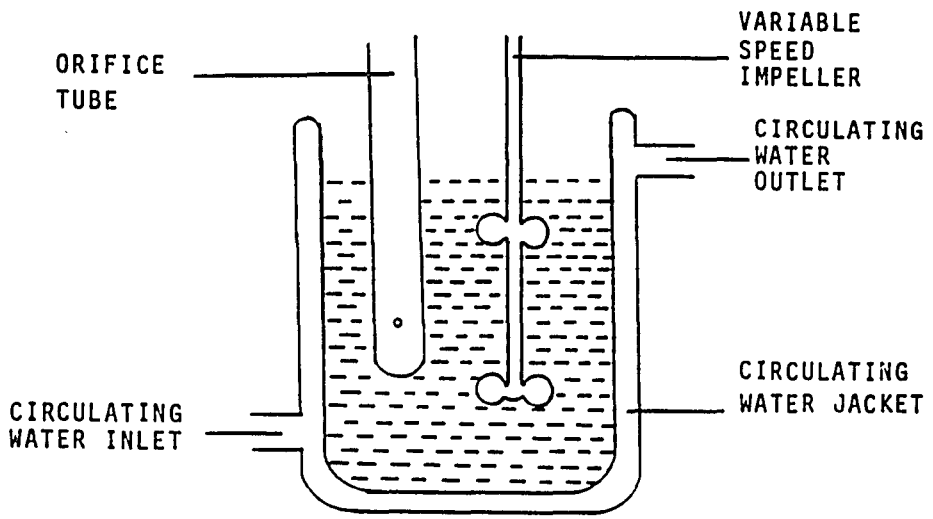

2.7 : GROWTH RATE OF THEOPHYLLINE MONOHYDRATE CRYSTALS

The growth rates of theophylline monohydrate crystals were determined at various degrees of super-saturation, temperatures and stirring rates in a batch crystallization method.

Ten minutes after the solution reached the desired temperature, a 0.5ml aliquot of the monohydrate seeds was introduced. The crystal size distribution and the arithmetic mean size of the crystals as a function of time were obtained. The growth rate was calculated as the increase of the arithmetic mean crystal size per unit time interval.

2.8 : DISSOLUTION RATE OF THEOPHYLLINE ANHYDROUS CRYSTALS

Two hundred ml pH 6 phosphate buffer, with a theophylline concentration which was undersaturated with respect to the anhydrous form, was brought to 10°C in the jacketed beaker. Fifty mg of the sieved theophylline anhydrous crystals were added to the solution and stirred at 750 RPM. The size distribution of the crystals as a function of time was obtained.

The dissolution rates of the crystals calculated as the decrease of the crystal diameter as a function of time (dL/dt, μm/min) from the cumulative number versus size distribution plots were obtained for the crystals at different initial diameters at various undersaturations.

2.9 : PHASE TRANSFORMATION PROCESSES

The experiments for the transformation of theophylline anhydrous crystals to the monohydrate crystals were conducted at 10°C with a stirring rate of 750 RPM.

The initial concentration of the solution was adjusted to the solubility of the anhydrous form. Ten minutes after the solution reached the desired temperature, 5.5g theophylline anhydrous crystals were added to the solution and stirred for 10 seconds, then an aliquot of the monohydrate seeds was added to the slurry and timing started. Two ml samples of solution were taken at different times, and the theophylline concentrations were measured.

The concentration profiles were obtained at a constant amount of theophylline anhydrous, 5.5 g, and by varying the amount of monohydrate seeds, 0%, 0.5% (38mg) and 2% (152mg).

The concentration profile for the growth of 38mg monohydrate seeds in the absence of the anhydrous solid phase was also obtained.

The number versus size distributions of the crystals were monitored and photomicrographs were taken during the

transformation process. The samples at 20 minutes into the transformation were filtered, dried and identified as theophylline monohydrate by IR spectroscopy.

CHAPTER 3

RESULTS AND DISCUSSION

3.1 : SOLUBILITY

3.1.1 : Solubility of Theophylline Monohydrate

The typical concentration versus time profiles for theophylline monohydrate obtained by dissolving the anhydrous and the monohydrate forms at 23°C are shown in Figure 3.1. The system reached equilibrium very rapidly.

Due to the high solubility of the anhydrous form, the concentration of theophylline in solution rose very fast and reached a high value within 3 minutes by dissolving the anhydrous form. The high concentration achieved was supersaturated with respect to the monohydrate form. Then the monohydrate crystals nucleated and grew, and brought the concentration gradually down to the solubility of the monohydrate form.

For the experiment where the dissolution of the monohydrate form was examined, the concentration of

theophylline increased gradually and reached the solubility of the monohydrate form.

The solubility of the monohydrate form obtained from these two methods are in good agreement. The solubilities of theophylline monohydrate at various temperatures are shown in Table 3.1. The temperature dependence of the solubility follows the Van't Hoff equation as shown in Figure 3.2 and equation 3.1,

$$\log C_{SH} = -1715 \left(\frac{1}{T}\right) + 6.53 \qquad (3.1)$$

$$n = 13, \qquad r^2 = 0.995$$

where C_{SH} is the solubility of the monohydrate form in mg/ml and T is the absolute temperature.

3.1.2 : Estimation of the Solubility of Theophylline Anhydrous From Initial Dissolution Rate

The concentration versus time profiles obtained from the disk dissolution method for both the monohydrate and the anhydrous forms at 10°C and 23°C are shown in Figures 3.3a and 3.3b. The concentration of theophylline in the dissolution medium increases linearly with time for the monohydrate form.

There is a transition point in the dissolution profile of the anhydrous form. The rate of the increase of theophylline concentration in the dissolution medium is faster during the first 6 minutes, then the rate slows down gradually and parallels that of the monohydrate form. This phenomena can be explained by the gradual transition of the metastable anhydrous form to the stable monohydrate form at the surface of the disk (Desmidt, 1986).

The initial dissolution rate is obtained from the initial slope (dC/dt) of the concentration versus time profile. The initial dissolution rates for both forms at various temperatures are shown in Table 3.2.

By knowing the value of the solubility of the monohydrate form and the initial dissolution rates of both forms, the solubility of the anhydrous form at a given temperature is calculated from equation 3.2,

$$C_{SA} = \frac{IDR_A}{IDR_H} C_{SH} \qquad (3.2)$$

where C_{SA} and C_{SH} are the solubilities (mg/ml) of the anhydrous and the monohydrate forms, respectively. IDR_A and IDR_H are the initial dissolution rates (mg/ml/min) of the anhydrous and the monohydrate forms, respectively. The solubilities of the anhydrous form at various temperatures are shown in Table 3.1. The temperature dependence of the solubility is shown in Figure 3.2, and can be expressed by equation 3.3,

$$\log C_{SA} = -834 \left(\frac{1}{T}\right) + 3.88 \qquad (3.3)$$

$$n = 4, \quad r^2 = 0.976$$

where C_{SA} is the solubility of the anhydrous form in mg/ml, and T is the absolute temperature.

3.1.3 : Thermodynamic Parameters for Theophylline

The temperature dependence of the initial dissolution rate of theophylline anhydrous and monohydrate forms are shown in Figure 3.4 and equations 3.4 and 3.5,

$$\log IDR_H = -2680 \left(\frac{1}{T}\right) + 6.58 \qquad (3.4)$$

$$n = 4, \quad r^2 = 0.999$$

$$\log IDR_A = -1802 \left(\frac{1}{T}\right) + 3.95 \qquad (3.5)$$

$$n = 4, \quad r^2 = 0.994$$

Where IDR_H and IDR_A represent the initial dissolution rates (mg/ml/min) of the monohydrate and anhydrous forms. T is the absolute temperature. Both systems follow Arrhenius behavior.

The heat of dissolution, ΔH_{diss}, for each form can be calculated from equation 3.6, with the corresponding slope from equation 3.4 or 3.5.

$$\Delta H_{diss} = -2.3\ R \cdot slope \qquad (3.6)$$

The transition temperature, which is the intercept of the two lines in Figure 3.4, is calculated to be 60.0°C. The enthalpy of the transition (ΔH_{trans}), determined from the difference of the heat of dissolution of these two forms, is listed in Table 3.3 along with the data from the literature (Shefter and Higuchi, 1963; Wadke and Reier, 1972). The free energy (ΔG_T) and entropy (ΔS_T) of the transition at 25°C are calculated from equations 1.9 and 1.10, respectively, and are listed in Table 3.3.

The heat of solution of the anhydrous form (ΔH_{SA}) and the monohydrate form (ΔH_{SH}) are determined from equation 1.7 with the respective solubility versus temperature data. The activation energy of the diffusion process (Ea in equation 1.6) is calculated by subtracting the value of the heat of solution from the value of the heat of dissolution, and calculated to be 4.4 kcal/mole for theophylline in this study.

3.1.4 : Comparison with Literature Results and Discussion

Higuchi (1963) and Reier (1972) investigated the dissolution behavior of theophylline anhydrous and monohydrate. The thermodynamic parameters obtained from their investigations are listed in Table 3.3.

As mentioned by the above authors, the higher dissolution rate of theophylline anhydrous was not only a contribution from the higher solubility of the anhydrous form, but also was a result of the geometric factors. The effective surface area, in terms of number of molecules exposed per unit area, is different for these two solid states of theophylline. Thus, in equation 1.5, the constant K_A which incorporates an area term, would not be the same for these two crystalline forms. The dissolution data should be expressed in terms of the effective surface area.

One way to correct for the difference in the surface area is to divide the observed dissolution rate by the respective density of each form with the assumption that there is no significant difference in the densities of the compressed tablets and crystals, and the densities

are independent of the temperatures under investigation. The densities for the anhydrous and the monohydrate crystals are 1.44g/ml and 1.52g/ml, respectively (Suter, 1958, Nagvi, 1981). The thermodynamic parameters obtained in this study are corrected for the geometric factor according to the method mentioned above and are listed in Table 3.3.

There are substantial differences in some of the parameters obtained in the present study compared to the literature data even after the correction. In the present study, the transition temperature is 10°C lower than the one reported in previous work, and the heats of solution for both forms and the entropy of transition are also lower.

The major experimental difference between the previous and the present studies is the dissolution medium used. pH 6 phosphate buffer with an ionic strength of 0.15 was used in the present study; whereas, water was used in other studies. The pH values of water and theophylline saturated water are 5.6 and 5.3, respectively. With a pKa value of 8.6 (Cohen, 1975), theophylline exists as unionized molecules in water and pH 6 buffer. Therefore, the difference in the pH value

of the dissolution medium cannot explain the difference in the solubilities and other thermodynamic parameters.

It has been shown that the solubility of theophylline will be altered in the presence of several inorganic salts (Cohen, 1975). For example, NaI, KI, NaSCN will increase the solubility while NaCl, KCl, Na_2SO_4 decrease it. The change in the solubility can be attributed to salt formation as well as hydrophobic interactions (Leuallen, 1949). It is expected that the ionic strength and the electrolytes present in the solution will influence the solubility, transition temperature and other thermodynamic parameters of theophylline.

Figure 3.5 compares the solubilities of theophylline monohydrate and anhydrous obtained from Higuchi (1963), Reier (1972) and the present study. It is clear that the transition temperature is lower in the phosphate buffer.

The study of the kinetics of the transformation process was done at 10°C in the present study, where the differences in solubilities would have a significant influence on the interpretation of the kinetic data.

Figure 3.1 : Concentration versus Time Profile for the Determination of Theophylline Monohydrate Solubility by the Equilibrium Method at 23°C

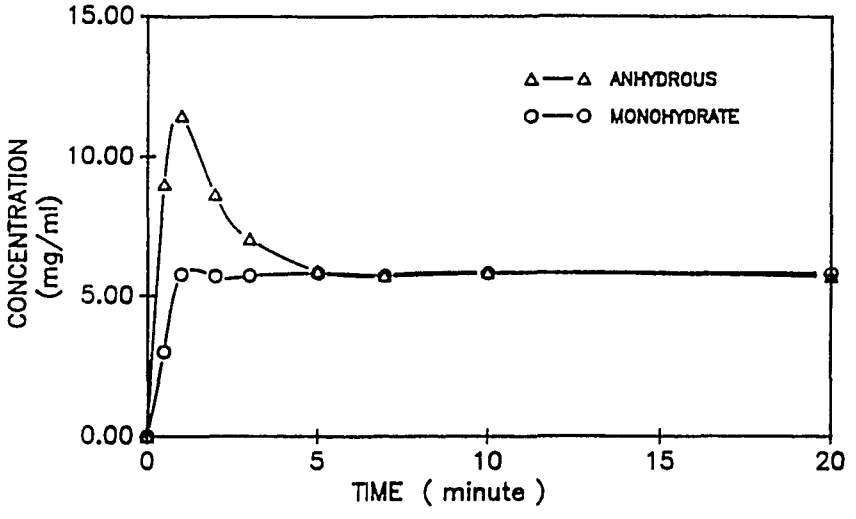

Figure 3.2 : Solubility-Temperature Dependence of Theophylline Monohydrate and Anhydrous.

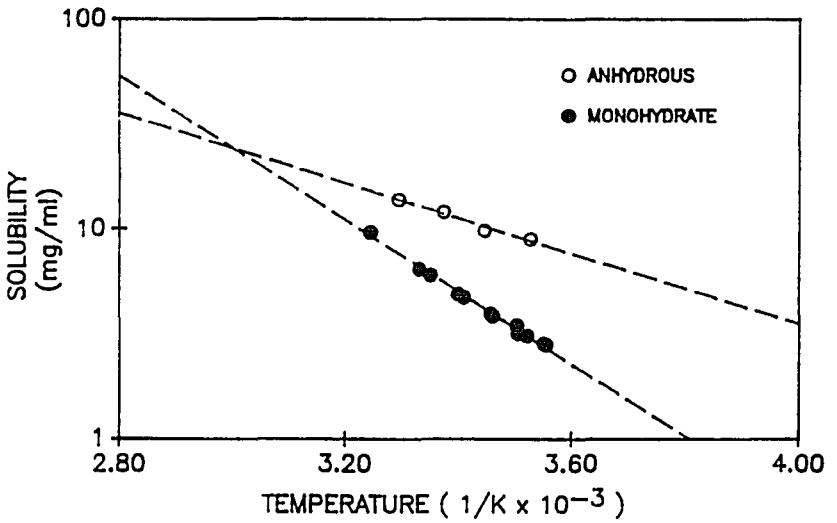

Figure 3.3 : Concentration Versus Time Profile for Disk Dissolution of Theophylline Monohydrate and Anhydrous at **(A)** 23°C and **(B)** 10°C.

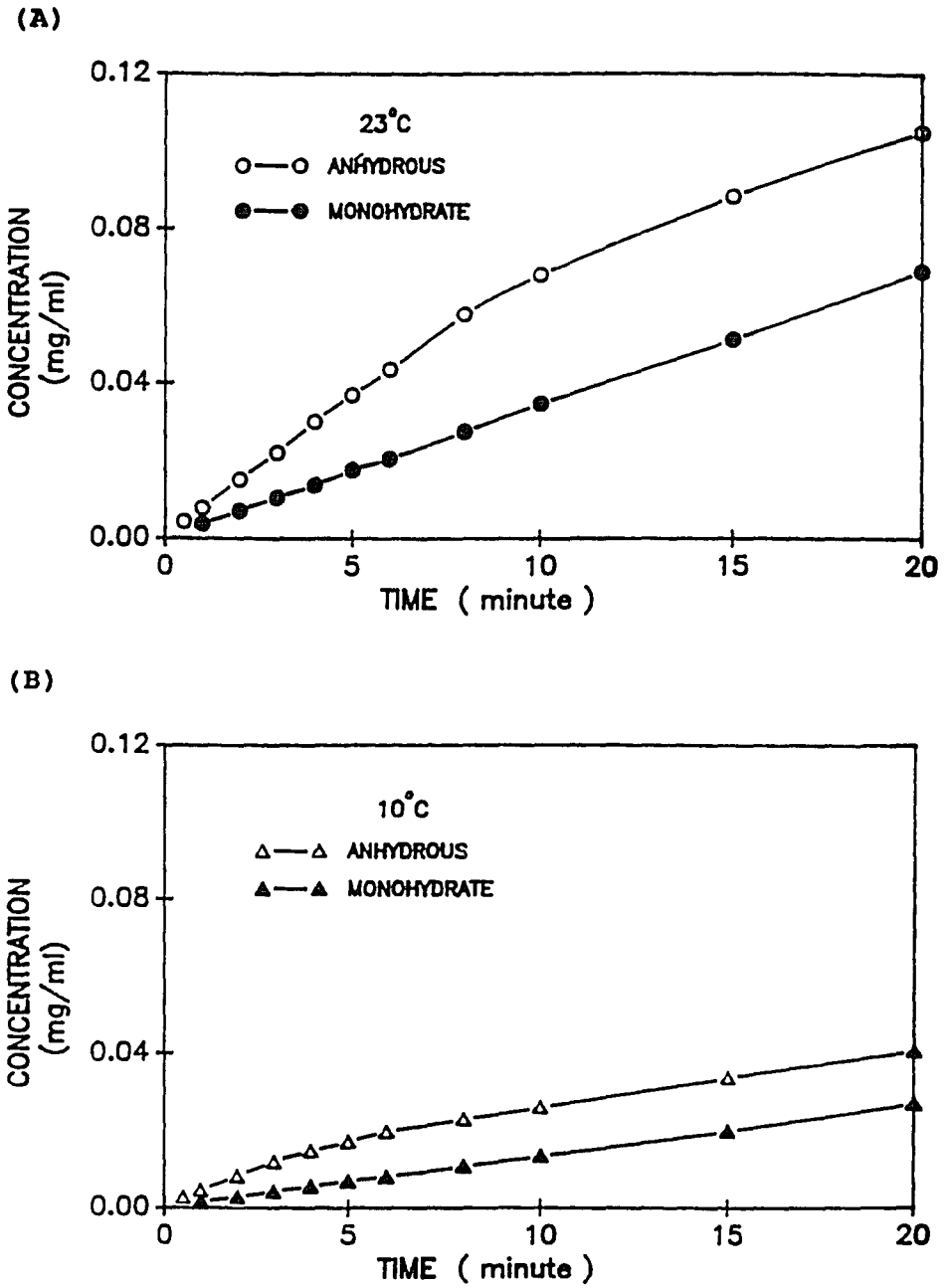

Figure 3.4 : The Dependence of Dissolution Rate on Temperature for Theophylline Monohydrate and Anhydrous.

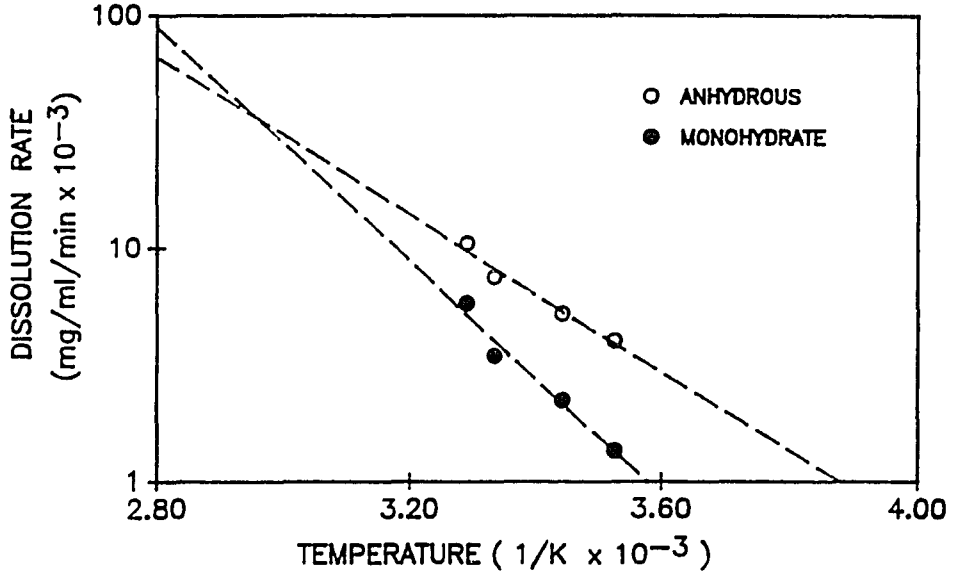

Figure 3.5 : Solubility-Temperature Dependence of Theophylline in water (—— Anhydrous,— — Monohydrate; Higuchi, 1963) and Phosphate Buffer with an Ionic Strength of 0.15 (Δ Anhydrous, ▲ Monohydrate).

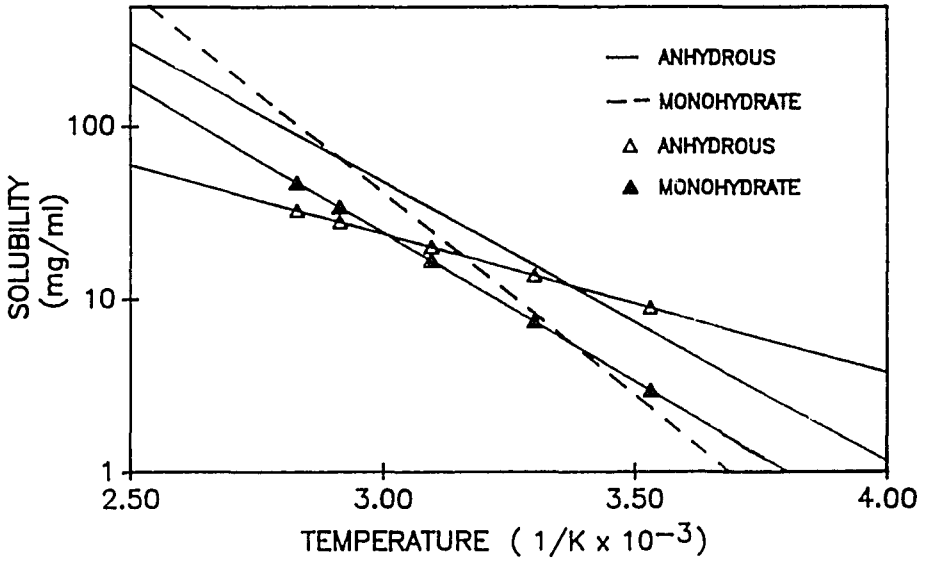

TABLE 3.1 : Solubilities of Theophylline in pH 6 Phosphate Buffer at Various Temperatures

	Solubility (mg/ml)	
Temperature(°C)	Monohydrate	Anhydrous
8.1	2.78	
8.4	2.81	
10.3	3.00	8.91
10.8	3.08	
12.1	3.15	
12.3	3.44	
15.8	3.83	
16.1	3.91	
17.0	4.14	9.78
20.2	4.68	
21.1	4.85	
23.3	5.52	12.01
25.3	5.95	
27.1	6.33	
30.5	7.58	13.71
35.1	9.56	

TABLE 3.2 : Initial Dissolution Rates of Theophylline in pH 6 Phosphate Buffer at Various Temperatures

	Initial dissolution rate (dC/dt, $\mu g\ ml^{-1}\ min^{-1}$)	
Temperature(°C)	Monohydrate	Anhydrous
10.3	1.3	4.0
17.0	2.2	5.2
23.3	3.4	7.5
30.5	5.8	10.4

Table 3.3 : Calculated Thermodynamic Parameters for Theophylline Anhydrous and Monohydrate

Parameter	Present study	Ref.1[a]	Ref.2[b]
Transition Temp.(°C)	59.8 63.2[c]	73.0	69.7 73.6[c]
ΔH_{SA} (kcal/mole)	3.7	7.4	
ΔH_{SH} (kcal/mole)	7.9	10.7	
E_a (kcal/mole) (Diffusion)	4.4		2.9
ΔH_{dissA} (kcal/mole)	8.3		10.3
ΔH_{dissH} (kcal/mole)	12.3		13.4
ΔH_{trans} (kcal/mole)	-4.0	-3.3	-3.1
ΔG_T (cal/mole, 25°C)	-423 -455[c]	-410	-355 -411[c]
ΔS_T e.s.u. (25°C)	-12.6 -12.5[c]	-10.0	-9.2 -9.0[c]

a: Shefter E. and Higuchi T., *J.Pharm.Sci.*, **52**, 781, 1963.
b: Wadke A. and Reier E., *J.Pharm.Sci.*, **61**, 869, 1972.
c: corrected for geometric factor.

3.2 : THEOPHYLLINE MONOHYDRATE SEEDS AND ANHYDROUS CRYSTALS

Crystal size distribution (CSD) of theophylline monohydrate seeds, shown in Figure 3.6a, can be approximated by a log normal distribution with an arithmetic mean of 22.5 μm and standard deviation of 4.6 μm. The seed suspension contains 76mg monohydrate crystals in one milliliter. The mass of the monohydrate seeds obtained from multiplying volume by density is within 10% error of the mass obtained from weighing.

The CSD of the anhydrous crystals is shown in Figure 3.6b. The mass of the anhydrous crystals obtained from weighing and from the volume and density terms agree with each other within 10% error.

Figure 3.6 : Crystal Size Distributions for
(A) Theophylline Monohydrate Seeds and
(B) Theophylline Anhydrous Crystals.

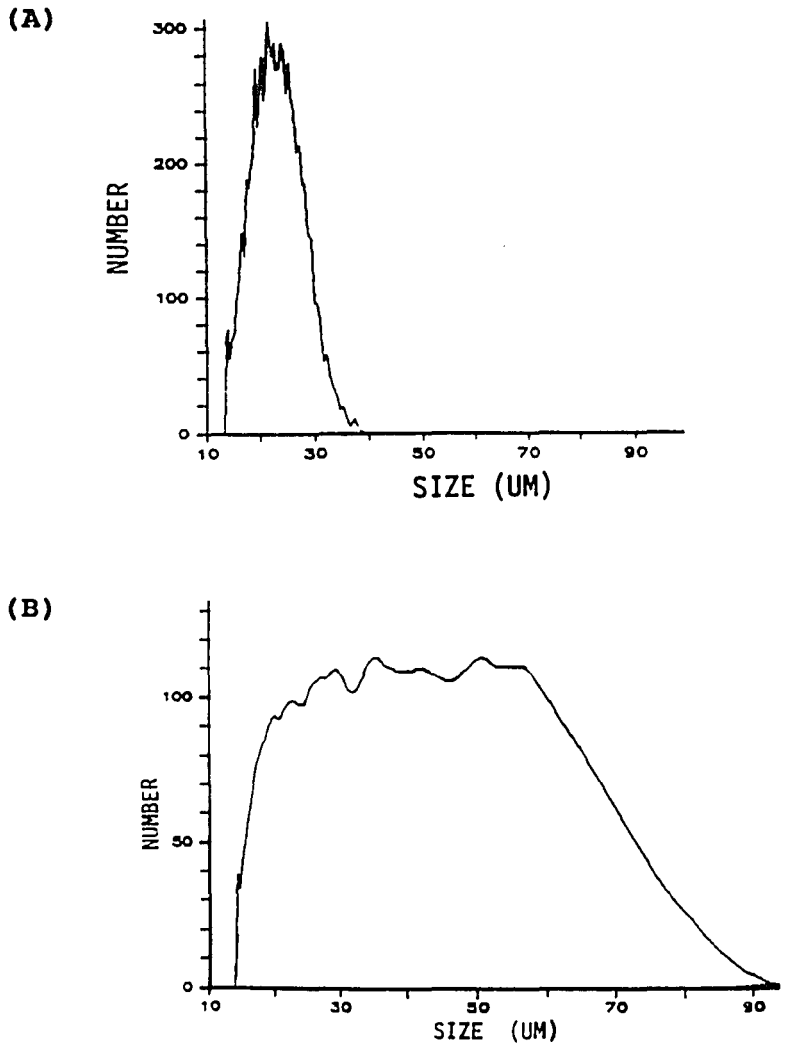

3.3 : GROWTH KINETICS OF THEOPHYLLINE MONOHYDRATE

3.3.1 : Evaluation of Growth Rate and Supersaturation

Figure 3.7a shows the crystal size distribution as a function of time with a supersaturation of 0.48 at 20°C; Figure 3.7b shows that the corresponding cumulative crystal size distribution shifts towards large size as the crystals grow. The cumulative curves parallel each other, so the McCabe's ΔL law (McCabe, 1929) is valid in the present study. McCabe's ΔL law states that the growth rate is independent of the particle size.

Since McCabe's ΔL law is valid, the growth rate of the monohydrate crystals can be expressed as the increase of the arithmetic mean particle size as a function of time, as shown in equation 3.7,

$$G = \frac{dLm}{dt} \qquad (3.7)$$

where G is the growth rate (μm/min), dLm is the change in the mean particle size during the time interval dt. A typical plot of mean size versus time at various initial

supersaturations is shown in Figure 3.8. The initial growth rate is obtained from the initial slope of each curve. The data of the mean size as a function of time and the growth rate calculated for each experiment are summarized in Appendix II.

The supersaturation, S, is expressed as,

$$S = \frac{(C - C_{SH})}{C_{SH}} \qquad (3.8)$$

where C is the concentration of theophylline in the solution (mmole/ml), and C_{SH} is the solubility of theophylline monohydrate at the given temperature.

The change in the supersaturation in the first few minutes of each experiment is negligible, so the initial growth rate corresponds to the initial supersaturation for each experiment.

The growth rates obtained at various supersaturations and temperatures at a stirring rate of 750 RPM are listed in Table 3.4. The range of the initial supersaturation used is from 0.2 to 0.5 for 20°C, 30°C and 40°C, and from 0.2 to 2 for 10°C. The linear and logarithmic plots of the growth rate versus super-

saturation at 10°C are shown in Figures 3.9a and 3.9b. The plots of growth rate versus supersaturation at various temperatures are shown in Figure 3.10a and the corresponding logarithmic plot is shown in Figure 3.10b.

Figure 3.7 : Crystal Size Distribution as a Function of Time for (A) Differential Distribution, and (B) Cumulative Distribution at a Supersaturation of 0.48 at 20°C.

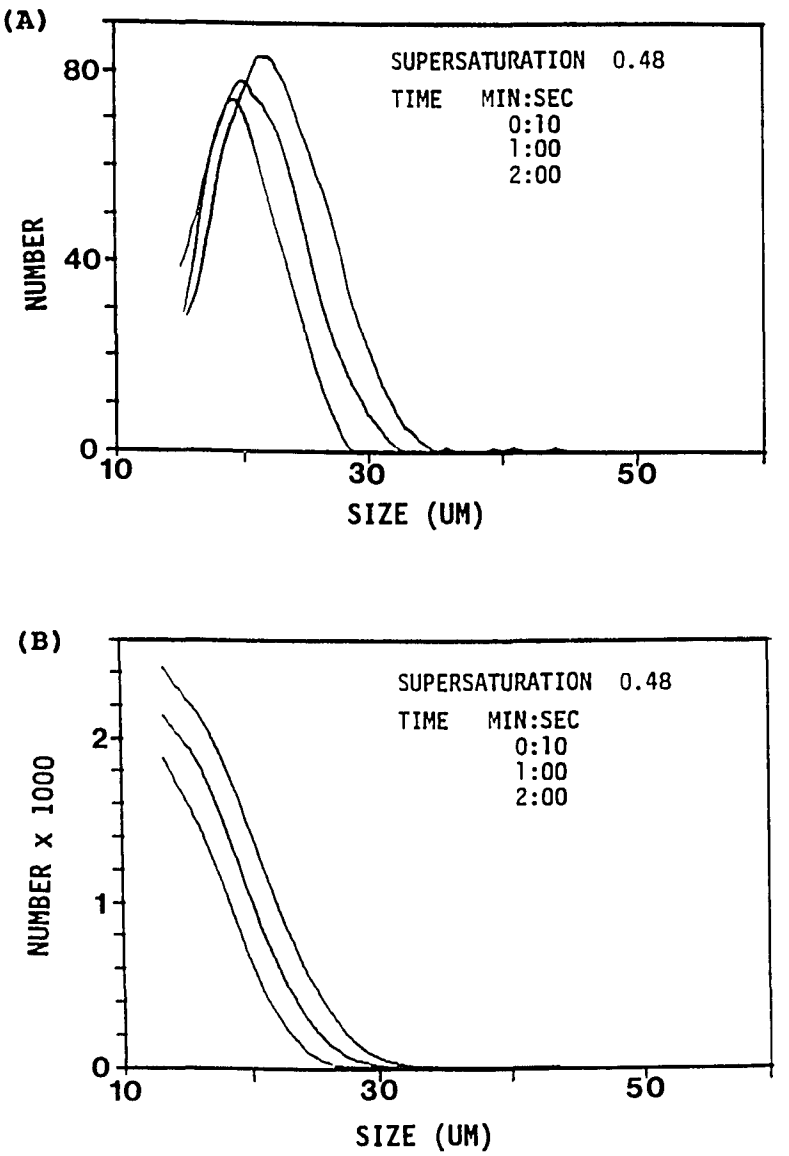

Figure 3.8 : Mean Crystal Size as a Function of Time for Theophylline Monohydrate at Various Initial Supersaturations at 20°C

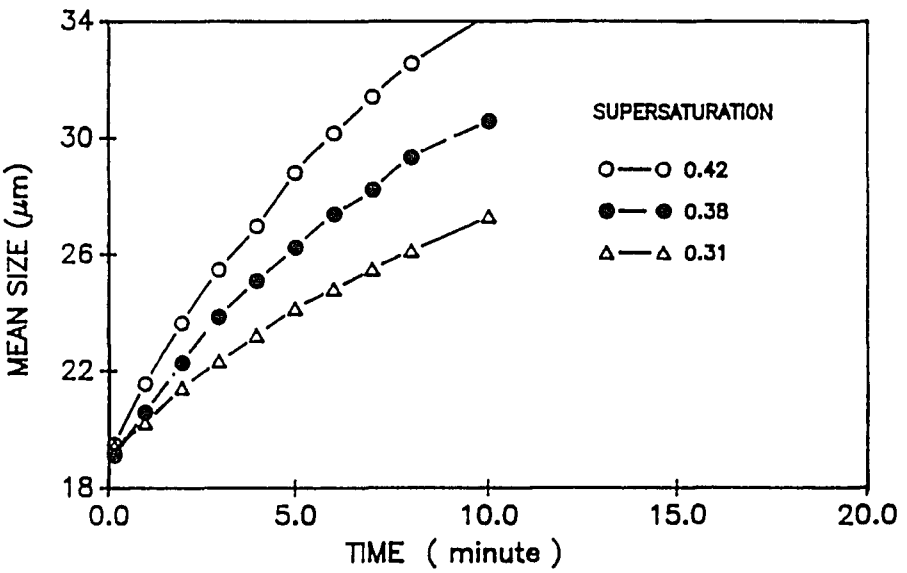

Figure 3.9 : Growth Rate Versus Supersaturation at 10°C. (A) Linear Plot, and (B) Logarithmic Plot.

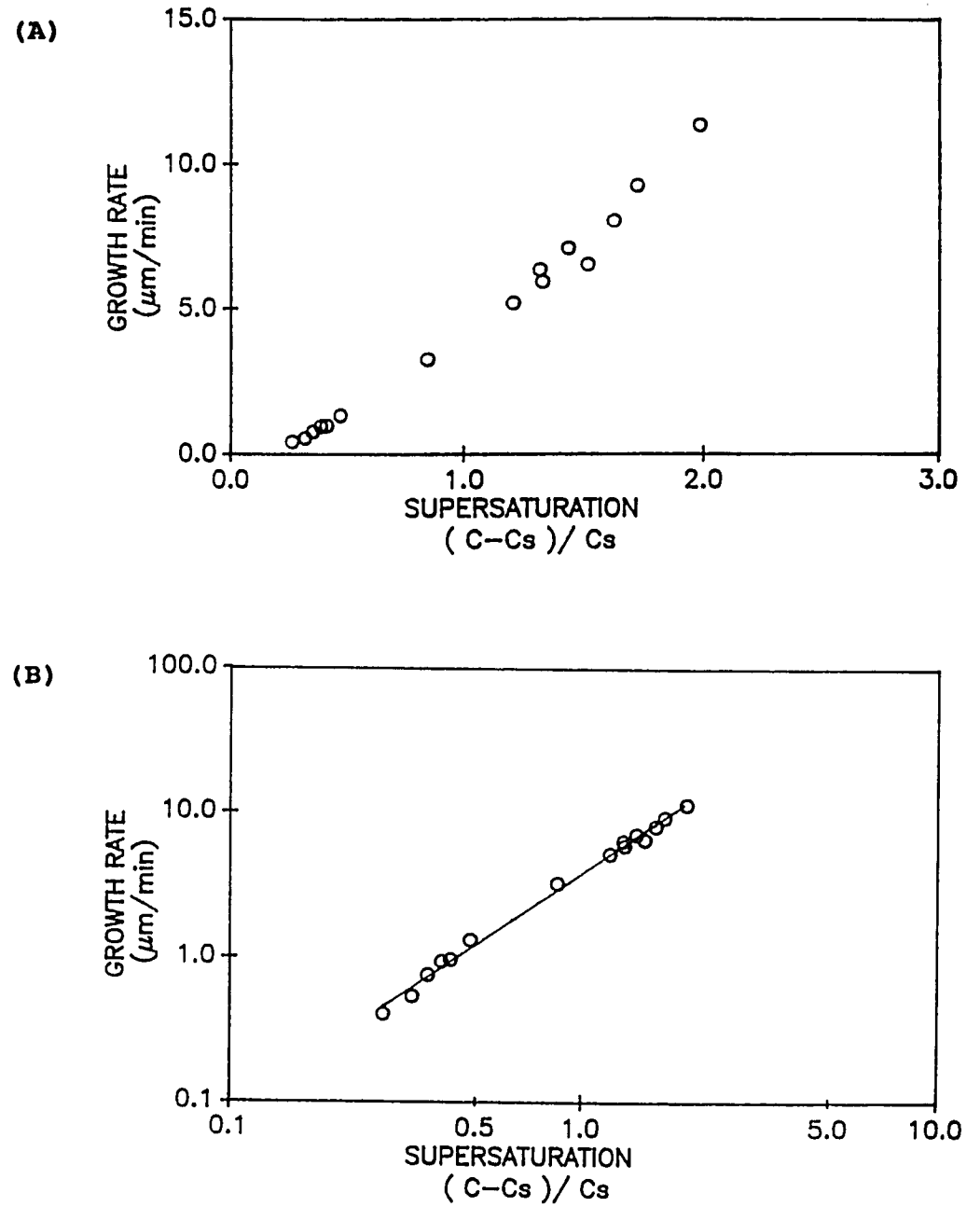

Figure 3.10 : Growth Rate Versus Supersaturation at Various Temperatures. **(A)** Linear Plot, and **(B)** Logarithmic Plot.

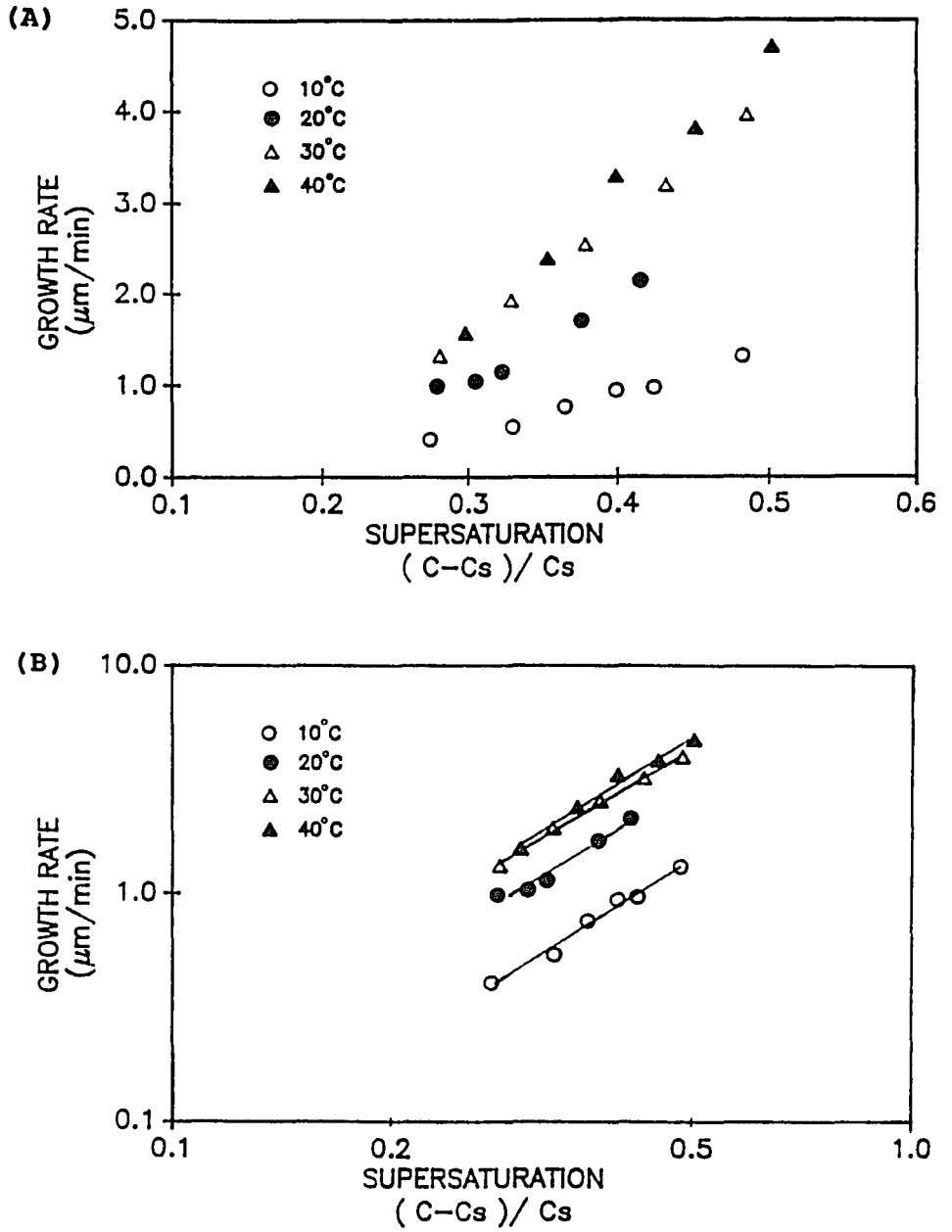

Table 3.4 : Growth Rate of Theophylline Monohydrate at Various Supersaturations and Temperatures in pH 6 Phosphate Buffer.

TEMPERATURE (°C)	SUPERSATURATION (C-Cs)/Cs	GROWTH RATE G (μM/MIN)
40.0	0.30	1.6
40.0	0.35	2.4
40.0	0.40	3.3
40.0	0.45	3.8
40.0	0.50	4.7
30.0	0.28	1.3
30.0	0.33	1.9
30.0	0.38	2.5
30.0	0.43	3.2
30.0	0.48	4.0
20.0	0.28	1.0
20.0	0.30	1.0
20.0	0.32	1.2
20.0	0.38	1.7
20.0	0.42	2.1
10.0	0.27	0.4
10.0	0.33	0.6
10.0	0.36	0.8
10.0	0.40	0.9
10.0	0.42	1.0
10.0	0.48	1.3
10.0	0.85	3.4
10.0	1.20	5.2
10.0	1.31	6.3
10.0	1.32	6.0
10.0	1.43	7.1
10.0	1.51	6.5
10.0	1.62	8.0
10.0	1.72	9.3
10.0	1.98	11.3

3.3.1 : Growth Models

The growth data were fitted to the following models, (a) exponential model, (b) BCF model,and (c) birth and spread model by a nonlinear regression program with the simplex algorithm and least square criterion. The diffusion model was fitted by linear regression. The equations for the models mentioned above are summarized here according to the order they are mentioned.

$$G = K_g S^a \tag{1.27}$$

$$G = \frac{K_1}{K_2} S \, ln(1+S) \tanh\left(\frac{K_2}{ln(1+S)}\right) \tag{1.20}$$

$$G = A S^P e^{(-B/S)} \tag{1.16}$$

$$G = K S \tag{1.14}$$

The results of the regression for the exponential model at various temperatures are included in Table 3.5. The average value of the exponent **a** is found to be 1.9 (±0.2) from 10°C to 40°C. This indicates that the growth process is not transport limited but may be surface controlled (Durbin and Feher, 1986).

Values of the parameters evaluated for the birth and spread model, BCF model and the diffusion model are shown in Table 3.6. The fitted curves for all the models are shown in Figure 3.11.

It is clear from Table 3.6 and the fitted curves that the diffusion model is not suitable to describe the growth process.

Both the BCF and birth and spread models fit the experimental data pretty well in this study. Due to the small supersaturation range used in this study, it is difficult to discriminate between these two models from the fitted curves. To be able to discriminate between these two models, we should do the growth experiment at a higher and lower supersaturation, however, such an approach presents some practical difficulties. At very high supersaturation, bulk nucleation occurs; while accuracy is limited at very low supersaturation. Discrimination between the BCF model and the birth and spread model is extremely difficult based on the experimental growth rate-supersaturation data only. Previous investigations by Garside (1975) and Bourne (1976) have also noted this limitation.

However, the exponential growth model fit the data very well with the **a** value of 2 from 10°C to 40°C in the present study. Although this relation is not a result of a detailed theory, it is generally assumed that for screw dislocation growth, **a** = 2, while **a** > 2 is taken to indicate surface nucleation (Nelson, 1984). From the supersaturation range used in the present study and the above argument, the growth of theophylline monohydrate in the present study may belong to the BCF model.

Figure 3.11 : Growth Rate Data of Theophylline Monohydrate Fitted by Different Growth Models at **(A)** 10°C, **(B)** 20°C, **(C)** 30°C, and **(D)** 40°C.

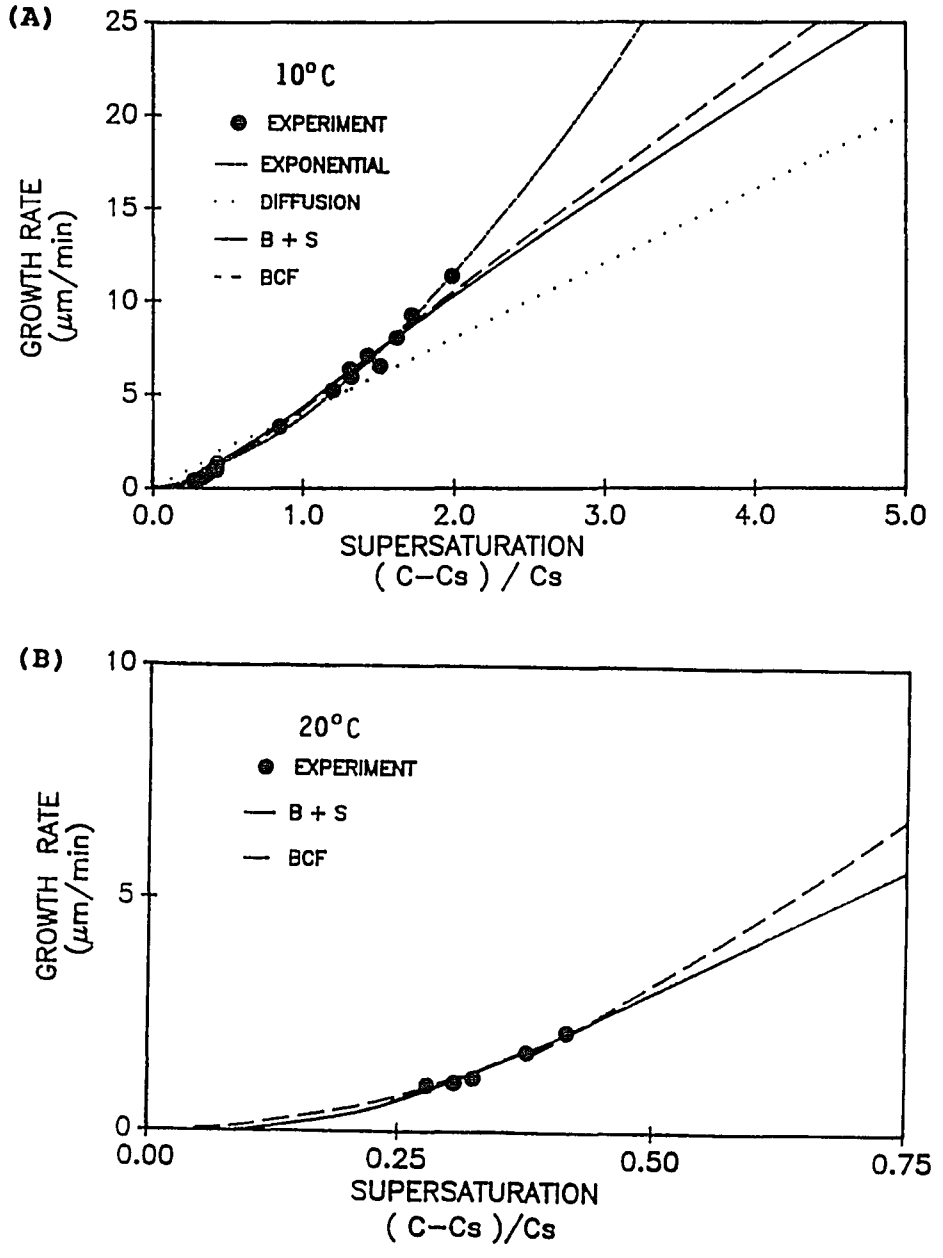

Figure 3.11 : Continued.

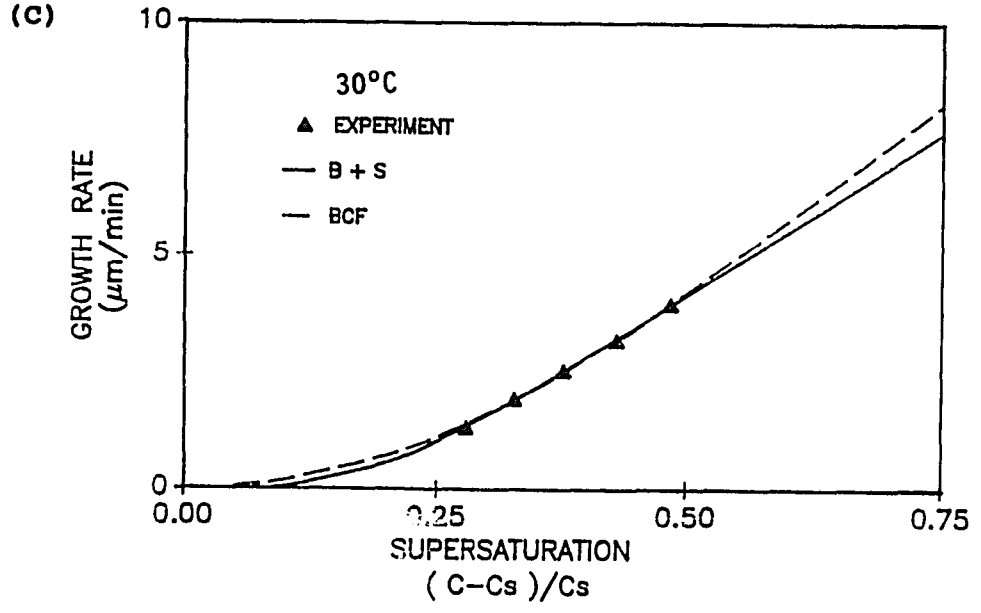

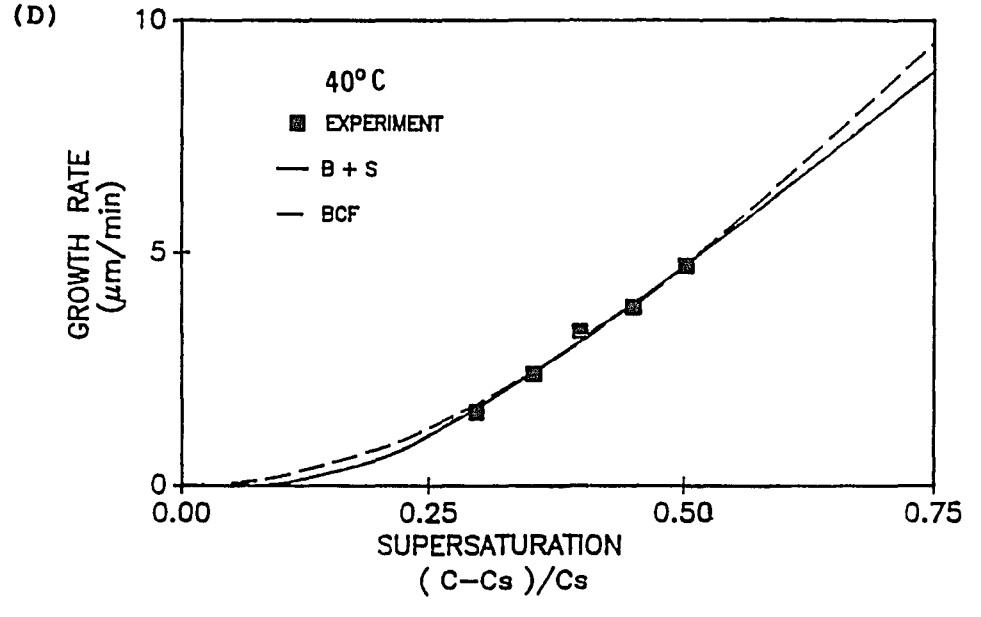

Table 3.5 : Values of the Parameters of Exponential Growth Model* for Theophylline Monohydrate Crystals at Various Temperatures

TEMPERATURE	K_g*	a*	CORRELATION
10°C	3.8(0.1)[b]	1.6(0.1)[b]	0.995
20°C	12.3(1.1)	2.0(0.2)	0.963
30°C	17.0(1.0)	2.0(0.1)	0.996
40°C	20.4(1.1)	2.1(0.2)	0.985

* : Exponential Growth Model, $G = K_g S^a$

b : The number in the parenthesis represents the standard deviation.

Table 3.6 : Values of the Parameters in Various Growth Rate Equations for Theophylline Monohydrate at **(A)** 10°C **(B)** 20°C, 30°C and 40°C.

(A) 10°C

MODEL	PARAMETER	SUM OF WEIGHTED SQUARED RESIDUALS	CORRELATION
BCF	K_1 = 6.9(0.5) K_2 = 1.1(0.1)	0.40	0.995
B+S	A = 7.7(0.3) B = 0.6(0.1)	0.56	0.993
EXPONENTIAL	K_g = 3.8(0.1) a = 1.6(0.1)	0.38	0.997
DIFFUSION	K = 4.0(0.4)	10.2	0.992

$$\text{BCF} : G = \frac{K_1}{K_2} S \, ln(1+S) \tanh\left(\frac{K_2}{ln(1+S)}\right)$$

$$\text{B+S} : G = A \, S^{(5/6)} \, e^{(-B/S)}$$

$$\text{EXPONENTIAL} : G = K_g \, S^a$$

$$\text{DIFFUSION} : G = K \, S$$

$$S = (C - C_{SH})/C_{SH}$$

Table 3.6 : Continued.

(B) 20°C, 30°C AND 40°C

MODEL EQUATION	PARAMETER	SUM OF WEIGHTED SQUARED RESIDUALS	CORRELATION
20°C			
BCF	K_1 = 35.3 K_2 = 2.5	0.04	0.988
B+S	A = 13.1(2.8) B = 0.5(0.1)	0.09	0.987
EXPONENTIAL	K_g = 12.3(1.1) a = 2.0(0.2)	0.02	0.963
30°C			
BCF	K_1 = 78.4 K_2 = 3.8	0.02	0.999
B+S	A = 16.8(0.5) B = 0.4(0.1)	0.03	1.000
EXPONENTIAL	K_g = 17.0(1.0) a = 2.0(0.1)	0.02	0.996
40°C			
BCF	K_1 = 66.2 K_2 = 2.9	0.12	0.993
B+S	A = 20.7(2.5) B = 0.5(0.1)	0.14	0.995
EXPONENTIAL	K_g = 20.4(1.1) a = 2.1(0.1)	0.13	0.985

3.3.3 : Dependence of the Growth Rate on the Stirring Intensity

The dependence of the growth rate on the agitation intensity at 10°C and 20°C are shown in Table 3.7. The growth rates are not affected by the stirring rates from 400 RPM to 1200 RPM with a supersaturation of 0.85 at 10°C and a supersaturation of 0.34 at 20°C. This phenomena suggests that the growth of theophylline monohydrate crystals is not controlled by the solute transport process in the present study.

Table 3.7 : Growth Rate as a Function of Stirring Rate for Theophylline Monohydrate at **(A)** 10°C and **(B)** 20°C.

(A) 10°C, Supersaturation = 0.85

	GROWTH RATE (μM/MIN)	
RPM	RUN 1	RUN 2
400	3.2	3.2
600	3.3	3.2
1200	3.3	3.2

(B) 20°C, Supersaturation = 0.34

	GROWTH RATE (μM/MIN)	
RPM	RUN 1	RUN 2
530	1.8	1.9
750	1.6	
1200	1.8	1.8

3.3.4 : Temperature Dependence of the Growth Rate Constant

The growth rate constant Kg in equation 1.27 is temperature dependent. The values of Kg at various temperatures are summarized in Table 3.5. Since the growth order **a** has the same value from 10°C to 40°C, the apparent activation energy of crystallization can be obtained from the temperature dependence of Kg. A plot of log Kg versus 1/T is shown in Figure 3.12. The dependence of Kg on temperature does not follow Arrhenius behavior.

The activation energy of crystallization between 10°C and 20°C is 11.7 kcal/mole. The activation energy for the diffusion of theophylline is 4.4 kcal/mole as obtained in section 3.1.3. The high value of the activation energy for the crystal growth also confirms the observation in section 3.3.2 and 3.3.3 that the growth process at 10°C to 40°C is controlled by a surface reaction mechanism rather than by a transport process.

The activation energy of crystallization decreases as the temperature increases. This phenomena may be explained by : (a) The crystallization process is an

exothermic reaction. According to LeChatelier's principle, the reaction rate for an exothermic process will decrease as temperature increases. Further study by solution calorimetry would allow to determine the amount of the heat evolved in this crystallization process and how the heat and temperature affect the crystallization. (b) The crystallization mechanism may change as temperature increase. (c) Theophylline may form dimers or higher aggregates in solution (Thakkar, 1971; Guttman, 1971), and make it difficult for a growth unit to attach itself onto the lattice. The formation of dimers or aggregates may be temperature dependent (Nishijo, 1986). However, we do not have enough information to arrive at a definite conclusion.

Figure 3.12 : Growth Rate Constant versus Temperature For Theophylline Monohydrate in pH 6 Phosphate Buffer.

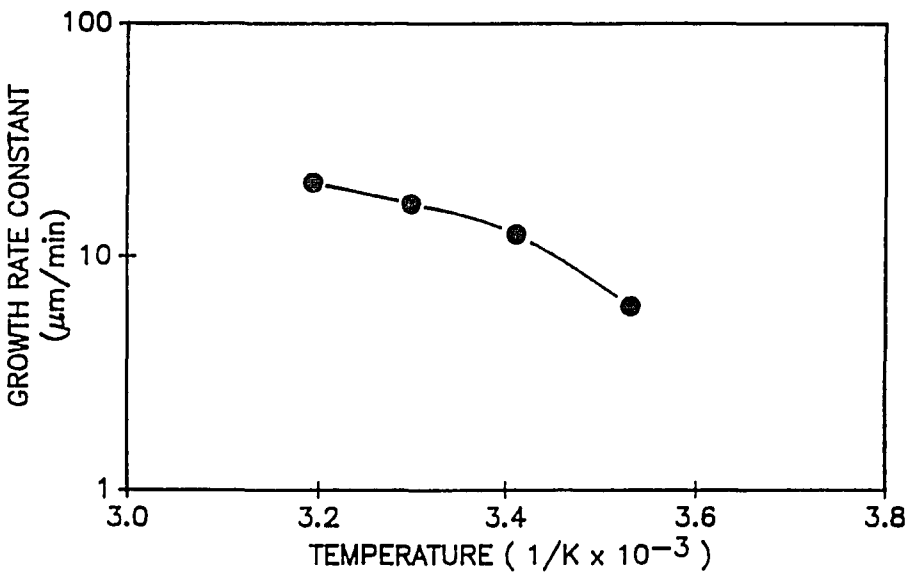

3.4 : DISSOLUTION KINETICS OF THEOPHYLLINE ANHYDROUS CRYSTALS

3.4.1 : Evaluation of the Undersaturation and Dissolution Rate

The undersaturation, Su, is defined as follow,

$$Su = \frac{(C_{SA} - C)}{C_{SA}} \qquad (3.9)$$

where C is the concentration (mmole/ml) of theophylline in the solution and C_{SA} is the solubility (mmole/ml) of theophylline anhydrous. The dissolution experiments were conducted at an undersaturation range from 0.06 to 0.3. The differential and cumulative number versus size distributions of the crystals with an undersaturation of 0.21 are shown in Figures 3.13a and 3.13b. The total number of the particles decreases as the crystals dissolve, and the differential and cumulative size distribution curves shift towards smaller size as a function of time. The shift in the distribution curves is not parallel in either the differential or the

cumulative curves. This phenomena indicates that the dissolution rate is size dependent. The cumulative curves show that the smaller crystals dissolve faster than the larger ones.

The initial dissolution rate (dL/dt, μm/min) of the anhydrous crystals at various initial sizes and undersaturations were calculated by equation 1.30, and are listed in Table 3.8. The concentration change is negligible in the first few minutes during the dissolution process, so the initial dissolution rate obtained corresponds to the initial undersaturation of each experiment.

Figure 3.13 : Size Distribution of Theophylline Anhydrous Crystals During Dissolution at 10°C with an Undersaturation of 0.29, **(A)** Differential Distribution, **(B)** Cumulative Distribution. The Lines From Top to Bottom in Each Graph Represent the Distribution Curves Corresponding to the Time Listed.

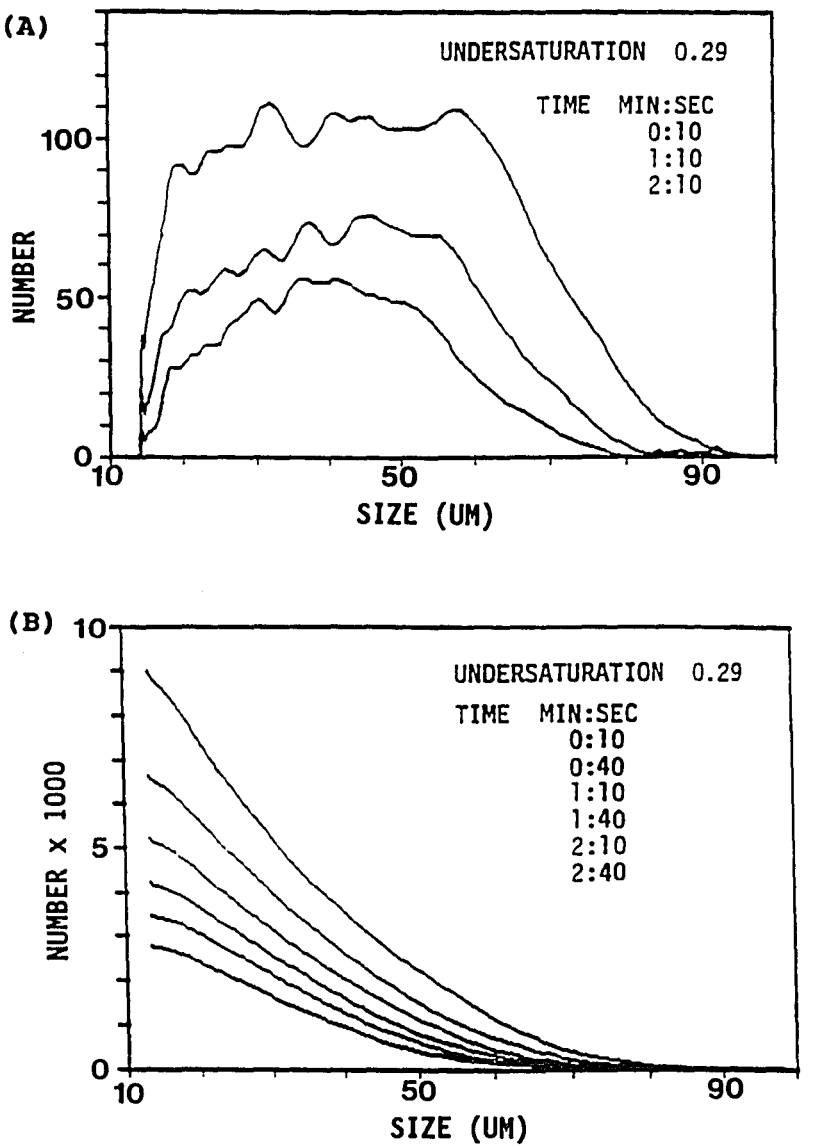

Table 3.8 : Experimental Dissolution Rate at Various Undersaturations and Particle Sizes for Theophylline Anhydrous Crystals

UNDERSATURATION (Cs-C)/Cs	SIZE (μM)	DISSOLUTION RATE (μM/MIN)
0.29	60.0	9.6
	56.1	10.0
	50.0	10.9
	45.4	11.4
	40.0	12.1
	37.5	12.6
	30.2	13.9
	30.0	13.9
	23.7	15.7
	20.0	16.6
	17.9	17.2
	15.0	19.0
0.21	60.0	5.7
	59.5	5.7
	50.0	6.6
	48.9	6.6
	40.8	7.5
	40.0	7.6
	33.5	8.3
	30.0	9.4
	27.9	9.6
	22.0	11.4
	20.0	11.0
	16.8	11.9
	15.0	13.5

Table 3.8 : Continued.

UNDERSATURATION (Cs-C)/Cs	SIZE (μM)	DISSOLUTION (μM/MIN)
0.17	60.1	2.8
	60.0	2.8
	50.1	3.0
	50.0	2.8
	42.3	3.6
	40.0	3.4
	35.4	3.3
	30.0	3.8
	29.7	3.9
	24.9	4.6
	20.0	5.5
	16.0	6.5
	15.0	7.1
0.08	64.5	1.0
	60.0	1.2
	54.9	1.4
	50.0	1.6
	47.3	1.6
	40.6	2.0
	40.0	2.1
	35.4	2.1
	30.6	1.9
	30.0	2.0
	26.5	1.9
	22.8	2.1
	20.0	2.1
	19.4	2.0
	16.0	2.5
	15.0	2.4

3.4.2 : The Dependence of the Dissolution Rate on the Crystal Size and Undersaturation for Theophylline Anhydrous Crystals

Figure 3.14 displays the plot of the dissolution rate versus crystal size at various undersaturations, it shows that the dependence of the dissolution rate on the crystal size is not linear. The linear and the logarithmic plots of the dissolution rate as a function of undersaturation at various initial sizes are shown in Figures 3.15a and 3.15b.

The correlation of the dissolution rate (DR), crystal size (equivalent sphere volume diameter) and undersaturation is analyzed by the Statistic Analysis System (SAS program) according to the linear form of equation 1.28, as shown here in equation 3.10,

$$\ln(DR) = K_R + Q \ln(Su) + R \ln(size) \qquad (3.10)$$

where K_R, Q, and R are constants. The results of the SAS analysis are shown in Table 3.9. The plot of the predicted versus the experimental dissolution rates is

shown in Figure 3.16, which shows a fairly good correlation.

Cheng (1984) and Christofferson (1984) demonstrated that for a diffusion controlled dissolution process, the dissolution rate depends on the first order of the undersaturation; while for a surface reaction controlled process, the dissolution rate depends on the second or higher order of the undersaturation. The results from the SAS analysis show that the dissolution rate of theophylline anhydrous crystal is dependent on the 1.5 power of the undersaturation. This suggests that the dissolution of the anhydrous crystals is not diffusion limited only, but may be controlled by a surface reaction or by the combination of both the surface reaction and diffusion.

The dissolution rate is inversely proportional to the square root of the crystal size in the present study. This phenomena may be explained by the following :

(a) Ostwald ripening. Ostwald ripening states that due to the higher surface energy of the small particles, the solubility and hence the dissolution rate are higher for small particles.

(b) The smaller anhydrous crystals may have a higher density of defects than the larger ones and this results in a higher dissolution rate.

(c) The diffusion boundary layer thickness, h, has been shown to be a function of the square root of the diameter of the dissolving particle (Bisrat and Nostrom, 1988). The mechanism of this observation can be related to the hydrodynamics of an agitated system of a suspended solid body. For flow pass a flat surface, the Prandtl boundary layer equation can be used to express the hydrodynamic boundary layer thickness, h_H,

$$h_H = K_H \frac{L^{0.5}}{V^{0.5}} \qquad (3.11)$$

where K_H is a constant, L is the length of the surface in the direction of flow and V is the relative velocity of the flowing liquid versus the flat surface. A decrease in particle size at a given intensity of agitation, would result in a larger decrease in L than in V. The net effect is a decrease in h_H. The diffusion boundary layer thickness, h, is proportional to the hydrodynamic boundary layer thickness, h_H. Therefore a decrease in

the diameter of theophylline anhydrous crystal would result in a shorter diffusional distance for the dissolved molecules and a faster dissolution rate.

The actual mechanism of the dissolution at molecular level can not be elucidated without further studies.

Figure 3.14 : Dissolution Rate versus Crystal Size for Theophylline Anhydrous at 10°C and Various Undersaturations.

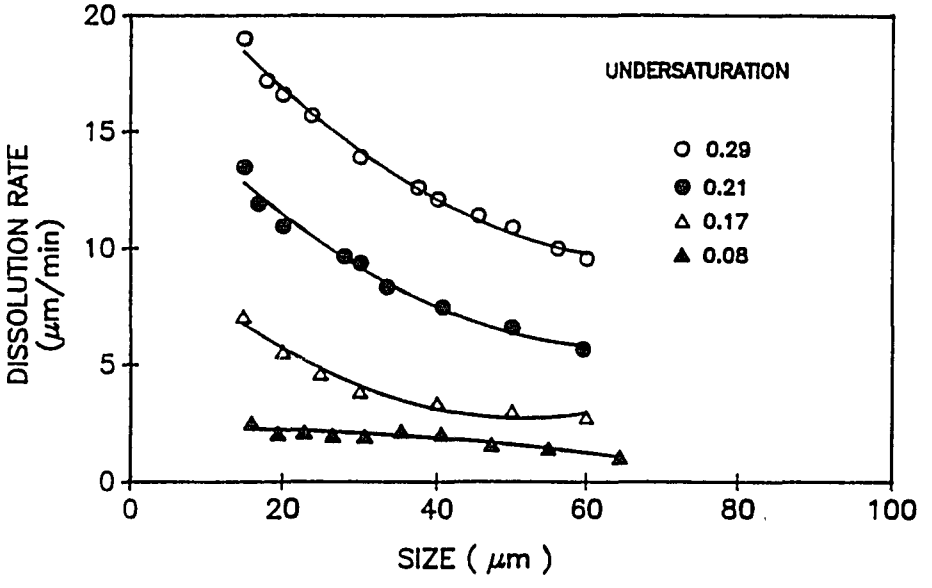

Figure 3.15 : Dissolution Rate as a Function of Undersaturation for Theophylline Anhydrous Crystals at 10°C. **(A)** Linear Plot and **(B)** Logarithmic Plot.

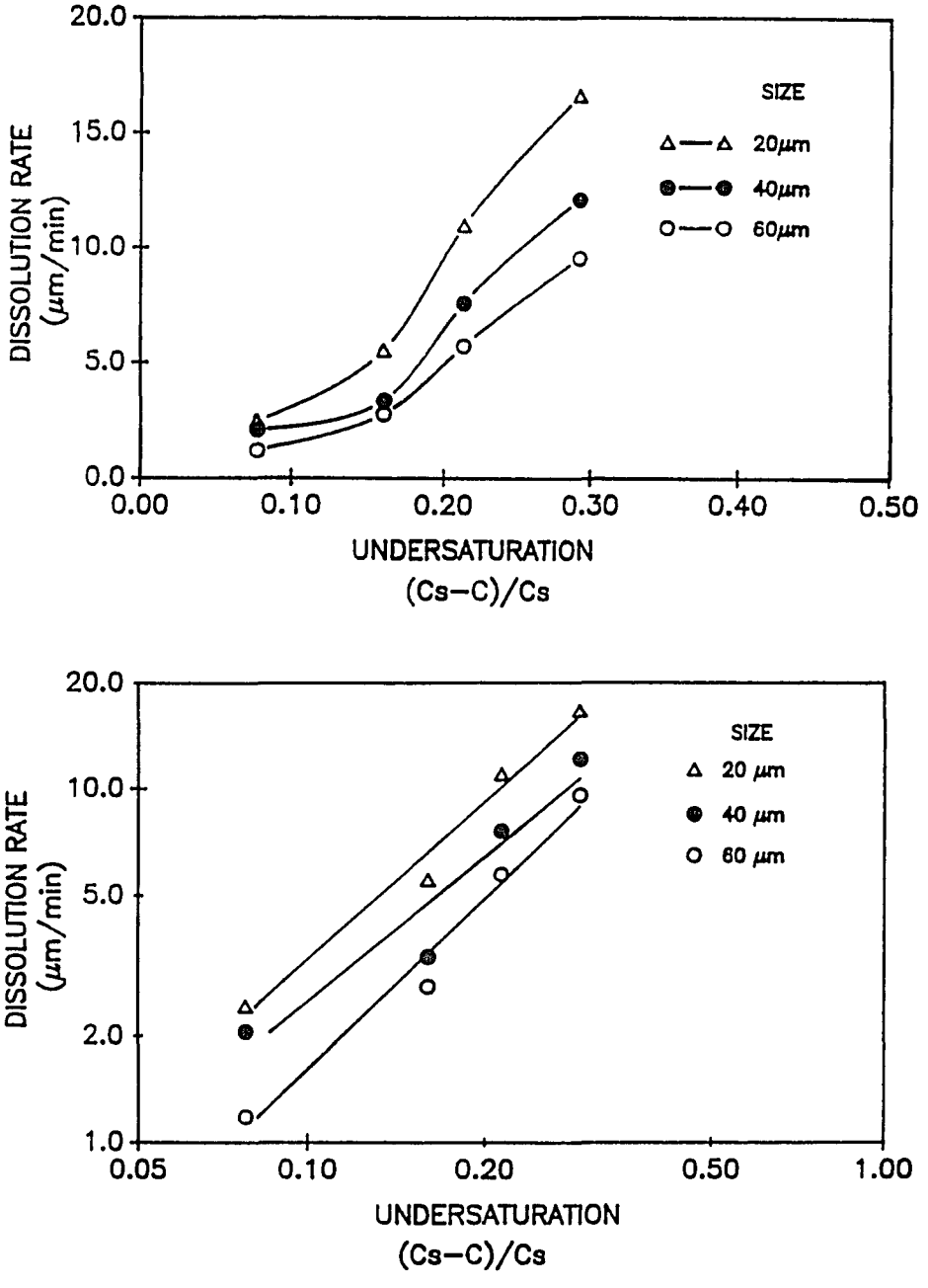

Figure 3.16 : Predicted Versus Experimental Dissolution Rate for Theophylline Anhydrous Crystals.

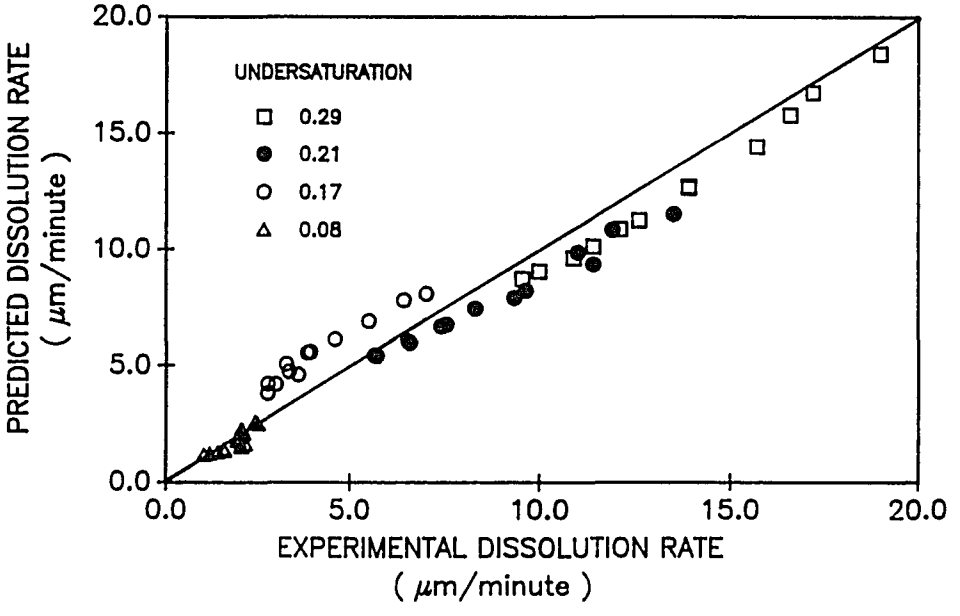

Table 3.9 : The Statistical Analysis (SAS) Results of the Dissolution Equation for Theophylline Anhydrous Crystals

DEP VARIABLE : ln(DR)

ANALYSIS OF VARIANCE :

SOURCE	DF	SUM OF SQUARES	MEAN SQUARE	F VALUE	PROB>F
MODEL	2	33.76	16.88	429.53	0.0001
ERROR	52	2.04	0.04		
C TOTAL	54	35.81			

ROOT MSE	0.19	R-SQUARE	0.94
DEP MEAN	1.59	ADJ R-SQ	0.94
C.V.	12.42		

PARAMETER ESTIMATES :

VARIABLE	DF	PARAMETER ESTIMATE	STANDARD ERROR	T FOR HO: PARAMETERS =0	PROB>|T|
INTERCEPT	1	(K_R) 6.21	0.23	27.08	0.0001
ln(Su)	1	(Q) 1.49	0.05	27.82	0.0001
ln(SIZE)	1	(R) -0.54	0.06	-9.18	0.0001

3.5 : The PHASE TRANSFORMATION OF THEOPHYLLINE

3.5.1 : Phase Diagram of Theophylline

The phase diagram of theophylline in the present study, constructed from the solubility versus temperature data, is shown in Figure 3.17. It shows that theophylline anhydrous is the stable phase when the temperature is above the transition point, 60.0°C; and the monohydrate form is the stable phase below the transition temperature.

The phase transformation of theophylline was studied at 10°C, where the monohydrate is the stable phase with a solubility of 2.99 mg/ml and the anhydrous form is the metastable phase with a solubility of 8.75 mg/ml. The transformation process starts at a solution composition at point A, which is saturated with respect to the anhydrous form and is supersaturated with respect to the monohydrate, and end at point B (which is saturated with respect to the monohydrate form) in the phase diagram.

Figure 3.17 : Phase Diagram of Theophylline. A is the Initial Solution Composition of the Transformation Process, B is the End Point of the Transformation.

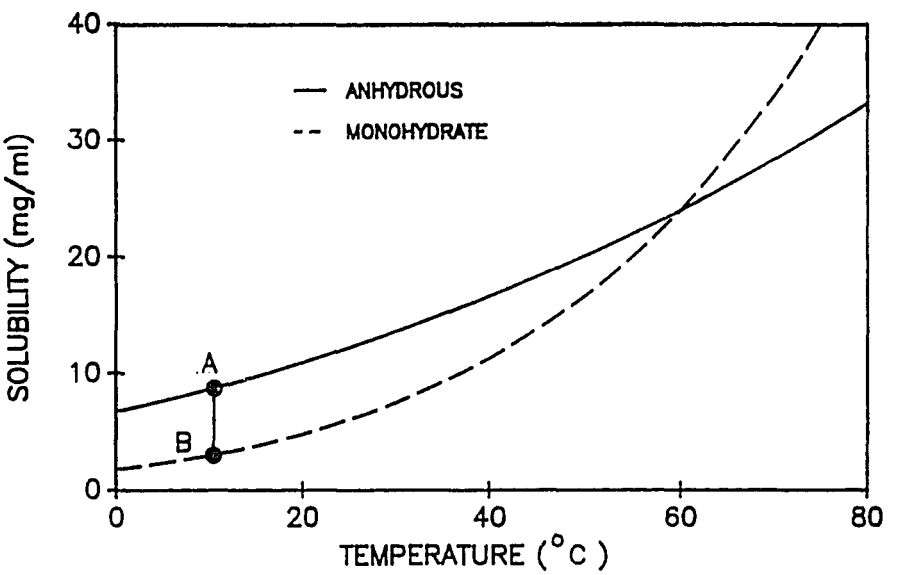

3.5.2 : The Appearance of the Crystals During the Phase Transformation Process

The phase transformation started at the moment the monohydrate seeds were added to the slurry and was completed when the supersaturation dropped to zero with respect to the monohydrate form. The microscopic pictures of the crystals, for the experiment with 5.5g anhydrous crystals and 38mg monohydrate seeds, taken before and at 3, 6 and 20 minutes into the transformation are shown in Figure 3.18. Before the addition of the monohydrate seeds, all the crystals exist as anhydrous form with a flat plate shape and they are opaque under the light microscope. As the transformation proceeds, the monohydrate seeds grow to long plate shape crystals and are transparent. The pictures taken at 3 and 6 minutes show that both the anhydrous and the monohydrate crystals exist. When the transformation approaches completion, only the monohydrate crystals exist. These pictures also suggest that there is no relationship between the morphologies of these two phases and, therefore, that the transformation is indeed solvent-

mediated rather than involving structural rearrangement within the solid phase.

Figure 3.18 : Optical Microscopic Pictures of **(A)** Anhydrous Theophylline Crystals. **(B)** A Mixture of Theophylline Anhydrous and Monohydrate Crystals Taken at 3 Minutes into the Transition and **(C)** at 6 Minutes. **(D)** Theophylline Monohydrate Crystals After the Transition is Complete.

(A)

(B)

Figure 3.18 : Continued.

(C)

(D)

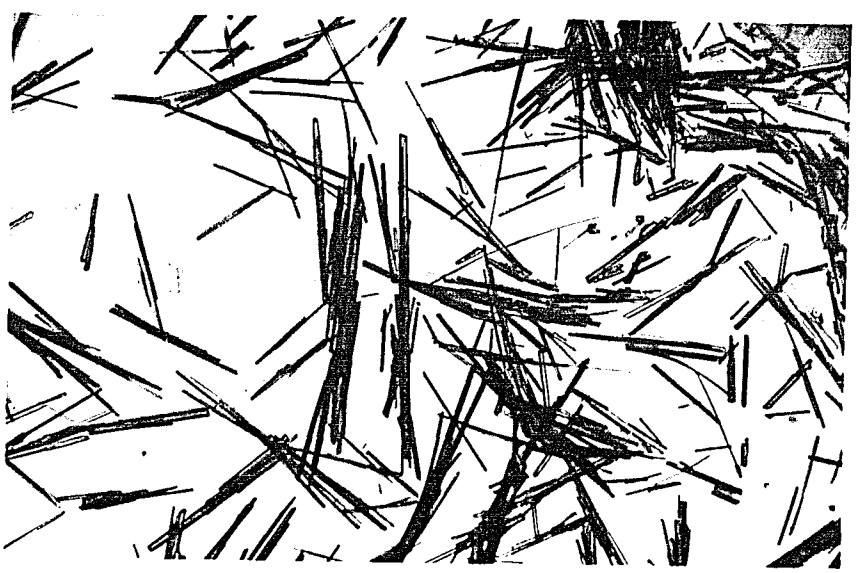

3.5.3 : Supersaturation Profile During the Phase Transformation Process

The concentration versus time data for the experiments with the same amount, 5.5g, of the anhydrous crystals and various amounts of the monohydrate seeds are shown in Table 3.10, and the corresponding supersaturation profiles are shown in Figure 3.19. As shown in these profiles, the supersaturation, S, approaches zero as the transition approaches completion in 15 minutes. The desupersaturation profile for the experiment with no monohydrate seeds shows a plateau at an early stage of the transformation. This might be due to the lag time needed for the formation of the nuclei of the monohydrate. Once the nuclei form and start to grow, the supersaturation decreases rapidly. When more seeds are added, the earlier the supersaturation begins to drop. The trend of the desupersaturation profiles seem to fall into the dissolution controlled category as shown in Figure 1.9, where the plateau supersaturation level is very low.

The supersaturation profiles for the systems with 38mg monohydrate seeds in the absence and presence of the anhydrous phase are shown in Figure 3.20.

The details of the desupersaturation profiles and the the simulation of the concentration profiles for the transformation will be discussed later.

Figure 3.19 : Supersaturation Profile as a Function of Time for the Transformation of Theophylline in pH 6 Phosphate Buffer Started With 5.5 g Anhydrous Crystals and Different Amounts of Monohydrate Seeds at 10°C.

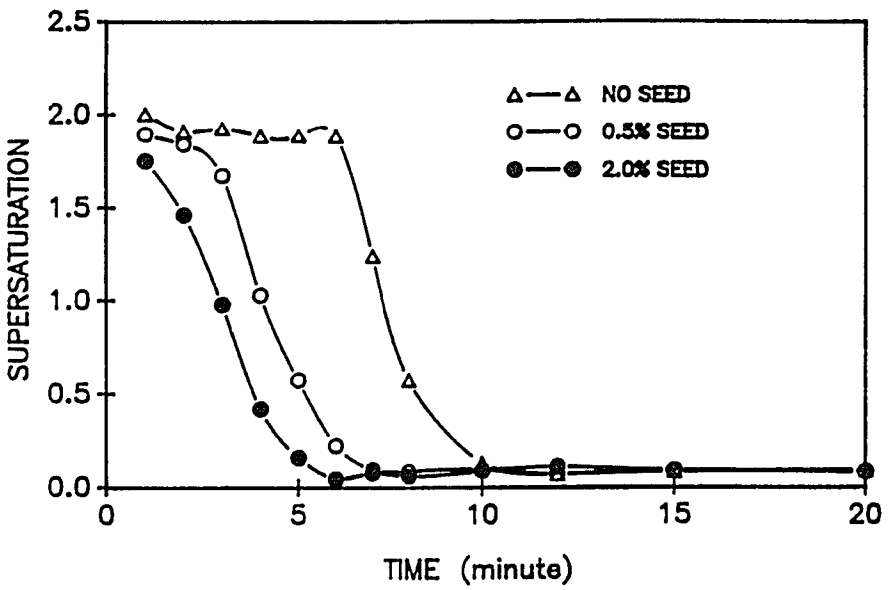

Figure 3.20 : Supersaturation Profile as a Function of Time for the Phase Transformation From 5.5g Theophylline Anhydrous Crystals to the Monohydrate Crystals with 38mg Monohydrate Seeds, and the Supersaturation Profile for the Growth of 38mg Monohydrate Seeds in the Absence of the Anhydrous Crystals at 10°C.

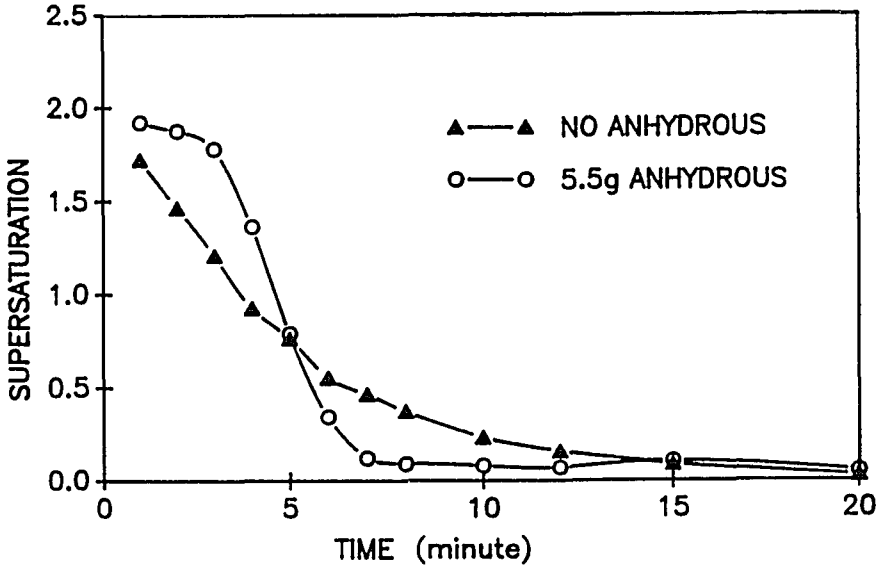

Table 3.10 : Concentration as a Function of Time for the Transformation of Theophylline in pH 6 Phosphate Buffer at 10°C.

	Run 1	Run 2	Run 3	Run 4
Anhydrous added	5.5g	5.5g	5.5g	0.0g
Monohydrate seed added	0.0ml	0.5ml	2.0ml	0.5ml
Time(minute)	Concentration (mg/ml)			
1	8.90	8.65	8.22	8.14
2	8.69	8.45	7.36	7.37
3	8.74	7.99	5.92	6.61
4	8.62	6.07	4.25	5.76
5	8.62	4.71	3.46	5.28
6	8.41	3.65	3.12	4.65
7	6.69	3.26	3.21	4.38
8	4.70	3.24	3.16	4.10
10	3.37	3.27	3.24	3.68
12	3.19	3.19	3.31	3.46
15	3.23	3.25	3.25	3.25
20	3.25	3.23	3.24	3.07
25	3.17	3.21	3.18	
30	3.21	3.33	3.16	
35		3.13	3.15	
50		3.01		

a : Monohydrate seed suspension contains 76mg/ml of theophylline monohydrate.

3.5.4 : Nucleation During the Transformation Process

Basically the transformation process of theophylline can be described by the growth of the monohydrate crystals at the expense of the dissolution of the anhydrous crystals. In order to investigate the effect of growth and dissolution on the transformation process in a better defined system, the monohydrate seeds were added to avoid the nucleation of the monohydrate. However, we found that extensive nucleation occurred in our experiments despite the addition of the monohydrate seeds. So we need to take into consideration the nucleation process during the transformation.

3.5.4.1 : Analysis of the Experimental Data :

(a) Total Number and Size Distribution of the Final Monohydrate Crystals :

The number of the monohydrate seeds added to the system before the transformation and the total number of the monohydrate crystals after the transformation was complete are shown in Table 3.11. Three important results are obtained from these data,

Table 3.11 : The Initial and Final Total Number of Theophylline Monohydrate Crystals before and after the Phase Transformation.

Anhydrous Crystals Added	Number of Initial Monohydrate Seed Crystals Added	Final Total Number of the Monohydrate Crystals[a]
5.5 g	1.6×10^7	1.5×10^8
5.5 g	6.4×10^6	1.4×10^8
5.5 g	0	1.4×10^8
2.0 g	0	5.0×10^7
1.0 g	0	1.6×10^7
0.0 g	6.4×10^6	6.5×10^6 [b]

a : There is a 15% error associated with this data.
b : There is a 5% error associated with this data.

(1) For the systems with same amount of anhydrous crystals but different amounts of monohydrate seeds, the final total number of the monohydrate crystals is much higher than the number of the seeds added initially in each system, and the number is independent of the amount of seeds added.

(2) For the systems with same amount of monohydrate seeds but different amounts of the anhydrous crystals, the final total number of the monohydrate crystals increases significantly in each system and the increase is dependent on the amount of the anhydrous crystals added.

(3) For the system with monohydrate seeds only, the total number of crystals does not change significantly.

From the above results we can conclude that the nucleation during the transformation process for theophylline is not dependent on the monohydrate seeds added but depends on the anhydrous crystals added. This suggests a heterogeneous nucleation mechanism.

It is also clear that nucleation occurred during the transformation process by examining the crystal size distributions of the crystals before and after the transformation. The size distribution of the seeds is

shown in Figure 3.21a with an arithmetic mean of 22 μm. The size distributions of the final monohydrate crystals, started with different amounts of monohydrate seeds, are shown in Figures 3.21b, 3.21c and 3.21d. The mean size of the seeds is expected to increase to 100 μm if no nucleation occurs. As shows in Figures 3.21b, c, and d that in addition to some big crystals there are a lot of small crystals present, the number of the small crystals is much greater than the number of the larger crystals and the mean size of the small crystals is 25 μm. The larger crystals in the system may result from the growth of the monohydrate seeds added, and the small crystals may result from the nucleation process during the transformation. There is no significant difference in these distributions, which suggests that the nucleation does not depend on the monohydrate seeds added.

The nucleation process generates a lot of small crystals and consumes a considerably large amount of theophylline molecules, which will otherwise have been available for growth.

(b) Crystal Size Distributions During the Phase Transformation :

Due to the fast nucleation and transformation processes, it is difficult to monitor the relative amount and the size distribution of the anhydrous and the monohydrate crystals during the transformation process. However, the combined crystal size distribution of both forms in the slurry was obtained as a function of time for the experiment with 5.5g anhydrous crystals and 380mg monohydrate seed added, as shown in Figure 3.22.

Figure 3.22a shows the initial size distribution of the monohydrate seeds . Due to the static charge of anhydrous crystals, it is difficult to get rid of some small crystals by sieving, and Figure 3.22b shows the initial size distribution of the anhydrous crystals.

Figure 3.22c shows the crystal size distribution at 2 minutes into the transformation. The first peak in Figure 3.22c may be the combination of some monohydrate nuclei and the smaller particles of the anhydrous crystals, the second peak is the monohydrate seeds added and the third peak is the other part of the anhydrous crystals.

Figure 3.22d shows the crystal size distribution at 4 minutes into the transformation, the distribution changes significantly. Due to the formation of a large amount of monohydrate nuclei, the relative number in the first peak increases drastically, this makes the peaks of the monohydrate seeds and the anhydrous crystals relatively very low.

Figure 3.22e shows the distribution at 6 minutes into the transformation, which is the same as those at 4 minutes.

(c) Desupersaturation Profile :

The desupersaturation profiles during the transformation, as shown in Figure 3.19, can be explained by the nucleation during the transformation. The declining part of the supersaturation profile for the experiment without any monohydrate seeds added is due to the formation and the subsequent growth of a very large number of the monohydrate nuclei. The formation of the large amount of the monohydrate nuclei provides a very significant surface area for the attachment of theophylline molecules from the solution, so the

depletion of the molecules from the solution is very fast.

The supersaturation profiles for the experiments with different amounts of monohydrate seeds can also be explained by the nucleation process. The initial decline of the supersaturation is due to the growth of the seeds; after a certain lag time, there is a big drop in the supersaturation due to both the growth of the seeds and the formation and subsequent growth of a large amount of monohydrate nuclei. The number of the nuclei is much greater than the initial seeds added, once the nuclei form, the supersaturation drops very fast and the declining slope of the desupersaturation curve is almost the same as that in the experiment without seeds. The contribution of the growth of the seeds to the decrease in the supersaturation profile can only be detected initially, it is overwhelmed by the huge amount of nuclei formed later.

(d) The Lag Time of Nucleation :

The presence of the monohydrate seeds influences the lag time for the nucleation process, as shown in Figure

3.19, the larger the mass of the seeds added the earlier the supersaturation starts to decline.

3.5.4.2 : Primary Heterogeneous Nucleation Process for Theophylline Monohydrate

Nucleation during the transformation process in the present study can be summarized as : (1) The lag time for the nucleation process is dependent on the monohydrate seeds added. (2) The total number of the nuclei formed is independent of the amount of the monohydrate seeds added. (3) The formation of the monohydrate nuclei is associated with the presence of the anhydrous crystals, the more anhydrous crystal added, the more nuclei formed.

From the above summary, the nucleation during the transformation belongs to the primary heterogeneous nucleation process. Theophylline anhydrous crystals in the solution act as nucleation substrates for the monohydrate crystals. The monohydrate nuclei form on the surface of the anhydrous crystals and they may be swept away into the solution and continue to grow. This kind heterogeneous nucleation processes have been observed in the phase transition process of anhydrous and dihydrate

uric acid crystals (Boistelle and Rinaudo 1981), and also in the crystallization of gypsum from a dense suspension of calcium sulfate hemihydrate (Amathieu and Boistelle, 1988).

3.5.4.3 : Comparison With Literature Results

Nucleation did not occur during the polymorphism phase transformation processes for copper phthalocyanine, dyestuff and paclobutrazol studied by Davey and Cardew (1985, 1986). The desupersaturation profiles of the above compounds reflect their relative growth and dissolution kinetics. The transformation between polymorph I and II of dyestuff at 60°C is a dissolution controlled process and the transition between polymorph α and β of paclobutrazol at 65°C is growth controlled, as shown in Figures 3.23a and 3.23b.

The occurrence of the nucleation during the transformation process complicates the kinetics of the transformation in the present study. The tremendous impact of the nucleation in this study overwhelms the kinetics of the growth and dissolution, and results in a dissolution controlled desupersaturation profile. The

dissolution of the anhydrous crystals can not keep up with the demand of the growth of the monohydrate seeds, and the formation and subsequent growth of the monohydrate nuclei.

Nucleation will pose a significant problem for some compounds with a relatively high solubility, since the higher the solubility, the easier and faster the nucleation will be (Adamson, 1982). The solubility of theophylline monohydrate is 2.99 mg/ml in the present study. The solubility of the other compounds mentioned above are very low. For example, the solubility of copper phthalocyanine is 0.25 mg/l, and the solubility of paclobutrazol is 0.01 mg/ml. The difference in the solubility may explain why, during the transformation process, nucleation occurs with theophylline but not for the other compounds.

Figure 3.21 : Number Versus Size Distributions for **(A)** the Monohydrate Seeds, and the Final Monohydrate Crystals for the System Started With **(B)** None **(C)** 0.5% and **(D)** 2% of the Monohydrate Seeds. The Scale for All the Plots Are the Same.

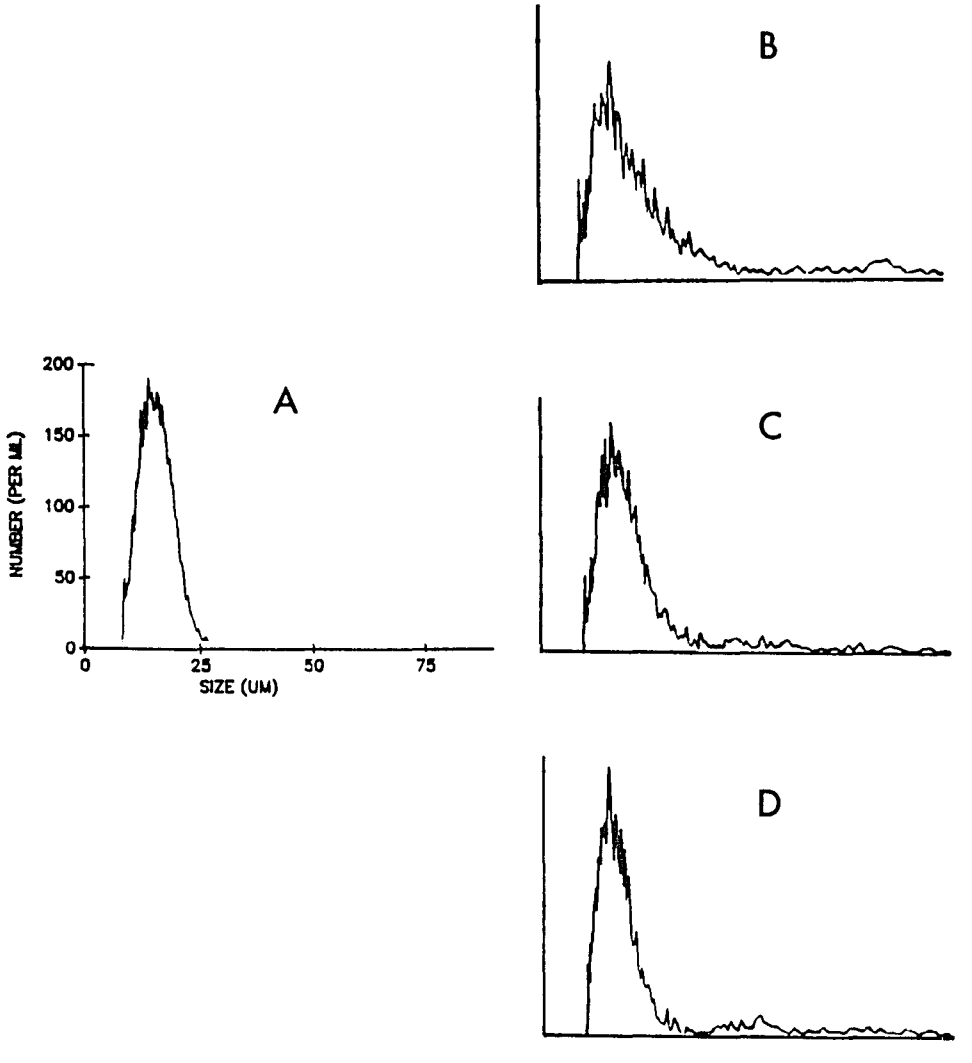

Figure 3.22 : Number Versus Size Distributions for **(A)** Monohydrate Seeds **(B)** Anhydrous Crystals Added Initially, and for the Combined Size Distributions of both the Anhydrous and Monohydrate Crystals at **(C)** 2 Minutes, **(D)** 4 Minutes and **(E)** 6 Minutes into the Transformation. The Scale for All the Plots Are the Same.

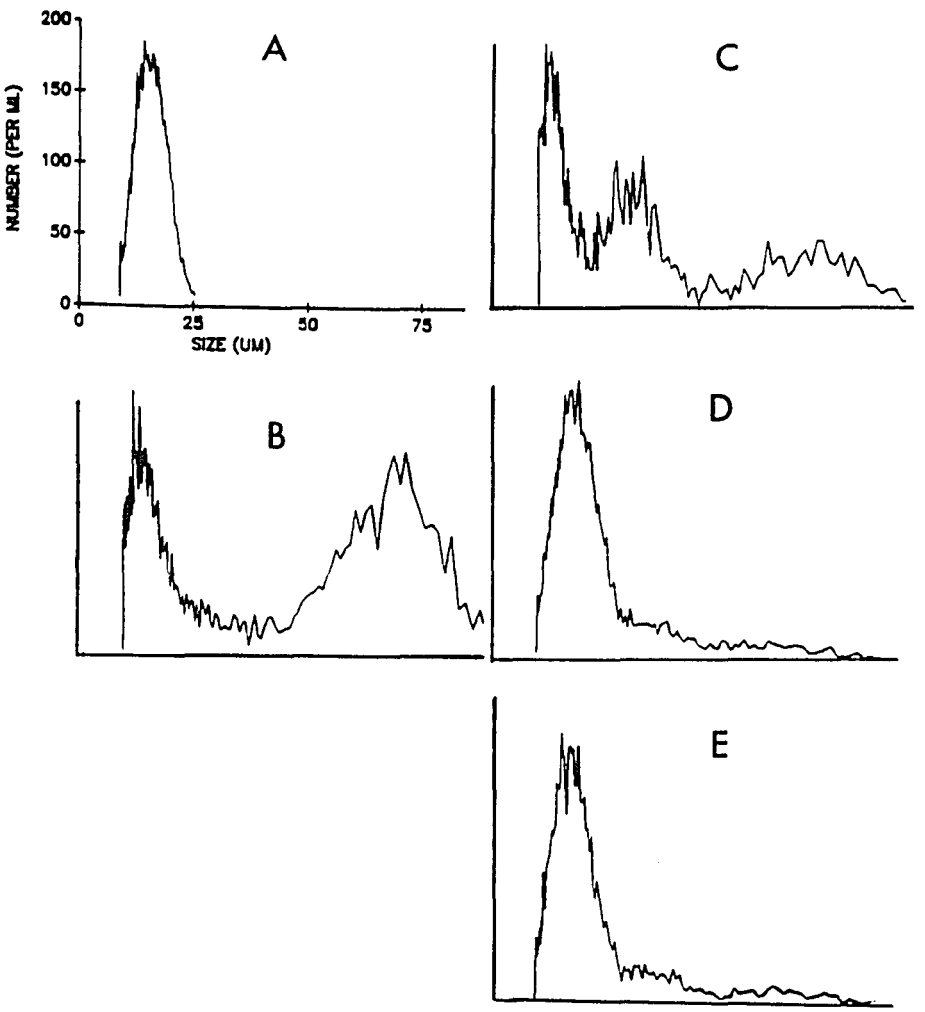

Figure 3.23 : Supersaturation as a Function of Time for the Transformations Between **(A)** Polymorph I and II of Dyestuff, **(B)** α and β Polymorph of Paclobutrazol. (Davey and Cardew, 1986)

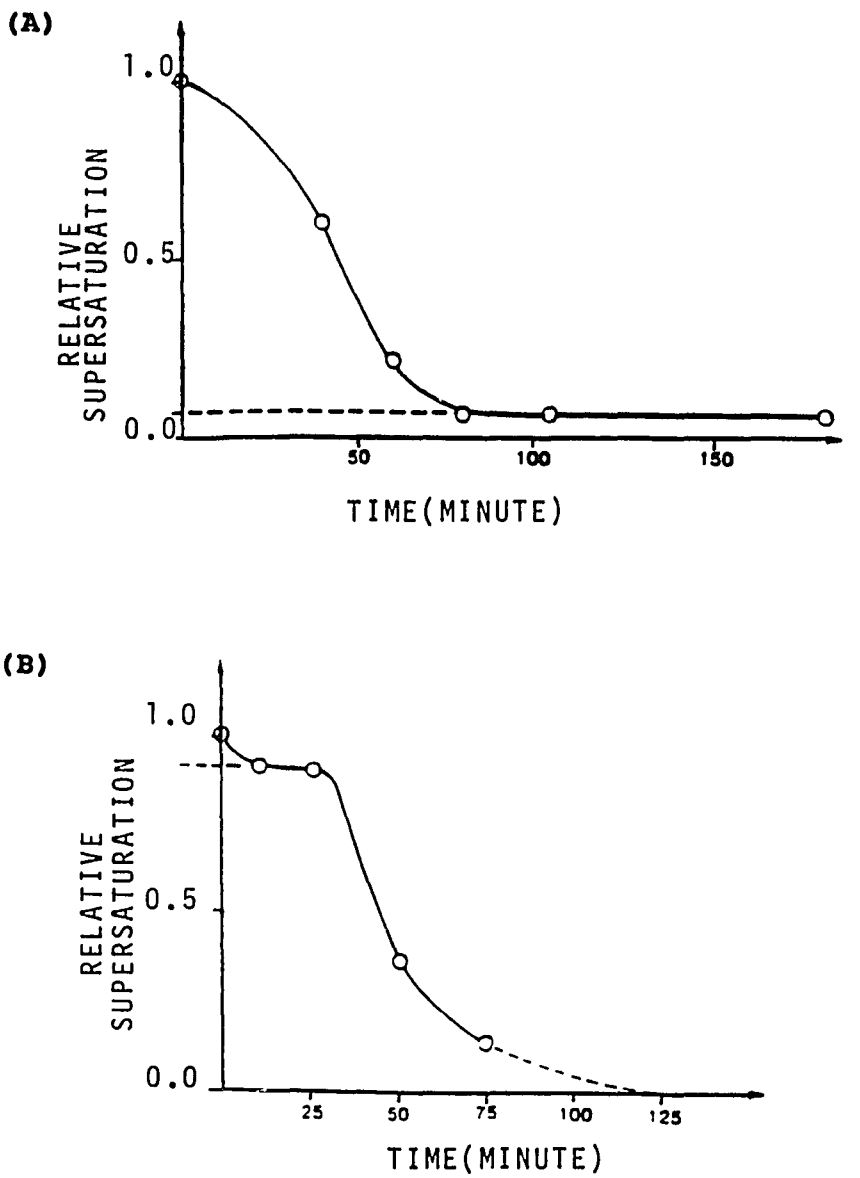

3.6 : SIMULATION OF THE CONCENTRATION PROFILE DURING THE PHASE TRANSFORMATION PROCESS

In order to model the phase transformation process for theophylline, a fortran program was written to simulate the concentration profile during the transformation at 10°C with the following input information :

(a) The density and molecular weight of theophylline anhydrous and monohydrate crystal.

(b) The amount and the number versus size distributions of the monohydrate seeds and the anhydrous crystals added into the system.

(c) The growth kinetics of the monohydrate crystals,

$$\log G = 1.63 \log(C-C_{SH})/C_{SH} + 0.59 \qquad (3.12)$$

(d) The dissolution rate of the anhydrous crystals as a function of the undersaturation and particle size,

$$\ln DR = 6.21 + 1.49 \ln[(C_{SA}-C)/C_{SA}] - 0.54 \ln(size) \qquad (3.13)$$

(e) The initial concentration of theophylline, 8.75mg/ml.

(f) The lag time for the nucleation process.

The lag time for each system is defined from the experimental desupersaturation profile as the time at which the following two lines intercept each other. (1) The straight line drawn through the decline part of the desupersaturation curve, and (2) the horizontal line which parallels X axis at a concentration level equal to the initial concentration. The lag time of the experiments with same amount of anhydrous crystals, 5.5g, and different amounts of the monohydrate seeds, 0%, 0.5% and 2.0% (weight by weight), are 6.0, 2.5 and 1.2 minutes, respectively, estimated from the above method.

(g) The number versus size distribution of the nuclei formed during the transformation process.

The size distribution of the nuclei is approximated from the number versus size distribution of the crystals after the transition is completed by taking into account the seeds added and the diameter grown during the transformation process.

The program is shown in Appendix III. In this simulation, the following assumptions are made. (1) The nucleation process is viewed as the formation of the monohydrate crystals in a burst after the lag time. (2)

The growth kinetics are the same for the seeds and the nuclei.

The simulations for the systems with same amount of anhydrous crystals, 5.5g, and different amounts of the monohydrate seeds are shown in Figure 3.24. Figure 3.24a shows the simulation including the nucleation process and Figure 3.24b shows the simulation without considering the nucleation. It is clear that the concentration profile is totally different in these two models and the model including the dissolution, growth and nucleation describes the data much better.

In order to gain a better understanding of how the growth and dissolution kinetics control the transformation process, a series of simulations were done by using theophylline as a model compound. The distribution of the monohydrate seeds and the anhydrous crystals are the same as in the present study, and nucleation was not allowed to occur. The simulation was performed at various amounts of the monohydrate seeds and anhydrous crystals, different growth and dissolution kinetics, as shown in Figures 3.25a, 3.25b and 3.25c. The relative amounts of the anhydrous and monohydrate crystals, and the relative dissolution and growth rates as a function

of time were obtained along with the concentration profile during the transformation processes, as shown in Figures 3.25 and 3.26. It is clear from the concentration profile that the plateau supersaturation occurs earlier and has a higher value when the growth rate is slow. The larger the amount of seeds added the faster the concentration is depleted.

Figure 3.24 : Simulated Concentration Profile for the Transformation of Theophylline (A) Including the Nucleation Process, (B) Without the Nucleation Process. The Lines in the Order From Left to Right in Each Graph Represent the Profiles for 2.0%, 0.5% and 0% Monohydrate Seeds Added Initially.

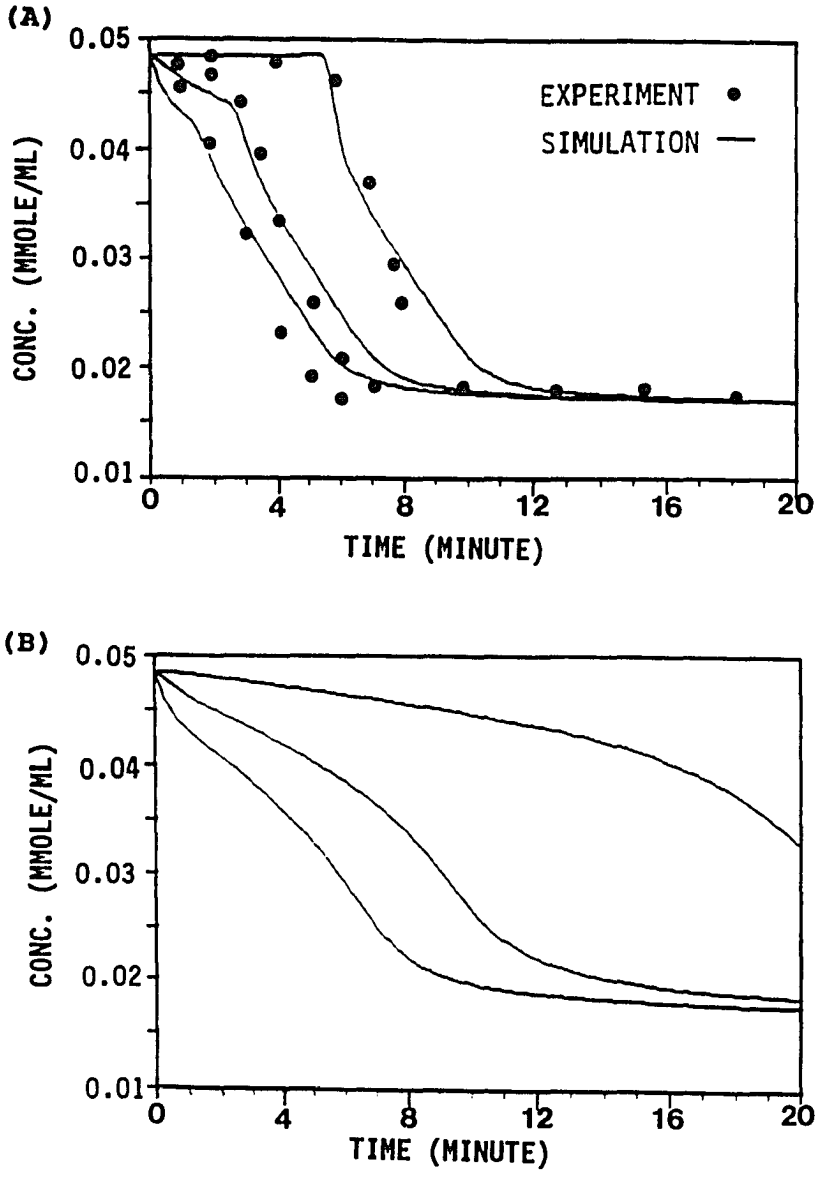

Figure 3.25 : Simulated Supersaturation Profile for the Transformation of Theophylline at Different **(A)** Growth Rates, **(B)** Dissolution Rates and **(C)** Amounts of Anhydrous, and With Various Amounts of Monohydrate Seeds, G, DR and A Represent Growth, Dissolution Rate and the Amount of the Anhydrous. The Lines in Each Graph in Order From Left to Right Represent the Profiles for 50%, 12.5%, 2.5%, and 0% seeds. All the Plots Have the Same Scale.

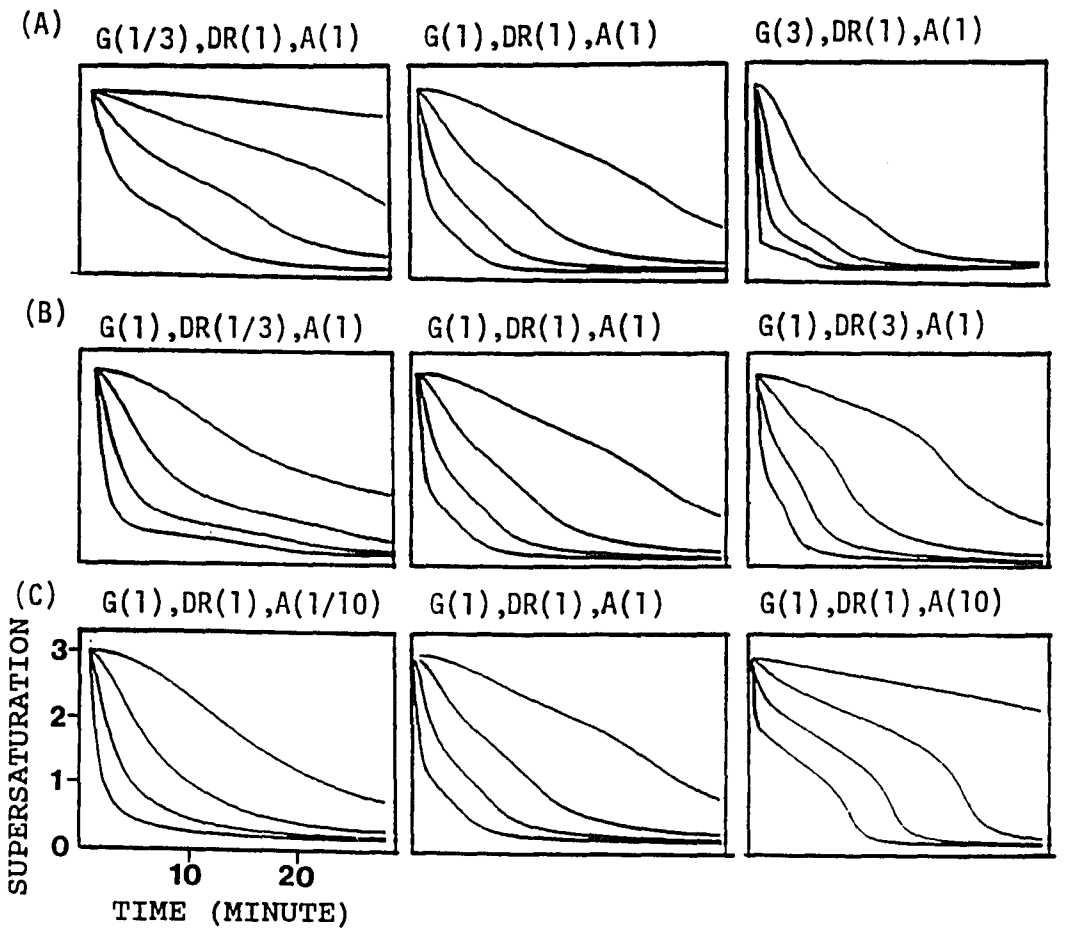

Figure 3.26 : Simulation, as a Function of Time, for **(A)** the Growth Rate (●) of the Monohydrate and the Dissolution Rate (▲) of the Anhydrous, **(B)** the Amount of the Monohydrate Crystals (○), Anhydrous Crystals (△) and the Theophylline in Solution (□) for the System with 2.5% Monohydrate Seeds at Various Initial Growth Rates (G).

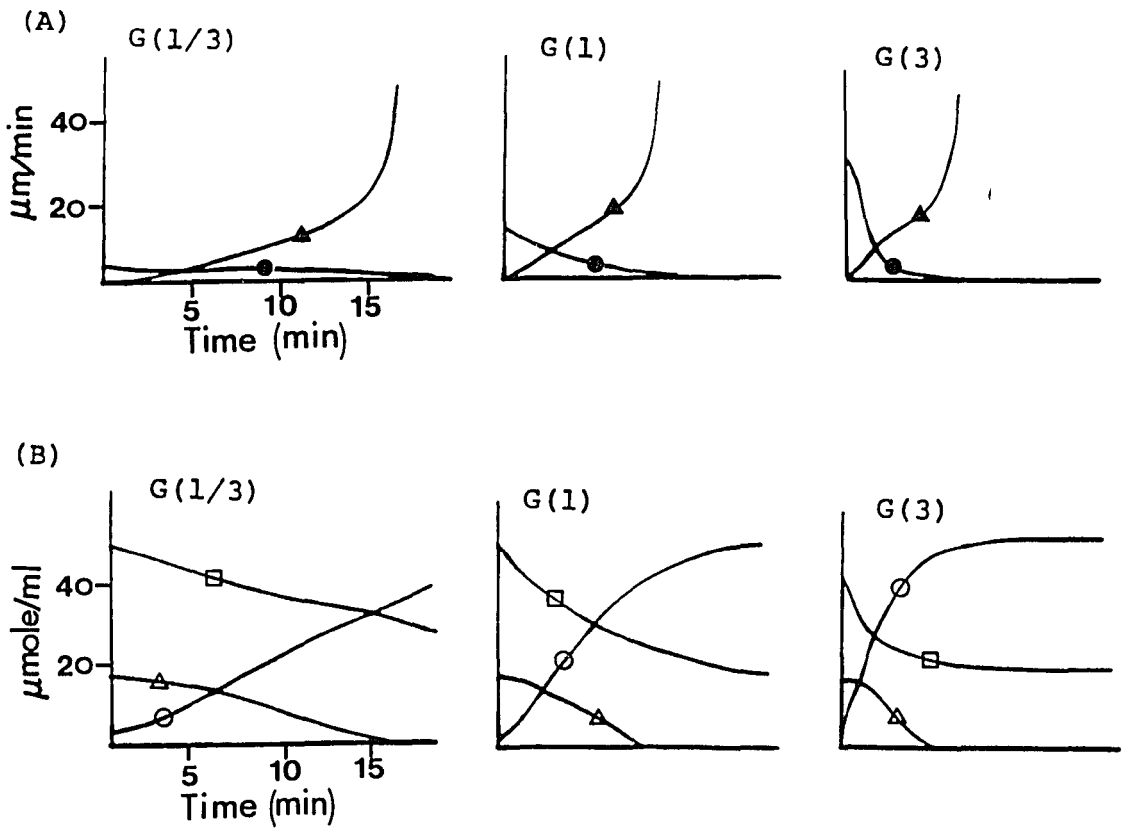

CHAPTER 4

CONCLUSIONS

In order to establish a model to describe the phase transformation process between the anhydrous form and the hydrated form for an organic compound, the following properties have been investigated in the present study by using theophylline as a model compound : (1) the solubilities and the disk dissolution behavior of both the anhydrous form and the monohydrate forms, (2) the growth kinetics of the monohydrate crystals at various supersaturations, temperatures and stirring rates, (3) the dissolution kinetics of the anhydrous crystals, and (4) the transformation process from the anhydrous form to the monohydrate form and the nucleation during the transformation.

4.1 : SOLUBILITY AND THERMODYNAMIC PROPERTIES OF THEOPHYLLINE :

Theophylline has a transition temperature of 60.0°C. The monohydrate form is the stable phase below the

transition temperature. The ionic strength and the electrolytes present in the system will affect the solubility, transition temperature and other thermodynamic properties of theophylline.

4.2 : GROWTH KINETICS OF THEOPHYLLINE MONOHYDRATE

The growth rate of the monohydrate crystals depends on the second order of the supersaturation and is independent of the stirring rate in the present study. These indicates that the growth is not a diffusion controlled process. The growth kinetics may be explained by a screw dislocation BCF model. The growth rate increases as temperature increases but which does not follow Arrhenius behavior.

4.3 : DISSOLUTION KINETICS OF THEOPHYLLINE ANHYDROUS CRYSTALS

The dissolution rate of the anhydrous crystals depends on the 1.5 order of the undersaturation and is inversely proportional to the square root of the crystal size.

4.4 : PHASE TRANSFORMATION PROCESS AND THE MODELLING OF THE PROCESS

The metastable anhydrous form undergoes transformation to the stable monohydrate form in an aqueous system below the transition temperature. The transformation process is characterized by the nucleation and growth of the monohydrate form at the expense of the dissolution of the anhydrous form. The addition of the monohydrate seeds initially does not prevent the bulk nucleation of the monohydrate form during the transformation process. Heterogeneous nucleation occurs regardless of the addition of the monohydrate seeds. The nucleation of the monohydrate form becomes the dominant mechanism of the transformation process and overwhelms the kinetics of the dissolution of the anhydrous form and the growth of the monohydrate form. Nucleation process will be a significant phenomena for the transformation processes of compounds with high solubility.

The model developed for the transformation process by taking into account the dissolution kinetics of the anhydrous form and the nucleation and growth kinetics of

the monohydrate form described the experimental data well.

4.5 : FUTURE WORK

This work provides some guidelines to study the kinetics of solvent-mediated phase transformation processes for organic solvates. It will be very interesting and promising to further investigate how to control transformation processes through the manipulation of the dissolution, nucleation and growth processes.

APPENDIX I

GROWTH KINETICS OF THYMINE MONOHYDRATE

5.1 : INTRODUCTION

Thymine, chemically known as 5-methyluracil, is a weak organic acid with a pka value of 9.94 at 25°C. Thymine can exist as anhydrous form or the monohydrate crystals with different crystal lattice and density (Gerdil 1961, Ozeki 1969). Solid state dehydration of thymine monohydrate has been investigated by Byrn and coworkers, the transition temperature was found to be 40°C in solid state (Byrn, 1982).

The solubility and crystal growth kinetics of thymine monohydrate in pH 6 phosphate buffer were investigated in the present study.

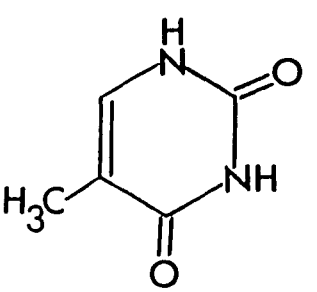

Structure of Thymine

5.2 : EXPERIMENTAL

5.2.1 : Materials and Equipments

Thymine anhydrous crystals were purchased from Sigma Company. The buffer system used in this study was Sorensen's pH 6 phosphate buffer prepared by the method as described in chapter 2. The ionic strength of the buffer was adjusted to 0.15 with potassium chloride.

The equipments used in this study are the same as those described in chapter 2.

5.2.2 : Assay of Thymine

The concentration of thymine in solution was measured by UV spectrophotometry at wave length of 270nm following proper dilution by 0.1N HCl. The standard curve for the assay is,

$$ABS = 62.52\ CONC + 0.0018 \qquad r^2 = 0.999 \qquad (5.1)$$

where ABS is the absorbance measured by UV spectrophotometry and CONC is the concentration of thymine in mg/ml.

5.2.3 : Solubility Measurement

The solubility of thymine monohydrate was obtained by dissolving an excess amount of thymine anhydrous crystals in the buffer solution with constant stirring for 24 hours. The concentration of the solution was measured as a function of time. Thymine anhydrous crystals transformed into the monohydrate crystals and the concentration of thymine in the buffer solution reached the solubility of the monohydrate form at the end of 24 hours. The solubility was measured at various temperatures.

5.2.4 : Preparation of Thymmine Monohydrate Seeds

One hundred and fifty ml of pH 6 phosphate buffer, saturated with thymine monohydrate at room temperature, was filtered and cooled in an ice bath (10g NaCl in 250 ml ice) with constant stirring. After 2 minutes, the monohydrate crystals appeared. The solution was stirred for another 3 minutes. The seeds were collected and aged in pH 6 phosphate buffer for two weeks.

5.2.5 : Growth Kinetics of Thymine Monohydrate

The growth experiments for thymine monohydrate were conducted in the same method as those described in chpater 2 for the growth of theophylline monohydrate. The grwoth rate was measured at varous supersaturations and temperatures in pH 6 phosphate buffer.

5.3 : RESULTS AND DISCUSSION

5.3.1 : Solubility

The solubility of thymine monohydrate at various temperatures in pH 6 phosphate buffer are shown in Table 5.1 and Figure 5.1. The dependence of the solubility on temperature can be expressed as equation 5.2,

$$\log S = -1401(1/T) + 5.23 \qquad r^2 = 0.998 \qquad (5.2)$$

where S is the solubility of thymine monohydrate in mg/ml and T is absolute temperature.

5.3.2 : Growth Kinetics of Thymine Monohydrate

The growth rate and supersaturation mentioned in this study have the same definitions as those discussed in chapter 3. The growth rate of thymine monohydrate crystals at various supersaturations and temperatures in pH 6 phosphate buffer are shown in Table 5.2.

The gorwth rates were fitted to the exponential growth model, as expressed in equation 1.27,

$$G = Kg\ S^{a} \qquad (1.27)$$

where all the terms have the same definitions as those described in chapter 1. The fitted parameters **Kg** and **a** at various temperatues are shown in Table 5.3. It is clear from the table that the growth order **a** changes significantly for thymine monohydrate as temperature increases from 14°C to 30°C and 43.5°C. This phenomena is very different from the growth of theophylline monohydrate, where the growth order did not change as temperature changes.

The profiles of growth rate versus supersaturation in pH 6 phosphate buffer at various temperatures are shown in Figure 5.2a and the corresponding logarithmic plots are shown in Figure 5.2b. The slope of the profile increases significantly as temperature increases, which corresponds to the increase in the growth order **a** as temperature increases.

The significant change in the growth order as a function of temperature may be explained by the change in the growth mechanism for thymine monohydrate as temperature increases. At 14°C, the growth may follow a screw dislocation mechanism with an **a** value of 2. At

higher temperatures, the growth mechanism may change to the surface nucleation model with an **a** value larger than 2. Further study is needed to investigate the details of how the growth mechanism chagnes with temperature.

Figure 5.1 : Solubility Versus Temperature for Thymine Monohydrate in pH 6 Phosphate Buffer

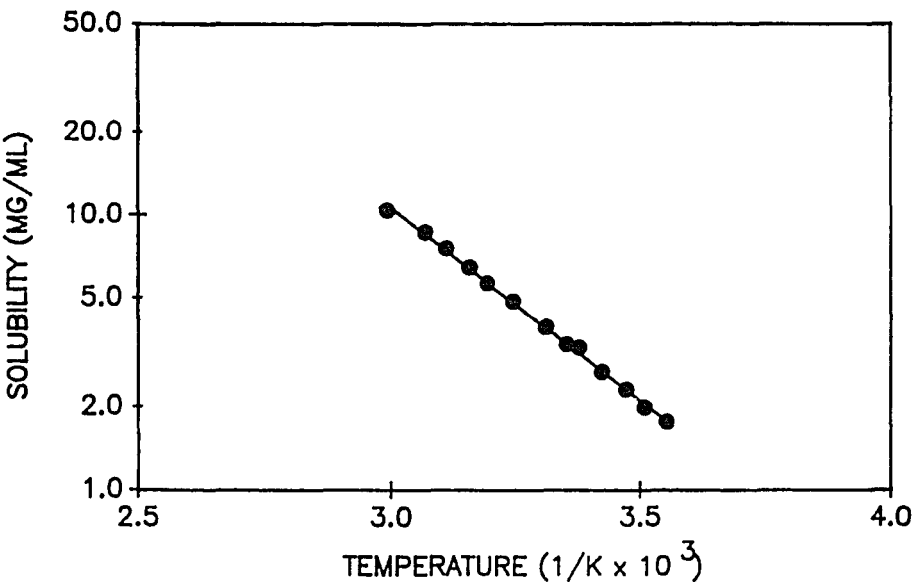

Figure 5.2 : Growth Rate Versus Supersaturation at Various Temperatures for Thymine Monohydrate Crystals in pH 6 Phosphate Buffer (A) Linear Plot (B) Logarithmic Plot

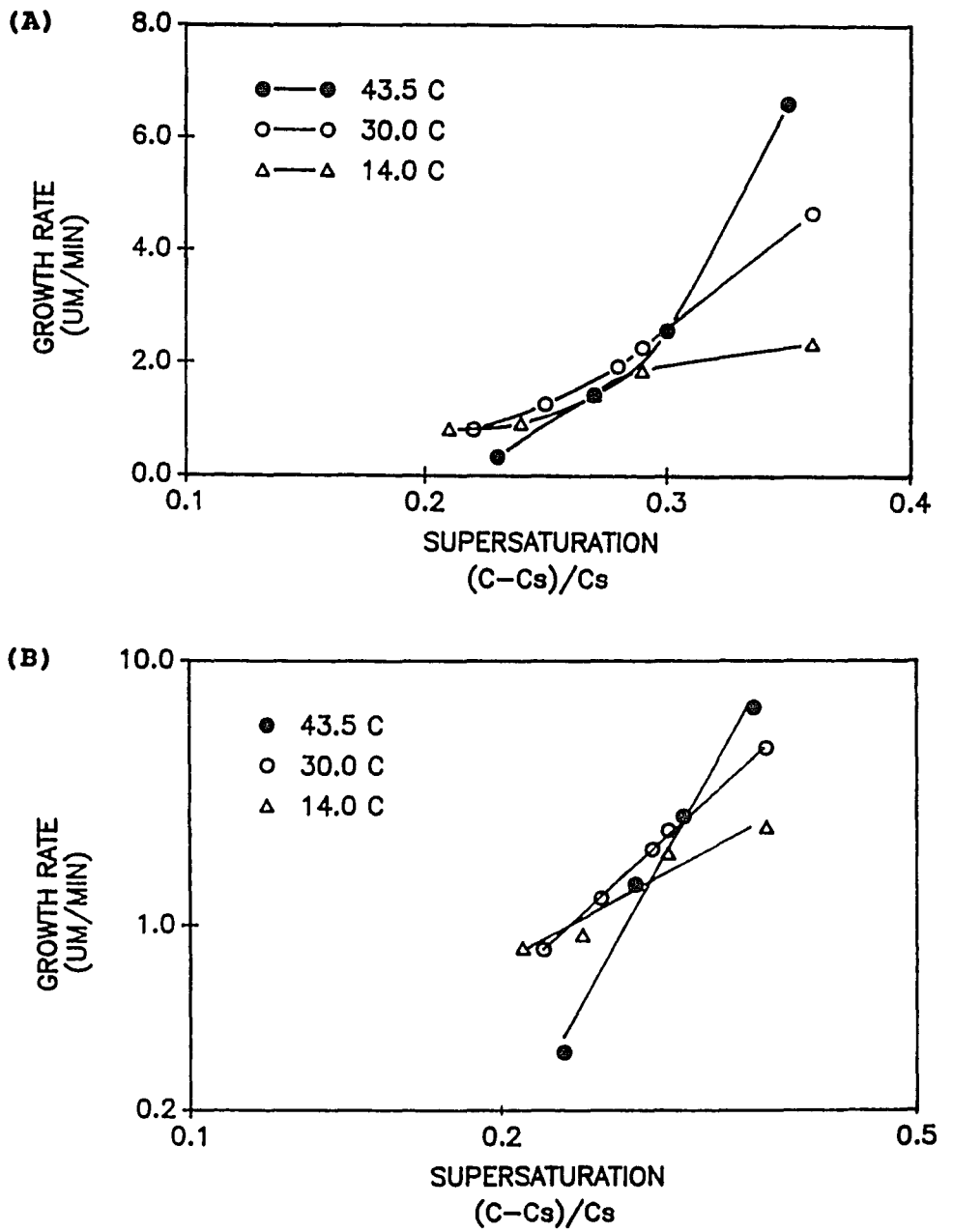

Table 5.1 : Solubility Versus Temperature for Thymine Monohydrate in pH 6 Phosphate Buffer

TEMPERATURE(°C)	SOLUBILITY (mg/ml)
8.3	1.76
11.8	1.99
14.9	2.31
19.0	2.68
23.0	3.29
25.2	3.39
29.0	3.92
35.0	4.85
40.0	5.64
43.6	6.43
48.4	7.53
52.8	8.64
61.0	10.37

Table 5.2 : Growth Rate for Thymine Monohydrate Crystals at Various Supersaturations and Temperatures in pH 6 Phosphate Buffer.

TEMPERATURE (°C)	SUPERSATURATION (C-Cs)/Cs	GROWTH RATE (μM/MIN)
43.5	0.23	0.33
43.5	0.27	1.42
43.5	0.30	2.57
43.5	0.35	6.60
30.0	0.22	0.81
30.0	0.25	1.26
30.0	0.28	1.93
30.0	0.29	2.27
30.0	0.36	4.65
14.0	0.21	0.82
14.0	0.24	0.92
14.0	0.27	1.43
14.0	0.29	1.86
14.0	0.36	2.34

Table 5.3 : Values of the Parameters for the Exponential Growth Model for Thymine Monohydrate at Various Temperatures in pH 6 Phosphate Buffer.

TEMPERATURE (°C)	Kg*	a*	r^2
43.5	4.1(0.1)	7.1(0.6)	0.986
30.0	2.3(0.0)	3.6(0.1)	0.999
14.0	1.4(0.1)	2.1(0.3)	0.933

* : Exponential Growth Model, $G = Kg\ S^a$

APPENDIX II

GENERAL DATA

Table 6.1 : Concentration Versus Time Profiles for the Dissolution Process of **(A)** Theophylline Monohydrate and **(B)** Anhydrous by Disc Dissolution Method at Various Temperatures.

(A) Theophylline Monohydrate :

TIME (MIN)	CONCENTRATION (μg/ML)			
	10.4°C	17.0°C	23.3°C	30.5°C
1.00	1.5	2.6	3.6	6.1
2.00	2.7	4.8	7.0	11.7
3.00	4.2	6.9	10.4	17.6
4.00	5.5	9.0	13.6	23.2
5.00	6.8	11.2	17.4	28.9
6.00	7.9	13.5	20.4	34.3
8.00	10.6		27.3	
10.00	13.2		34.5	
15.00	19.8		51.1	
20.00	26.8		68.9	

Table 6.1 : Continued.

(B) Theophylline Anhydrous

TIME (MIN)	CONCENTRATION (μg/ML)			
	10.4°C	17.0°C	23.3°C	30.5°C
0.50	2.6	2.8	4.2	5.9
1.00	4.6	5.2	7.7	10.8
2.00	8.2	10.0	15.1	21.0
3.00	11.9	14.3	22.3	31.1
4.00	14.7	17.1	30.2	38.7
5.00	17.0	19.8	36.9	45.5
6.00	19.6	22.3	43.3	53.0
8.00	22.8	27.4	57.6	67.8
10.00	25.9	31.6	67.8	82.3
15.00	33.6	44.1	88.1	120.1
20.00	40.4	54.8	105.3	152.4

Table 6.2[b] : Mean Size as a Function of Time and the Growth Rate for Theophylline Monohydrate at Various Supersaturations at 10°C.

TIME (MIN)	ARITHMETIC MEAN SIZE (μM)				
	S* 1.98	1.72	1.62	1.51	1.32
0.17	30.14	28.89	29.26	28.48	28.18
0.58	35.16	32.91	32.90		
1.00	38.97	36.26	35.78	34.88	34.09
1.58	42.51		39.48		
2.00	44.21	42.92	40.88	40.47	39.08
2.58		43.93	42.67		
3.00				44.32	42.45
4.00					44.97
	G* 11.3	9.3	8.0	6.5	6.0

TIME (MIN)	ARITHMETIC MEAN SIZE (μM)		
	S* 1.43	1.31	1.20
0.17	32.06	31.65	30.94
0.58	35.40	34.45	34.13
1.08	37.65	37.47	36.08
1.58	39.92	39.40	38.22
2.08	41.29	40.93	40.41
	G* 7.1	6.3	5.2

b : Table 6.2 continues on next page
* : S is the initial supersaturation, $(C-C_{SH})/C_{SH}$, G is the growth rate, μM/MIN.

Table 6.2 : Continued.

TIME (MIN)	ARITHMETIC MEAN SIZE (μM)				
	S* 0.48	0.42	0.40	0.36	0.36
0.17	19.01	19.00	19.00	18.46	18.71
1.00	20.04	19.94	19.51	19.27	19.31
2.00	21.59	20.75	20.51	19.93	20.08
3.00	22.79	21.79	21.31	20.68	20.55
4.00	23.95	22.53	21.94	21.44	21.21
5.00	25.14	23.11	22.91	21.69	21.88
	G* 1.3	0.9	0.9	0.7	0.8

TIME (MIN)	ARITHMETIC MEAN SIZE (μM)			
	S* 0.33	0.33	0.27	0.27
0.16	18.22	18.13	17.54	18.05
1.00	18.85	18.54	17.92	18.25
2.00	19.32	19.16	18.12	18.76
3.00	19.79	19.62	18.54	19.19
4.00	20.04	19.99	19.02	19.52
5.00	20.70	20.39	19.43	19.83
	G* 0.6	0.5	0.4	0.3

* : S is the initial supersaturation, $(C-C_{SH})/C_{SH}$.
G is the growth rate, μM/MIN.

Table 6.3 : Mean Size as a Function of Time and the Growth Rate for Theophylline Monohydrate at Various Supersaturations at 20°C.

TIME (MIN)	ARITHMETIC MEAN SIZE (μM)				
	S* 0.42	0.38	0.38	0.32	0.32
0.17	19.49	19.02	19.11	19.06	18.70
1.00	21.56	20.74	20.57	19.99	19.91
2.00	23.64	22.34	22.27	21.11	21.22
3.00	25.46	23.97	23.84	22.36	21.87
4.00	26.96	25.39	25.07	23.20	22.84
5.00	28.79	26.77	26.23	24.05	23.63
	G* 2.1	1.7	1.7	1.1	1.2

TIME (MIN)	ARITHMETIC MEAN SIZE (μM)		
	S* 0.30	0.28	0.28
0.17	19.31	18.63	18.50
1.00	20.23	19.46	19.54
2.00	21.41	20.47	20.55
3.00	22.33	21.37	21.34
4.00	23.21	22.04	21.88
5.00	24.13	22.76	22.62
	G* 1.0	1.0	1.0

* : S is the initial supersaturation, $(C-C_{SH})/C_{SH}$.
G is the growth rate, μM/MIN.

Table 6.4 : Mean Size as a Function of Time and the Growth Rate for Theophylline Monohydrate at Various Supersaturations at 30°C.

TIME (MIN)	ARITHMETIC MEAN SIZE (μM)				
	S* 0.48	0.43	0.38	0.38	0.33
0.17	20.30	20.18	19.88	19.73	19.61
1.00	24.45	23.27	22.34	22.42	21.49
2.00	28.53	26.88	25.03	24.89	23.49
3.00	31.87	28.34	27.09	26.91	25.15
4.00	34.74	30.41	28.77	28.84	26.57
5.00	37.15	33.00	30.52	30.49	27.48
	G* 4.0	3.2	2.6	2.5	1.9

TIME (MIN)	ARITHMETIC MEAN SIZE (μM)		
	S* 0.33	0.28	0.28
0.17	19.11	19.18	19.32
1.00	21.15	20.72	20.86
2.00	22.81	21.68	22.12
3.00	24.58	23.01	23.15
4.00	26.07	24.02	24.31
5.00	27.09	24.96	25.38
	G* 1.9	1.3	1.3

* : S is the initial supersaturation, $(C-C_{SH})/C_{SH}$.
G is the growth rate, μM/MIN.

Table 6.5 : Mean Size as a Function of Time and the Growth Rate for Theophylline Monohydrate at Various Supersaturations at 40°C.

TIME (MIN)	ARITHMETIC MEAN SIZE (μM)				
S*	0.50	0.45	0.40	0.35	0.30
0.17	21.30	20.96	20.38	19.90	19.60
1.00	26.02	24.57	23.15	22.04	21.03
2.00	29.96	27.97	26.41	23.92	22.21
3.00	33.32	32.29	28.29	25.92	23.27
4.00	35.95	34.67	30.74	26.96	24.25
5.00			31.85	28.37	25.12
G*	4.7	3.8	3.3	2.4	1.6

* : S is the initial supersaturation, $(C-C_{SH})/C_{SH}$.
G is the growth rate, μM/MIN.

Table 6.6 : Mean Size as a Function of Time and the Growth Rate for Theophylline Monohydrate at Various Stirring Rates and **(A)** Supersaturation of 0.85 and 10°C , and **(B)** Supersaturation of 0.34 and 20°C.

(A) Supersaturation of 0.85 and at 10°C

TIME (MIN)	ARITHMETIC MEAN SIZE (μM)					
RPM	400	400	700	700	1200	1200
0.17	22.32	22.32	22.58	22.61	22.56	23.03
1.00	25.30	25.07	25.46	25.75	25.86	26.18
2.00	28.29	28.22	28.67	28.54	28.65	28.86
3.00	31.02	30.95	31.10	31.21	31.13	31.48
4.00	33.83	33.67	33.84	33.83	33.48	33.59
5.00	35.89	35.77	36.21	36.26	35.37	35.54
G*	3.2	3.2	3.3	3.2	3.3	3.2

* : G is the growth rate, μM/MIN.

Table 6.6 : Continued.

(B) Supersaturation of 0.34 and at 20°C

TIME (MIN)	ARITHMETIC MEAN SIZE (μM)				
RPM	530	530	750	1000	1000
0.17	22.38	21.94	22.26	22.11	21.72
1.00	24.26	23.77	23.77	23.64	23.32
2.00	26.00	25.52	25.14	25.43	25.03
3.00	27.19	26.81	26.65	26.44	26.52
4.00	28.47	28.18	28.01		27.96
5.00	29.82	29.09	28.94		28.81
G*	1.8	1.9	1.6	1.8	1.8

APPENDIX III

THE PROGRAM TO SIMULATE THE TRANSFORMATION PROCESS

```
C     This program simulates the concentration profile in
C     the suspension for the transformation process from
C     anhydrous theophylline to theophylline monohydrate
C     in an aqueous buffer system.
C
C     All the unit used are based in mMole/ml
C
C-------------------------------------------------------
C
C The inputs are :
C
C    all the parameters associated with anhydrous : "A"
C    all the parameters associated with monohydrate : "B"
C
C        FA, FB : shape and density factor
C        SA, SB : solubility
C        V : total volume of the suspension
C        CON(1) initial concentration started with
C        TI : the unit increament of time
C        O : factor for the amount of the anhydrous put in
C            initially
C        P : factor for the amount of the monohydrate put
C            in initially
C        OA, PB : the number in the number distribution.
C        A, B : the different amount in terms of number
C               distribution of the anhydrous and mono-
C               hydrate crystal used in the simulation
C        ZA, ZB : the size in the number distribution
C        C,D : total mass of the anhydrous and monohydrate
C        E,F : new mass of the anhydrous and monohydrate
C
C
C     The program works by fixing the numbers but shifting
C     the size correspondently as a function of time
C
C-------------------------------------------------------
C
```

```
C
C
      INTEGER I,J,K,L,M,N,Q,U
      PARAMETER (M=400)
      REAL*8 E(M,130),F(M,130),ZB(M,130)
      REAL*8 ZA(M,130),C(M,130),D(M,130)
      REAL*8 FA,FB,SA,SB,V,CON(M),MT,P,O,OA(1,130),HY(M)
      REAL*8 R(M,130),G(M),A(1,130),B(1,130),TI,PB(1,130)
      REAL*8 PNN(1,130) NT,NQ,ZN(M,130),PN,NN(1,130)
      REAL*8 MN(M,130),CN(M,130)
      CHARACTER *15 FNAME,ONAME
      WRITE (*,900)
  900 FORMAT('   INPUT FILE NAME = ')
      READ (*,910) FNAME
  910 FORMAT (A)
      OPEN (3,FILE=FNAME,status='old')
      WRITE (*,911)
  911 FORMAT ('   OUTPUT FILE NAME =')
      READ (*,920) ONAME
  920 FORMAT (A)
      OPEN (4,FILE=ONAME,STATUS='NEW')
C
C
C
      READ (3,60) FA,FB,SA,SB,V,CON(1)
   60 FORMAT (3X,6F9.4)
      READ (3,61) TI,P,O,PN,NT
   61 FORMAT (3X,5F9.4)
C
C
      DO 10 J=1,128
      READ (3,66) ZB(1,J),PB(1,J),ZA(1,J),OA(1,J)
     *ZN(1,J),PNN(1,J)
   66 FORMAT (3X,9X,6F9.3)
      B(1,J)=P*PB(1,J)
      A(1,J)=O*OA(1,J)
      NN(1,J)=PN*PNN(1,J)
   10 CONTINUE
C
C
```

```
C
C-------------------------------------------------------
C   Calculation of the mass distribution.
C-------------------------------------------------------
C
C
      DO 12 J=1,128
      C(1,J)=(ZA(1,J)/10000.0)*(ZA(1,J)/10000.0)
     **(ZA(1,J)/10000.0)*A(1,J)*FA
C
      D(1,J)=(ZB(1,J)/10000.0)*(ZB(1,J)/10000.0)
     **(ZB(1,J)/10000.0)*B(1,J)*FB
C
   12 CONTINUE
C
C
C
C-------------------------------------------------------
C    Calculation of the cumulative mass
C-------------------------------------------------------
C
C
      E(1,1)=0
      F(1,1)=0
      DO 22 K=2,129
      L=K-1
      E(1,K)=E(1,L)+C(1,L)
      F(1,K)=F(1,L)+D(1,L)
   22 CONTINUE
C
C
C-------------------------------------------------------
C  E(1,129) : totol mass of anhydrous initially
C  F(1,129) : total mass of monohydrate initially
C  MT : total mass in the suspension
C-------------------------------------------------------
C
C
      MT=E(1,129)+F(1,129)+CON(1)
      WRITE (4,55) MT
   55 FORMAT (3X,'TOTAL MASS = ',F9.5)
      WRITE (4,56) CON(1)
   56 FORMAT (3X,F12.6)
C
```

```
C
C-------------------------------------------------------
C  Calculation of growth and dissolution rate :
C  Size independent growth and size dependent dissolution
C-------------------------------------------------------
C
C
      DO 31 I=2,M
      Q=I-1
      DO 33, K=1,128
      IF (ZA(Q,K).EQ.0.000) GO TO 11
C
C
      R(Q,K)=10**(((LOG(ABS((SA-CON(Q))/SA)))*1.49/2.303)
     *-((LOG(ABS(ZA(Q,K))))*0.54/2.303)+2.70)
      GO TO 33
   11 R(Q,K)=0
   33 CONTINUE
C
C
   14 IF ((CON(Q)-SB).LE.0.0000001) GO TO 16
      G(Q)=10**((LOG(ABS((CON(Q)-SB)/SB)))*2.11/2.303
     *+0.786)
      GO TO 18
   16 G(Q)=0.0
C
C
C-------------------------------------------------------
C Calculation of the 'new size' after unit time interval.
C Assign the size to be zero when the corresponding size
C is less than zero.
C-------------------------------------------------------
C
C
   18 DO 32 J=2,129
      K=J-1
      ZA(I,J)=ZA(Q,J)-R(Q,K)*TI
      IF (ZA(I,J).LT.0.0) THEN
      ZA(I,J)=0.0
      END IF
C
```

```
C
C-------------------------------------------------------
C  Calculate the new mass distribution
C-------------------------------------------------------
C
C
      C(I,J)=(ZA(I,J)/10000.0)*(ZA(I,J)/10000.0)
     **(ZA(I,J)/10000.0)*A(1,J)*FA
      ZB(I,J)=ZB(Q,J)+G(Q)*TI
      D(I,J)=(ZB(I,J)/10000.0)*(ZB(I,J)/10000.0)
     **(ZB(I,J)/10000.0)*B(1,J)*FB
   32 CONTINUE
C
C
C-------------------------------------------------------
C  Calculation of the new cumulative mass
C-------------------------------------------------------
C
C
      E(I,1)=0
      F(I,1)=0
      DO 41 J=2,129
      N=J-1
      E(I,J)=E(I,N)+C(I,N)
      F(I,J)=F(I,N)+D(I,N)
   41 CONTINUE
C
C-------------------------------------------------------
C   NUCLEATION PART
C-------------------------------------------------------
C
      NQ=NT/TI
      IF (Q.LT.NQ) GO TO 43
      GO TO 44
   43 ZN(I,J)=ZN(1,J)
      CN(I,129)=0.0
      GO TO 45
   44 DO 35 J=1,128
      ZN(I,J)=ZN(Q,J)+G(Q)*TI
      MN(I,J)=(ZN(I,J)/10000.0)*(ZN(I,J)/10000.0)
     **(ZN(I,J)/10000.0)*NN(1,J)*FB
   35 CONTINUE
C
```

```
C
C
      CN(I,1)=0.0
      DO 36 J=2,129
      U=J-1
      CN(I,J)=CN(I,U)+MN(I,U)
   36 CONTINUE
C
C
C-------------------------------------------------------
C    CALCULATE NEXT CONCENTRATION
C-------------------------------------------------------
C
   45 HY(I)=F(I,129)+CN(I,129)
      CON(I)=MT-E(I,129)-HY(I)
      WRITE (4,57) CON(I),E(I,129),CN(I,129),G(Q)
   57 FORMAT (3X,4F12.6)
   31 CONTINUE
C
C
C
      STOP
      END
```

REFERENCES

Adamson A., Physical Chemistry of Surface, 4th Ed., John Wiley and Sons, New York, p319, 1982.

Amathieu L and Boistelle R., *J. Crystal Growth*, **88**, 183, 1988.

Behme R.J., Brooke D., Farney R.F. and Kensler T.T., *J. Pharm. Sci.*, **74**, 1041, 1985.

Bennema P., *J. Crystal Growth*, **69**, 182, 1984.

Bisrat M. and Nyström C., *Int. J. Pharm.*, **47**, 223-231, 1988.

Bogan J.B., *J. Pharm. Sci.*, **72**, 837, 1983.

Boistelle and Astier, *J. Crystal Growth*, **90**, 14, 1988.

Boistelle R. and Astier J.P., *J. Crystal Growth*, **90**, 14-30, 1988.

Boistelle R. and Rinaudo C., *J. Cryst. Growth*, **53**, 1-9, 1981.

Botha S.A., Caira M.R., Guillory J.K and LÖtter A.P., *J. Pharm. Sci.*, **77**, 444-451, 1988.

Botha S.A., Caira M.R., Guillory J.K and LÖtter A.P., *J. Pharm. Sci.*, **78**, 28-34, 1989.

Botha S.A., Guillory J.K. and LÖtter A.P., *J. Pharm. Biomed. Anal.* **4**, 573-587, 1986.

Bourne J.R. and Davey R.J., *J. Crystal Growth*, **36**, 287, 1976.

Brener G., Roberts F.E., Hoinowski A., Budavavi J., Powell B., Hinkley D. and Schoenwaldt E., *Angew. Chem. Intl. ed.*, **8**, 975, 1969.

Breovic L. and Skrtic D., *J. Crystal Growth*, **74**, 399-408, 1986.

Brice J.C., Crystal Growth Process, John Wiley and Sons,

Brice J.C., Crystal Growth Process, John Wiley and Sons, New York, Blackie Glasgow and London, 1986.

Brooke D., *J. Pharm. Sci.*, **63**, 344, 1974.

Burt H.M. and Mitchell A.G., *Int. J. Pharm.* **5**, 239, 1980.

Burton W.K., Cabrera N. and Frank F.C., *Phil. Trans. Roy. Soc. London*, **A243**, 299, 1951.

Byrn S., Solid State Chemistry of Drug, P158, Academic Press, 1982.

Callow R.K., *Biochem. J.*, **25**, 79, 1931.

Carless J.E., Moustafa M.A. and Rapson H.D.C., *J. Pharma. Pharmac.*, **20**, 630, 1968.

Carstensen J.T. and Dhupar K., *J. Pharm. Sci.*, **65**, 1634, 1976.

Carstensen J.T. and Patel M., *J. Pharm. Sci.*, **64**, 1771, 1975.

Castellan G.W., Physical Chemistry, 3rd ed., Addison-Wesley Publishing Company, Reading, Massachusetts, 1983.

Cheng V., Coller B. and Powell J., *Faraday Discuss. Chem. Soc.*, **77**, 243, 1984.

Christoffersen J. and Christofferson M., *Faraday Discuss. Chem. Soc.*, **77**, 223, 1984.

Chu J.C., Kalil J. and Wetteroth W.A., *Chem. Engr. Prog.*, **49**, 141, 1953.

Clay R.J., Knevel A.M. and Byrn S.R., *J. Pharm. Sci.*, **71**, 1289, 1982.

Cohen J.L., *Analytical Profile of Drug Substance*, **4**, P476, 1975.

Cohen J.L., Ph.D. Dissertation, University of Wisconsin, Medison, 1969.

DeSmidt J.H., Fokkens J.G., Grijseeds H. and Cromnelin

DeSmidt J.H., Fokkens J.G., Grijseeds H. and Cromnelin D.J., *J. Pharm. Sci.*, **75**, 497, 1986.

Durbin S.D. and Feher G., *J. Grystal Growth*, **76**, 583, 1986.

Fokkens J.G. and de Blaey C.J., 1983 or Fokkens J.G., van Amelsfoort J.G.M., de Blaey C.J., de Kruif C.G. and Wilting J., *Int. J. Pharm.*, **14** (1), 79, 1983.

Gapon E.N., *Z. Elktrochem.*, **122**, 455, 1926.

Garside J. and Jancic S.J., *AIChe. Journal*, **22**, 887, 1976.

Garside J., *AIChe Symposium Series*, **80**, 23, 1984.

Garside J., Janseen-Van Rosmalen R. and Bennema P., *J. Crystal Growth*, **29**, 353, 1975.

Gerdil R., *Acta Cryst.* **14**, 333, 1961.

Gilmer G.H. and Jackson K.A., in Crystal Growth and Materials, eds. Kaldis E. and Scheel H.J., P79-114, North-Holland, Amsterdam, 1979.

Gohar P. and Cournil M., *Materials Chemistry and Physics*, **14**, 427, 1986.

Guttman D. and Higuchi T., *J. Pharm. Sci.*, **60**, 1269, 1971.

Haleblian J. and McCrone W.C., *J. Pharm. Sci.*, **58**, 911, 1969.

Haleblian J., Koda R. and Biles J., *J. Pharm. Sci.*, **60**, 1485, 1971.

Haleblian J.K., *J. Pharm. Sci.*, **64**, 1269, 1975.

Hartmann P., ed., Crystal Growth : An Introduction. North-Holland, Amsterdam, 1973.

Hiemenz, Principles of Colloidal and Surface Chemistry, P231, 1986.

Higuchi W.I., *J. Pharm. Sci.*, **56**, 315, 1967.

Higuchi W.I., *J. Pharm. Sci.*, **56**, 315, 1967.

Higuchi W.I., Prakongpan S. and Young F., *J. Pharm. Sci.*, **62**, 945, 1973.

Higuchi W.I., Rowe E.L. and Hiestand E.N., *J. Pharm. Sci.*, **52**, 162, 1963.

Hillig W.B., *Acta. Met.*, **14**, P1968, 1966.

Hixson A. and Crowell J., *Ind. Eng. Chem.*, **23**, 923, 1931.

Hsia D.C., Kim C.K. and Kildsig D.O., *J. Pharm. Sci.*, **66**, 960, 1977.

Jetten L.A., Human H.J., Bennema P. and Van der Erden J.P., *J. Crystal Growth*, **68**, 503, 1984.

Kahalil S., Moustafa M., Ebian A. and Motawi M., *J. Pharm. Sci.*, **61**, 1615, 1972.

Konak A.R., *Chem. Eng. Sci.*, **29**, 1785, 1974.

Kuhnert-Branstätter M. and Aepkers M., *Mikroskopie*, **16**, 181, 1961.

Kuhnert-Branstätter M. and Grimm H., *Sci. Pharm.*, **35**, 287, 1967.

Kuhnert-Branstätter M. Hoffman R. and Senn M., *Mikrochem. J.*, **7**, 357, 1963.

Langenbucher, *J. Pharm. Sci.*, **58**, 1265, 1969.

Lesson L.J. and Carstensen J.T., Dissolution Technology, Academy of Pharmaceutical Sciences, Washington DC, 1974.

Leuallen E. and Osol A., *J. Amer. Pharm. Assoc., Sci., Ed.*, **38**, 92, 1949.

Lin C.T. and Byrn S.R., *Mol. Cryst. Liq. Cryst.*, **50**, 99, 1979.

Linek K. and Peciai C., *Chem. Zvesti.*, **16**, 692, 1962.

Liu C.Y., Tsuei H.S. and Youngquist G.R., *AICHE* Symposium

Liu C.Y., Tsuei H.S. and Youngquist G.R., *AICHE* Symposium Series, **67**, 43, 1971.

Liu C.Y., Tsuei H.S. and Youngquist G.R., *AIChe. Process Symposium Series*, **67**, 43, 1971.

Marshall K. and Meakin B.C., *J. Pharm. Pharmacol. suppl.* **24**, 151, 1972.

Mauger J. and Howard S., *J. Pharm. Sci.*, **65**, 1043, 1976.

Maulding H.V. and Zoglio M.A., *J. Pharm. Sci.*, **60**, 309, 1971.

McEwan D. and Sadler D.E., *J. Crystal Growth*, **79**, 648, 1986.

McNamara P. and Amidon G.L., *J. Pharm. Sci.*, **75**, 858, 1986.

Mesley R.J. and Houghton E.E., *J. Pharm. Pharmacol*, **20**, 341, 1968.

Moustafa M., Ebian A., Khalil S. and Motawi M., *J. Pharm. Pharmacol.*, **23**, 868, 1971.

Nagvi A.A. and Bhattacharyya G.C., *J. Appl. Cryst.*, **14**, 464, 1981.

Nicklasson M. and Brodin A., *Acta. Pharm. Suec.* **19**, 109, 1982.

Niebergall P.J., Milosovich G. and Goyan J.E., *J. Pharm. Sci.*, **52**, 236, 1963.

Nielsen A.E., Kinetics of Precipitation, Pergamon, Oxford, P69, 1964.

Nielsin A.E. and Toft J.M., *J. Crystal Growth*, **67**, 278, 1984.

Nishijo J., Yonetani I., Tagahara K., Suzuta Y. and Iwamoto E., *Chem. and Pharm. Bull.*, **34**(11), 4451,1986.

Noyes A. and Whitney W., *Z. Phys. Chem.*, **23**, 689, 1897.

Noyes-Nernst A.A. and Whitney W.R., *J. Am. Chem. Soc.*,

Noyes-Nernst A.A. and Whitney W.R., *J. Am. Chem. Soc.*, **19**, 930, 1897.

Nyström C. and Bisrat M., *J. Pharm. Pharmacol*, **38**, 420, 1986.

Nyström C., Mazur J., Barnett M.I. and Glazer M., *J. Pharm. Pharmacol*, **37**, 217, 1985.

Nyvlt J., Industtrial Crystallization from Solution, Butterworths, London, 1971.

Ohara M. and Reid R.C., Modeling Crystal Growth Rates From Solution, P47, Englewood Cliffs, NJ, 1973.

Ostwald, *Z, Phys. Chem.*, **22**, 289, 1897.

Ozeki K., Sakabe N. and Tanaka J., *Acta Cryst.*, **B25**, 1038, 1969.

Pamplin B.R., ED., Crystal Growth, 2nd ed., Pergamon, Oxford, 1980.

Pearson J.T. and Varney G., *J. Pharm. Pharmac. Suppl*, **21**, 60s, 1969.

Pearson J.T. and Varney G., *J. Pharm. Pharmac. Supply*, **21**, 60s, 1969.

Randolph A.D. and Larson M.A., P20, Theory of Particulate Process, Academic Press, New York and London, 1988.

Rosenberger F., Fundamentals of Crystal Growth I, Springer-Verlag, Berlin, Heidelberg, New york, 1979.

Rowe E.L. and Anderson B.D., *J. Pharm. Sci.*, **73**, 1673, 1984.

Salunke D.M., Veerapandian B., Kodandapani R. and Vijayan M., *Acta. Cryst*, **B41**, 431, 1985.

Seitz J.A., Ph.D. thesis, University of Wisconsin, Madison, 1958.

Shah A.C. and Nelson K.G., *J. Pharm. Sci.*, **64**, 1519, 1975.

Shefter E. and Higuchi T., *J. Pharm. Sci.*, **52**, 781, 1963.

Shefter E. and Higuchi T., *J. Pharm. Sci.*, **52**, 781, 1963.

Simmons P.L., Ranz R.J., Gyanchandani N.D. and Picotte D., *Can. J. Pharm. Sci.*, **7**, 121, 1972.

Strickland-Constable R.F., Kinetics and Mechanisms of Crystallization, Academic Press, New York, 1968.

Summers M.P., Enever R.P. and Carless J.E., in Paritcle Growth in Suspensiion, Smith A.C., ed., Academic Press. P247, 1973.

Sutor D.J., *Acta. Cryst.*, **11**, 83, 1958.

Tawashi R., *J. Pharm. Pharmacol.*, **21**, 701, 1969.

Thakkar A.L., Tensmeyer L.G. and Wilham W.L., *J. Pharm. Sci.*, **60**, 1267, 1971.

Tingstad J.E. and Riegelman S., *J. Pharm Sci.*, **59**, 692, 1970.

Van der Eerdem J.P., Bennema P. and Cherepanova T.A., *Prog. Crystal Growth Charact.*, **1**, 219, 1978.

Veng Pedersen P. and Brown K.F., *J. Pharm. Sci.*, **64**, P1981, 1975.

Wadke D.A. and Reier G.E., *J. Pharm. Sci.*, **61**, 869, 1972.

Wagner J.G., Biopharmaceutics and Relevant Pharmacokinetics, Drug Intelligence, Hamilton, Illinois, P98-174, 1971.

Wagner J.G., *Drug Intell. Clin. Pharm.*, **4**, 77,1970.

Weeks J.D. and Gilmer G.H., *Advan Chem. Phys.*, **40**, 157, 1979.

Wey J.S. *Chem. Eng. Commun.*, **35**, 231, 1985.

Wong D.T., Wright P. and Aulton M.E., *Drug Development and Industrial Pharmacy*, **14**, 2109-2126, 1988.

Wurster D.E. and Taylor P.W., *J. Pharm. Sci.*, **54**, 169, 1965.